FAST HISTORY MATCHING OF FINITE-DIFFERENCE MODEL, COMPRESSIBLE AND THREE-PHASE FLOW USING STREAMLINE-DERIVED SENSITIVITIES

A Dissertation

by

HAO CHENG

Submitted to the Office of Graduate Studies of
Texas A&M University
in partial fulfillment of the requirements for the degree of

DOCTOR OF PHILOSOPHY

August 2005

Major Subject: Petroleum Engineering

FAST HISTORY MATCHING OF FINITE-DIFFERENCE MODEL, COMPRESSIBLE AND THREE-PHASE FLOW USING STREAMLINE-DERIVED SENSITIVITIES

A Dissertation

by

HAO CHENG

Submitted to the Office of Graduate Studies of
Texas A&M University
in partial fulfillment of the requirements for the degree of

DOCTOR OF PHILOSOPHY

Approved by:

Chair of Committee,	Akhil Datta-Gupta
Committee Members,	W. John Lee
	Daulat Mamora
	Yalchin Efendiev
Head of Department,	Stephen A. Holditch

August 2005

Major Subject: Petroleum Engineering

ABSTRACT

Fast History Matching of Finite-Difference Model, Compressible and Three-Phase Flow Using Streamline-Derived Sensitivities. (August 2005)

Hao Cheng, B.S., Xi'an Petroleum Institute, China;

Ph.D., University of Petroleum, Beijing, China

Chair of Advisory Committee: Dr. Akhil Datta-Gupta

Reconciling high-resolution geologic models to field production history is still a very time-consuming procedure. Recently streamline-based assisted and automatic history matching techniques, especially production data integration by "travel-time matching," have shown great potential in this regard. But no systematic study was done to examine the merits of travel-time matching compared to more traditional amplitude matching for field-scale application. Besides, most applications were limited to two-phase water-oil flow because current streamline models are limited in their ability to incorporate highly compressible flow in a rigorous and computationally efficient manner.

The purpose of this work is fourfold. First, we quantitatively investigated the nonlinearities in the inverse problems related to travel time, generalized travel time, and amplitude matching during production data integration and their impact on the solution and its convergence. Results show that the commonly used amplitude inversion can be orders of magnitude more nonlinear compared to the travel-time inversion. Both the travel-time and generalized travel time inversion (GTTI) are shown to be more robust and exhibit superior convergence characteristics.

Second, the streamline-based assisted history matching was enhanced in two important aspects that significantly improve its efficiency and effectiveness. We utilize streamline-derived analytic sensitivities to determine the location and magnitude of the changes to improve the history match, and we use the iterative GTTI for model updating. Our approach leads to significant savings in time and manpower.

Third, a novel approach to history matching finite-difference models that combines the efficiency of analytical sensitivity computation of the streamline models with the versatility of finite-difference simulation was developed. Use of finite-difference simulation can account for complex physics.

Finally, we developed an approach to history matching three-phase flow using a novel compressible streamline formulation and streamline-derived analytic sensitivities. Streamline models were generalized to account for compressible flow by introducing a relative density of total fluids along streamlines and a density-dependent source term in the saturation equation. The analytical sensitivities are calculated based on the rigorous streamline formulation.

The power and utility of our approaches have been demonstrated using both synthetic and field examples.

DEDICATION

To my wife, to my parents and parents-in-law, to my teachers, and to my friends.

ACKNOWLEDGMENTS

I would like to express my deep gratitude to my graduate advisor Dr. Akhil Datta-Gupta for his inspiration, invaluable advice, academic guidance, financial support, time and efforts contributed to my papers and presentations, and various help to make my four-year life at Texas A&M memorable.

I would like to thank Dr. Lee, Dr. Mamora, and Dr. Efendiev for serving as committee members. I acknowledge their helpful comments and suggestions in shaping this dissertation.

I wish to take this opportunity to acknowledge Xian-Huan Wen, William Milliken, Wen Chen, and Alan Bernath in ChevronTexaco Energy Technology Company for their constant support and discussion in history matching during my summer internship in San Ramon. Thanks to Woody, Djuro, Ritesh, Ricardo, Steve Johnson and many other colleagues for an enjoyable summer in Houston.

I want to thank my friends in the reservoir characterization group: Ahmed Daoud, Arun, Dayo, Eduardo, Ichiro, Leonardo, Mishal, Xianlin, Chengwu and Zhong He for their precious help and discussion.

I would like to thank Dr. Lee and Ms. Darla-Jean Weatherford for teaching me how to make presentations.

I would like to acknowledge financial support from members of the Joint Industry Project on reservoir data integration and also from the U.S. Department of Energy. The facilities and resources provided by the Petroleum Engineering Department, Texas A&M University, are gratefully acknowledged.

Thank God.

TABLE OF CONTENTS

Page

Page

Page

LIST OF FIGURES

FIGURE Page

FIGURE Page

FIGURE Page

FIGURE Page

FIGURE Page

CHAPTER I

INTRODUCTION AND STUDY OBJECTIVES

Reconciling geologic models to dynamic data such as multiphase production history is still by far the most time-consuming aspect of the workflow for both geoscientists and engineers. Although significant advancements have been made in this area over the last decade, current industry practice still involves iterative trial and error methods and often utilizes arbitrary permeability multipliers that can result in geologically unrealistic discontinuities in reservoir properties. Such manual history matching is time-consuming, manpower intensive and highly subjective in nature. This makes model assessment very difficult. The situation is further complicated by compressible and three-phase flow. This chapter presents the motivation and objectives of the research in this dissertation.

1.1 Introduction

Geological models derived from static data alone often fail to reproduce the production history of a reservoir. Reconciling geologic models to the dynamic response of the reservoir is critical to building reliable reservoir models. This process is referred as "history matching."

1.1.1 Static vs. Dynamic Data

Geostatistical reservoir models are widely used to model the heterogeneity of reservoir petrophysical properties, such as permeability and porosity. These geostatistical reservoir models are usually upscaled from fine-scale geologic/geocellular models to

---

This dissertation follows the style and format of the *SPE Journal*.

coarser reservoir simulation models for field development studies and performance predictions.

It is imperative that geostatistical reservoir models incorporate as much available, site-specific information as possible in order to reduce the uncertainty in the subsurface characterization. Available information on reservoir heterogeneity can be broadly categorized into two major types: static and dynamic. Static data are time-invariant direct or indirect measurements of reservoir properties, such as core measurements, well logs, and seismic data. These data can, relatively easily, be integrated into geostatistical models using the traditional geostatistical algorithms.[1] Dynamic data are the time dependent measurements of flow responses that are related to the reservoir properties through the flow equations, such as pressure, flow rate, fractional flow rate, saturation or tracer responses. Integration of dynamic data generally leads to an inverse problem.[2-3]

1.1.2 History Matching Workflow Overview

There are many possibilities for choosing parameters for history matching. These include porosity, permeability, fluid properties, relative permeabilites or boundary conditions such as fluid contacts, aquifer strength, fault transmissibilities etc. The reservoir response can be water-cut data, pressure measurements, tracer response, 4-D seismic etc. The key parameters in history matching are not always apparent. Also, the parameter and data uncertainties are often unknown and the constraints on the parameters are not well-defined. All these make field scale history matching a challenging and time consuming task. Modern history matching follows a hierarchical workflow to account for uncertainties at various scales. To start with, generally a geologic model screening is carried out to identify the impact of large-scale features such as structures, fluid contacts, reservoir architecture/stratigraphy and boundary conditions on the production response. This step consists of performing flow simulations through a suite of realizations representing large-scale subsurface uncertainties. The outcome of this step is a selected set of realizations for detailed history matching by changing spatially varying properties such as permeability, porosity or facies

distribution. This step involves localized changes and is typically the most time-consuming aspect of the workflow. Fortunately, streamline models are most advantageous at this stage because of the unique information content in the streamlines and sensitivities. Finally, history matching also involves adjusting physical property models such as relative permeabilities and fluid properties. Because typically there are only a few parameters involved here, we can conveniently examine their significance using experimental design. This dissertation mainly focuses on changing of spatially varying properties, in particular permeability for history matching finite-difference or streamline models using streamline-derived sensitivities.

1.1.3 Assisted History Matching

Traditionally, history matching is performed manually on the upscaled reservoir model and frequently uses local or regional multipliers to reservoir properties. By adjusting the regions and multipliers, a history match could be achieved using mostly trial and error. The trial-and-error involves considerable subjective judgment and personal bias and most importantly may create artificial discontinuities inside the reservoir, potentially destroying the correlation built into the initial geologic model.

A more systematic approach to history matching, called Assisted History Matching (AHM), utilizes unique information-content in streamlines in terms of injector-producer relationship to facilitate history matching.[4-6] The AHM is also a manual approach. However, changes to the model can be limited to the streamlines contributing to the production history of the well of interest and the amount of changes can be computed using some simple semi-analytical methods. The approach is a significant improvement over the traditional manual history matching but still could be time consuming, particularly when there are a large number of wells. This is complicated by the coupled nature of the flow equations which makes matching individual wells difficult without impacting other wells also. Finally, if we limit changes along streamlines only, it can introduce ‘tube like’ artifacts into the geologic model.

1.1.4 Automatic History Matching

Geostatistically-based automatic history matching (production data integration) has been an active area of research and a number of techniques have been reported in the literature in the past decade. The main goal here is to match well production data by modifying the initial model in such a way that it preserves the underlying geostatistical features built into the initial model. Yeh[7] and Wen et al.[8] provided a review of these inverse techniques. Both finite difference and streamline fluid flow modeling can be used in automated history matching.[9] Typically, an inverse technique is needed for production data integration, and requires multiple solutions of the flow equations within a nonlinear optimization procedure.[10-12] And this brings a hurdle to the practical applications. Streamline based inverse techniques have shown great potential in this regard[13-18] and they only require a single solution of the flow equations per minimization iteration.[13-14] The sensitivities of production data with respect to reservoir properties can be computed analytically using a single forward simulation. This renders substantial time-saving. For automatic history matching, there are many aspects which need to be addressed here, including different matching approaches, minimization techniques, sensitivity calculation, streamline versus finite-difference modeling, compressible and three-phase flow issues.

Matching Approach: Travel Time vs. Amplitude Matching. In recent years several techniques have been developed for integrating production data into reservoir models.[5,10,12,13,15,18-27] The theoretical basis of these techniques is generally rooted in the least-squares inversion theory that attempts to minimize the difference between the observed production data and the model predictions. This can be referred to as "amplitude" matching. The production data can be water-cut observations, tracer response, or pressure history at the wells. It is well known that such inverse problems are typically ill-posed and can result in nonunique and unstable solutions. Proper incorporation of static data in the form of a prior model can partially alleviate the problem. However, there are additional outstanding challenges that have deterred the

routine integration of production data into reservoir models. The relationship between the production response and reservoir properties can be highly nonlinear. The nonlinearity can result in multiple local minima in the misfit function. This can cause the solution to converge to a local minimum, leading to an inadequate history match. All these can make it difficult to obtain a meaningful estimate of the parameter field, particularly if the initial model is far from the solution. Another approach is "travel-time matching" that is analogous to seismic tomography. Instead of matching the production data directly, the observed data and model predictions are first "lined up" at the breakthrough time. This is typically followed by a conventional amplitude match, whereby the difference between the observed and calculated production response is minimized. A major part of the production data misfit reduction occurs during the travel-time inversion, and most of the large-scale features of heterogeneity are resolved at this stage.[19,21,22] A more efficient approach is "generalized travel-time" inversion.[9] The generalized travel-time inversion ensures matching of the entire production response rather than just the breakthrough times and at the same time retains most of the desirable properties of the travel-time inversion. The concept follows from wave-equation travel-time tomography and is very general, robust, and computationally efficient.[26,28] The generalized travel-time inversion has been utilized to extend the streamline-based production data integration methods to changing field conditions involving rate changes and infill drilling.

The advantages of the travel-time inversion compared to amplitude inversion mainly stems from its quasilinear properties. The advantages of travel-time inversion are well-documented in the context of seismic inversion.[28] However, no systematic study has been done to examine the benefits of travel-time inversion for production-data integration in terms of nonlinearity and convergence properties. Characterizing the degree of nonlinearity can be as important as finding the solutions to the inverse problem itself. However, quantitative measures of nonlinearity for the inverse problems related to production data integration have not been adequately addressed.

Minimization Techniques. Integration of dynamic data typically requires a least-square based minimization to match the observed and calculated production response. There are several approaches to such minimization and these can be broadly classified into three categories: gradient-based methods, sensitivity-based methods and derivative-free methods. The derivative-free approaches such as simulated annealing or genetic algorithms require numerous flow simulations and can be computationally prohibitive for field-scale applications.[20] Gradient-based methods have been widely used for automatic history matching, although the convergence rates of these methods are typically slower than the sensitivity-based methods such as the Gauss-Newton or the LSQR method.[13,19,23,25] An integral part of the sensitivity-based methods is the computation of sensitivity coefficients. These sensitivities are simply partial derivatives that define the change in production response because of a small change in reservoir parameters.

Sensitivity. There are several approaches to calculating sensitivity coefficients and these generally fall into one of the three categories: perturbation method, direct method and adjoint state methods.[7] Conceptually, the perturbation approach is the simplest and requires the fewest changes in an existing code. Sensitivities are estimated by simply perturbing the model parameters one at a time by a small amount and then computing the corresponding production response. Such an approach requires (N+1) forward simulations where N is the number of parameters. Obviously, this can be computationally prohibitive for reservoir models with many parameters. In the direct or sensitivity equation method,[7] the flow and transport equations are differentiated to obtain expressions for the sensitivity coefficients. Because there is one equation for each parameter, this approach can require the same amount of work. A variation of this method, called the gradient simulator method,[29] utilizes the discretized version of the flow equations and takes advantage of the fact that the coefficient matrix remains unchanged for all the parameters and needs to be decomposed only once. Thus, sensitivity computation for each parameter now requires a matrix-vector

multiplication.[12,19] This method can also be computationally expensive for large number of parameters.Finally, the adjoint state method requires derivation and solution of adjoint equations that can be significantly smaller in number compared to the sensitivity equations. The adjoint equations are obtained by minimizing the production data misfit with flow equations as constraint and can be quite cumbersome for multiphase flow applications.[30] Furthermore, the number of adjoint solutions will generally depend on the amount of production data and thus, length of the production history.

Streamline vs. Finite-Difference. With the streamline method, the sensitivities can be computed analytically using a single flow simulation.[13,26] Because the sensitivity calculations involve evaluation of 1-D integrals along streamlines, the method scales very well with respect to model size or the number of parameters. Although the streamline models have been extremely successful in bridging the gap between geologic modeling and flow simulation, they are currently limited in their ability to incorporate complex physical processes and cross-streamline mechanisms in a computationally efficient manner.[13] Thus, an efficient and robust approach to production data integration using finite-difference models will be particularly useful in characterizing reservoirs dominated by mechanisms such as compressibility and gravity effects, transverse dispersion and other complex physical mechanisms.

Since streamline models are limited in their ability to incorporate highly compressible flow and cross-streamline mechanisms in a rigorous and computationally efficient manner, most of the streamline-based history matching applications have been limited to two-phase water-oil flow.

1.2 Objectives

From the above section, several problems in reservoir characterization raised, including quantification of measure of nonlinearity for travel-time and amplitude matching,

enhancement of assisted history matching approach, history matching finite-difference models, and history matching compressible, three-phase flow. Thus the objectives of this research are as follows.

1.2.1 Nonlinearity Quantification

We discuss the mathematical foundation for the measure of nonlinearity and its implications on the production-data integration. We quantitatively investigate the extent of nonlinearity in travel-time inversion and amplitude inversion. We illustrate our results using both synthetic and field applications.

1.2.2 Assisted vs. Automatic History Matching

We enhance the streamline-based assisted history matching in two important aspects that can significantly improve its efficiency and effectiveness. First, we utilize streamline-derived analytic sensitivities to determine the spatial distribution and magnitude of the changes needed to improve the history-match. These sensitivities are then incorporated into an optimization algorithm to update the reservoir model during flow simulation. Secondly, a "generalized travel-time inversion (GTTI)"[24,26] is used for inverse modeling. The GTTI is robust because of its quasi-linear properties[31] resulting in rapid convergence even if the prior model is far from the solution. We demonstrate our approach using two field examples with over 100 wells and more than 30 years of production history.

1.2.3 History Matching Finite-Difference Models

We propose a novel approach to history matching finite-difference models that combines the advantage of the streamline models with the versatility of finite-difference simulation. We first generate streamlines using the velocity field derived from a finite-difference simulator. The streamlines are then used to compute the parameter sensitivities for updating the reservoir model. The updated model is then used in the finite-difference simulation to predict reservoir performance and the process is repeated

until a satisfactory history match is obtained. For history matching, we use ‘a generalized travel-time inversion’ that is shown to be extremely robust because of its quasi-linear properties and converges in only a few iterations. We illustrate the power and practical feasibility of the method using synthetic and field examples.

1.2.4 History Matching Compressible, Three-Phase Flow

We generalize streamline models to compressible flow using a rigorous formulation while retaining most its computational advantages. Our new formulation is based on three major elements and requires only minor modifications to existing streamline models. We introduce a relative density for the total fluids along the streamlines and incorporate a density-dependent source term in the saturation equation that accounts for the pressure effects during saturation calculations for compressible flow. We can history match three-phase flow using the rigorous streamline flow simulation. In addition, history matching three-phase flow using finite-difference flow simulation and streamline-based sensitivity is another option. The analytic sensitivities are calculated along the streamlines using the rigorous compressible streamline formulation. A synthetic example is used to illustrate the procedure, and a field-scale example is shown to validate this method.

CHAPTER II

TRAVEL-TIME VS. AMPLITUDE MATCHING FOR PRODUCTION DATA INTEGRATION*

The traditional approach to reconciling geologic models to production data involves an "amplitude matching," that is, matching the production history directly. These include water-cut, tracer concentration, and pressure history at the wells. It is well known that such amplitude matching results in a highly nonlinear inverse problem and difficulties in convergence, often leading to an inadequate history match. The nonlinearity can also aggravate the problem of nonuniqueness and instability of the solution. Recently, production data integration by "travel-time matching" has shown great promise for practical field applications. In this approach, the observed data and model predictions are lined up at some reference time such as the breakthrough or "first arrival" time. Further extensions have included amplitude information by a "generalized travel-time" inversion. Although the benefits of travel-time inversion are well documented in the context of seismic inversion, no systematic study has been done to examine its merits for field-scale history matching.

In this chapter, we quantitatively investigate the nonlinearities in the inverse problems related to travel time, generalized travel time, and amplitude matching during production data integration and their impact on the solution and its convergence. In our previous works, we speculated on the quasilinear nature of the travel-time inversion without quantifying it. Our results here show, for the first time, that the commonly used

---

*Part of this chapter is reprinted with permission from "A Comparison of Travel-Time and Amplitude Matching for Field-Scale Production Data Integration: Sensitivity, Non-Linearity and Practical Implications" by Cheng, H., Datta-Gupta, A., and He, Z., 2003. paper SPE 84570 presented at the 2003 SPE Annual Technical Conference and Exhibition , Denver, CO, October 5-8.

amplitude inversion can be orders of magnitude more nonlinear compared to the travel-time inversion. We also examine the resulting implications in field-scale history matching. The travel-time inversion is shown to be more robust and exhibits superior convergence characteristics. The travel-time sensitivities are more uniform between the wells compared to the amplitude sensitivities that tend to be localized near the wells. This prevents overcorrection near the wells.

We have demonstrated our results using a field application involving a multiwell, multitracer interwell tracer injection study in the McCleskey sandstone of the Ranger field, Texas. Starting with a prior geologic model, the traditional amplitude matching could not reproduce the field tracer response which was characterized by multiple peaks. Both travel time and generalized travel time exhibited better convergence properties and could match the tracer response at the wells with realistic changes to the geologic model.

2.1 Introduction

Geological models derived from static data alone often fail to reproduce the production history of a reservoir. Reconciling geologic models to the dynamic response of the reservoir is critical to building reliable reservoir models. In recent years several techniques have been developed for integrating production data into reservoir models.[5,10,12,13,15,18-27] The theoretical basis of these techniques is generally rooted in the least-squares inversion theory that attempts to minimize the difference between the observed production data and the model predictions. This can be referred to as "amplitude" matching. The production data can be water-cut observations, tracer response, or pressure history at the wells. It is well known that such inverse problems are typically ill-posed and can result in nonunique and unstable solutions. Proper incorporation of static data in the form of a prior model can partially alleviate the problem. However, there are additional outstanding challenges that have deterred the routine integration of production data into reservoir models. The relationship between the production response and reservoir properties can be highly nonlinear. The

nonlinearity can result in multiple local minima in the misfit function. This can cause the solution to converge to a local minimum, leading to an inadequate history match. All these can make it difficult to obtain a meaningful estimate of the parameter field, particularly if the initial model is far from the solution.

Recently, streamline-based methods have shown significant potential for incorporating dynamic data into high-resolution reservoir models.[5,10,12,13,15,18-27] A unique feature of the streamline-based production data integration has been the concept of a "travel-time match" that is analogous to seismic tomography. Instead of matching the production data directly, the observed data and model predictions are first "lined up" at the breakthrough time. This is typically followed by a conventional amplitude match, whereby the difference between the observed and calculated production response is minimized. A major part of the production data misfit reduction occurs during the travel-time inversion, and most of the large-scale features of heterogeneity are resolved at this stage.[13,21,22]

The concept of travel-time inversion is not limited to streamline models. Recently, it has been extended for application to finite-difference models through a "generalized travel-time" inversion.[24] The generalized travel-time inversion ensures matching of the entire production response rather than just the breakthrough times and at the same time retains most of the desirable properties of the travel-time inversion. The concept follows from wave-equation travel-time tomography and is very general, robust, and computationally efficient.[26,28] The generalized travel-time inversion has been utilized to extend the streamline-based production data integration methods to changing field conditions involving rate changes and infill drilling.

The advantages of the travel-time inversion compared to amplitude inversion mainly stems from its quasilinear properties. The advantages of travel-time inversion are well-documented in the context of seismic inversion.[28] However, no systematic study has been done to examine the benefits of travel-time inversion for production-data integration in terms of nonlinearity and convergence properties. Characterizing the degree of nonlinearity can be as important as finding the solutions to the inverse problem

itself. However, quantitative measures of nonlinearity for the inverse problems related to production data integration have not been adequately addressed.

In this chapter, we discuss the mathematical foundation for the measure of nonlinearity and its implications on the production-data integration. We quantitatively investigate the extent of nonlinearity in travel-time inversion and amplitude inversion. In particular, we show that the nonlinearity in travel-time inversion is orders of magnitude smaller than that of the amplitude inversion. This leads to better convergence properties and a robust method for production-data integration. We illustrate our results using both synthetic and field applications. The field application is from the McCleskey sandstone, the Ranger field, Texas, and involves a multiwell, multitracer interwell tracer injection study. The results clearly demonstrate the benefits of travel-time inversion for field-scale production-data integration. In particular, the generalized travel-time inversion appears to outperform both travel-time and amplitude inversion in reconciling the geologic model to the field-tracer response.

2.2 Background and Approach

2.2.1 Travel-Time Inversion, Amplitude Inversion, and Generalized Travel-Time Inversion

Travel-time inversion attempts to match the observed data and model predictions at some reference time, for example, the breakthrough time or the peak arrival time. Thus, we are lining up the production response along the time axis. **Fig. 2.1a** illustrates the travel-time inversion. On the other hand, the amplitude inversion attempts to match the production response directly. This is illustrated in Fig. 2.1b, wherein we match the observed tracer concentration and model predictions at the producing well. Creatively, we can combine the travel-time inversion and amplitude inversion into one step while retaining most of the desirable features of a travel-time inversion. This is the "generalized travel-time inversion" and follows from the work of Luo and Schuster[28] in the context of wave-equation travel-time tomography.

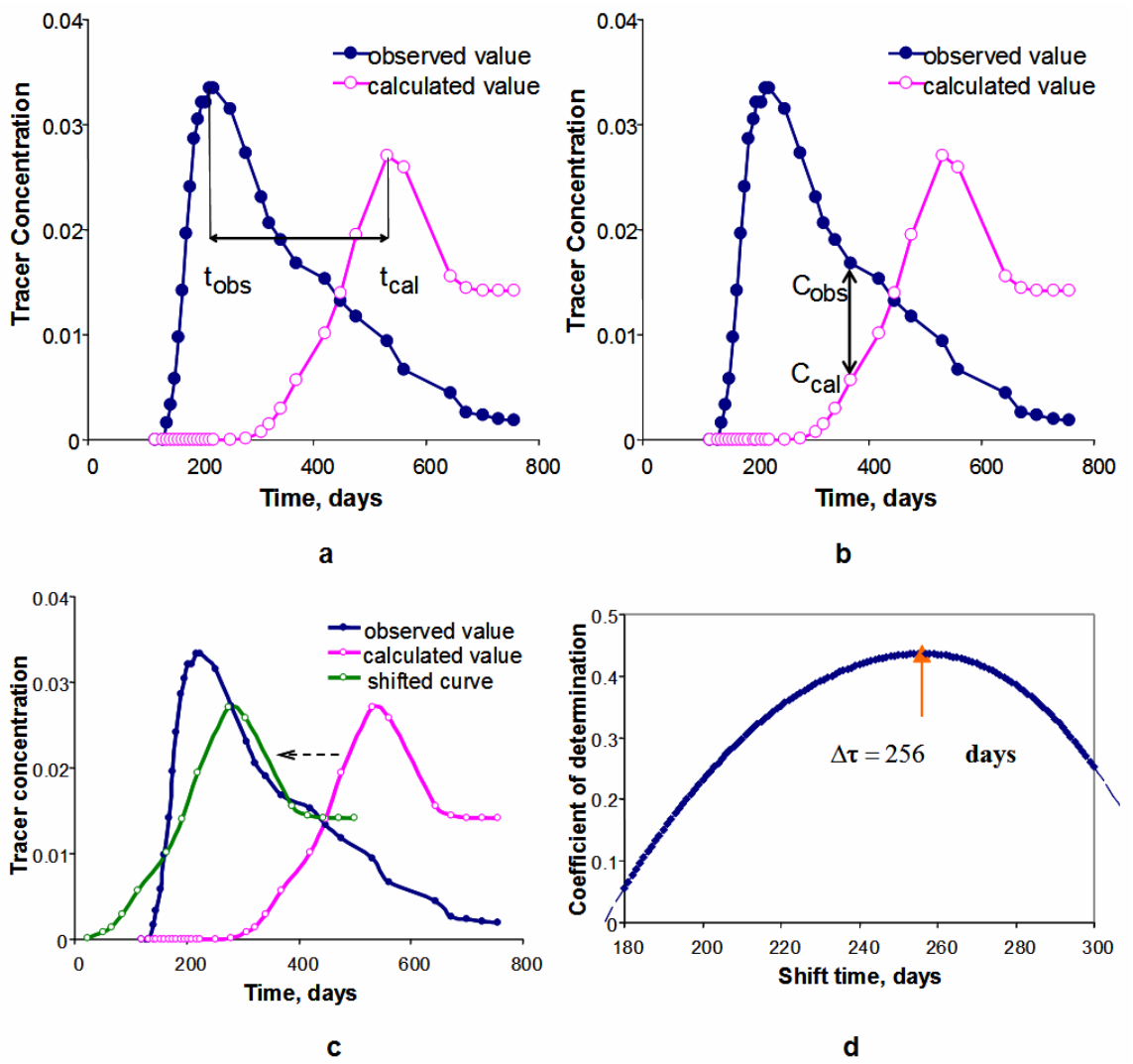

Figure 2.1 Illustration of (a) travel-time inversion, (b) amplitude inversion, (c) generalized travel-time inversion, and (d) best time shift.

A generalized travel-time or travel-time shift is computed by systematically shifting the computed production response toward the observed data until the cross-correlation between the two is maximized. The approach is illustrated in Figs. 2.1c and 2.1d. It preserves the robustness of a travel-time inversion and improves computational efficiency by representing the production data misfit at a well in terms of a single travel-

time shift. It can be shown to reduce to the more traditional least-squared misfit functional as we approach the solution.[26]

The advantages of travel-time inversion are well documented in the geophysics literature. For example, Luo and Schuster[28] pointed out that travel-time inversion is quasilinear as opposed to amplitude inversion, which can be highly nonlinear. Amplitude inversion typically works well when the prior model is close to the solution. This was the rationale behind our previously proposed two-step approach to production data integration: travel-time match followed by amplitude match.[13,21] In this chapter, we will quantitatively investigate the relative merits of the different methods in terms of nonlinearity and convergence properties.

2.2.2 Measures of Nonlinearity

Characterizing and assessing the nonlinearity in the parameter estimation problem is critical to designing efficient and robust approaches to production data integration. There are several methods for quantifying the degree of nonlinearity in inverse problems. In this paper, we will use the measure proposed by Bates and Watts[32] to examine the nonlinearities in travel-time and amplitude inversion. Grimstad and Mannseth[33,34] applied this measure to examine the relationship between nonlinearity, scale, and sensitivity in parameter-estimation problems. If F represents an outcome, for example, the tracer response, then the nonlinearity measure is defined as $\kappa=||F_{kk}||/||F_k||^2$, where F_k is the vector of the first-order derivatives with respect to the parameter vector k, that is, the sensitivity vector, and F_{kk} is the vector of second-order derivatives. This measure is based on the geometric concept of curvature and κ represents the inverse of a radius of the circle that best approximates the outcome locus F in the direction of F_k at k. Smoother and more linear outcome will have smaller curvature (larger radius) and thus a smaller measure of nonlinearity, as illustrated in **Fig. 2.2**.

In our application, we evaluate $\kappa=||F_{kk}||/||F_k||^2$ for every iteration during inversion. In addition, for amplitude inversion, we compute the measure for different observations and choose the maximum. The details of the computations, including the derivative

calculations for travel-time, amplitude, and generalized travel-time will be discussed later. In the following section, we first illustrate the approach using a synthetic example.

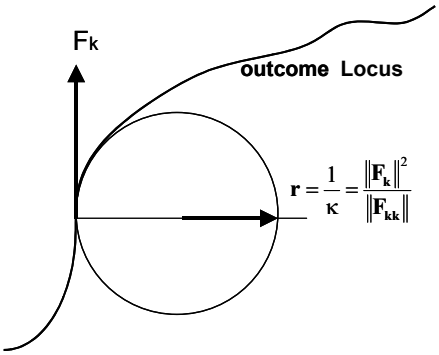

Figure 2.2 Geometric meaning of the measure of nonlinearity.

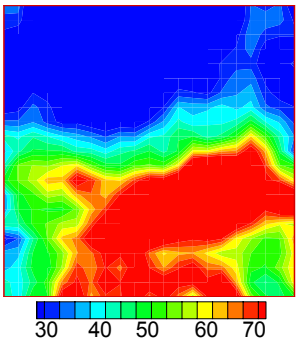

Figure 2.3 Synthetic permeability distribution for the 9-spot case.

2.2.3 Nonlinearity Measure in Production-Data Integration: A Simple Illustration

This example involves integration of tracer response in a heterogeneous nine-spot pattern, as shown in **Fig. 2.3**. The mesh size is 21×21. The reference permeability distribution consists of a low-permeability trend toward the north and a high-permeability trend toward the south. The tracer responses from the eight producers in the nine-spot pattern are shown in **Fig. 2.4a**. Also superimposed in Fig. 2.4a are the tracer

responses corresponding to our initial model, a homogeneous permeability field that is conditioned at the well locations.

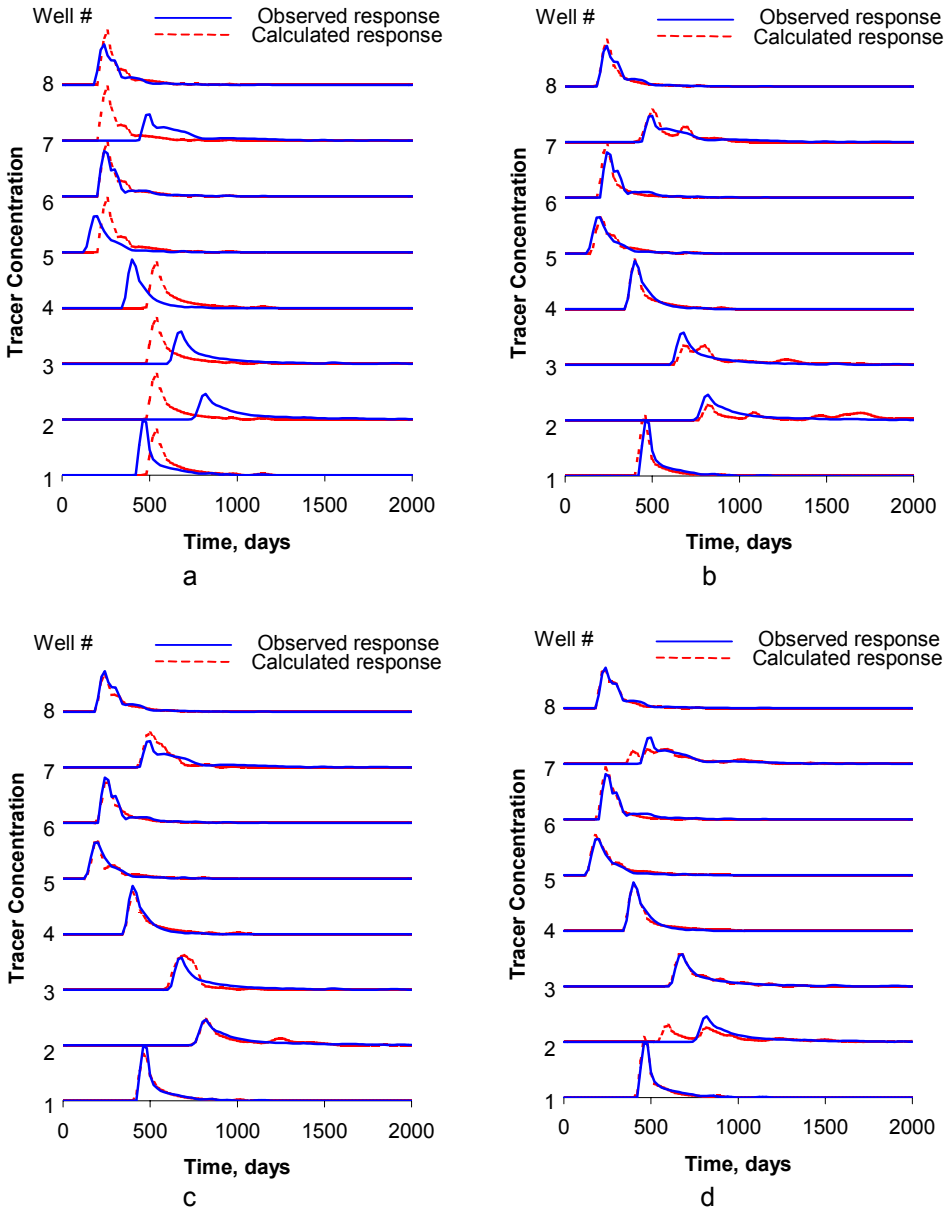

Figure 2.4 Tracer response (a) for uniform initial permeability, (b) after peak arrival-time inversion, (c) after generalized travel-time inversion, and (d) after direct amplitude inversion.

We compare the relative performance of travel-time, amplitude, and generalized travel-time inversion and also the nonlinearities inherent in these approaches. Fig. 2.4b shows the tracer concentration matches after travel-time inversion. All the peak times are now in agreement, although there are some discrepancies in the details of the tracer responses. Fig. 2.4c shows the tracer concentration matches after generalized travel-time inversion. Not only the peak arrival-times but also the amplitudes are matched much better compared to the travel-time inversion. Fig. 2.4d shows the tracer-responses match after the amplitude inversion. Although the matches are quite good for most wells, they are unsatisfactory for Wells 2 and 7. Incidentally, these are the two wells that exhibited maximum discrepancy based on the initial model.

Fig. 2.5 shows the convergence behavior for the three methods. Both travel-time and generalized travel-time inversion reproduce the arrival times perfectly. The generalized travel-time further reduces the tracer concentration misfit. In contrast, direct amplitude match shows high arrival-time misfit and is unable to reproduce the tracer response at two wells. **Fig. 2.6a** is the estimated permeability field after travel-time match. When comparing it to Fig. 2.3, we can identify the low-permeability areas and some of the moderate-to-high-permeability areas, although the high-permeability area is not well reproduced. Fig. 2.6b shows the permeability field derived by generalized travel-time inversion. It reproduces not only the low-permeability area but also the high-permeability regions. Fig. 2.6c shows the estimated permeability field after the amplitude inversion. Clearly, the results show signs of instability because of the high nonlinearity as discussed in the next section.

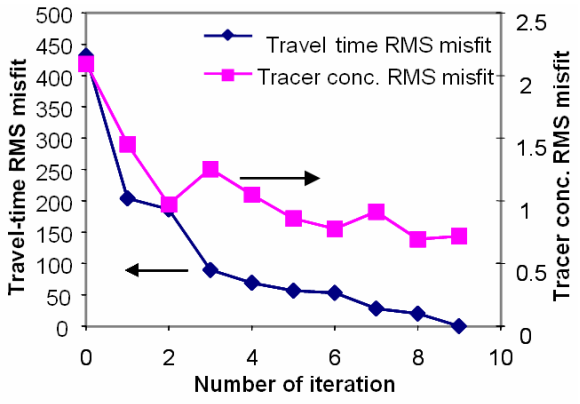

a

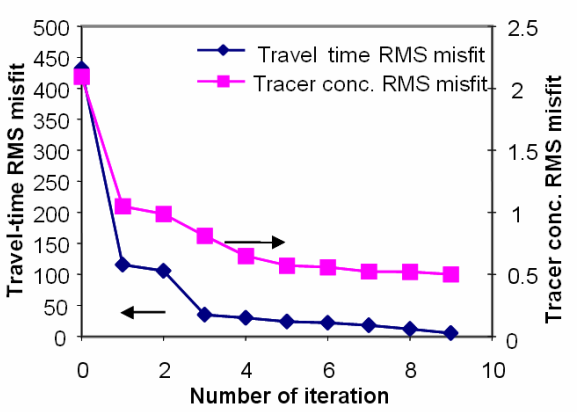

b

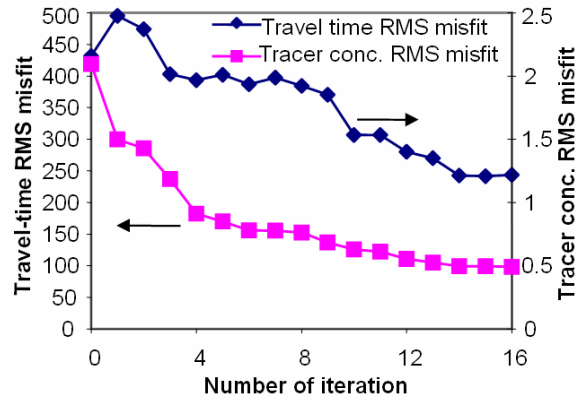

c

Figure 2.5 Travel-time and tracer concentration misfit for (a) travel-time, (b) generalized travel-time, and (c) amplitude inversion.

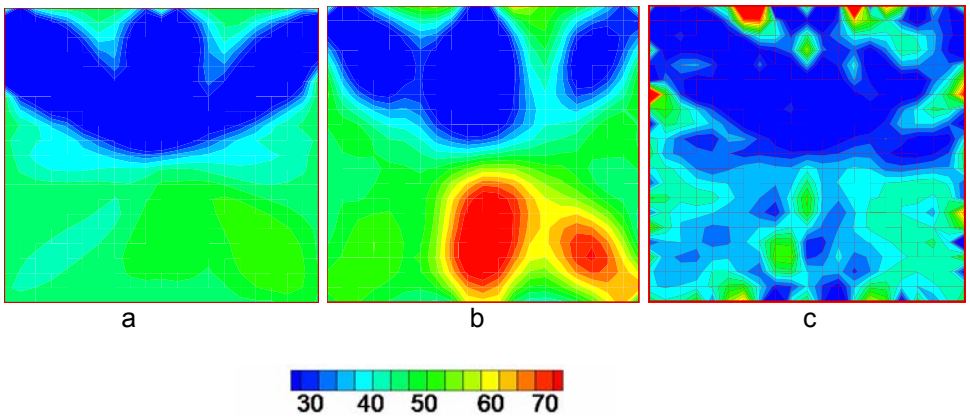

Figure 2.6 Estimated permeability distribution for the 9-spot case (a) after travel-time inversion, (b) after generalized travel-time inversion, and (c) after amplitude inversion.

Fig. 2.7 shows the measure of nonlinearity for the three approaches. We can see that both the travel-time and the generalized travel-time exhibit the same degrees of nonlinearity. In contrast, the amplitude inversion is three to four orders of magnitude more nonlinear than the travel-time inversion. This is partly the reason for the failure of the amplitude inversion when the initial model is far from the solution. The generalized travel-time inversion appears to retain most of the desirable features of a travel-time inversion while obtaining an adequate amplitude match.

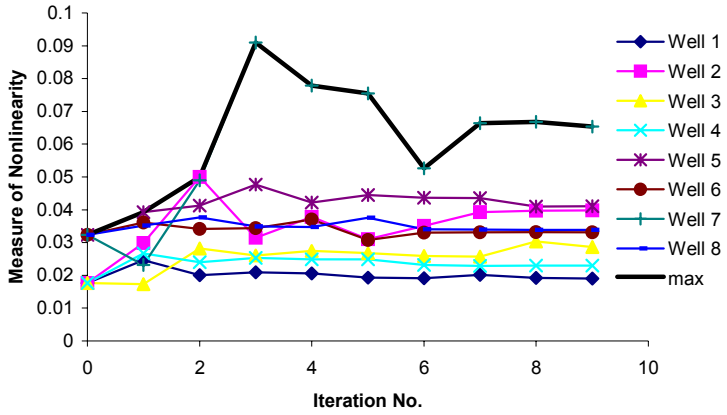

a

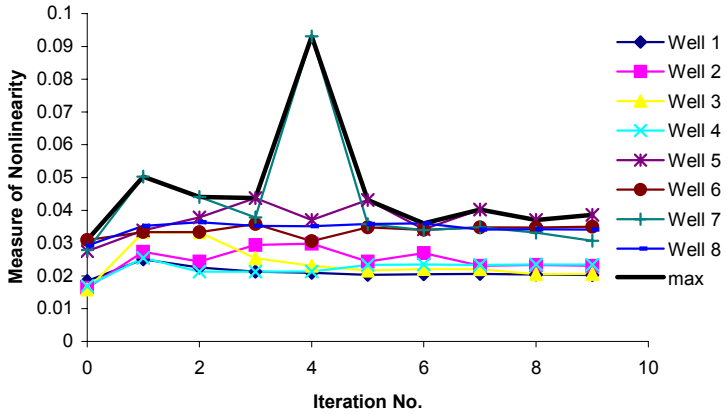

b

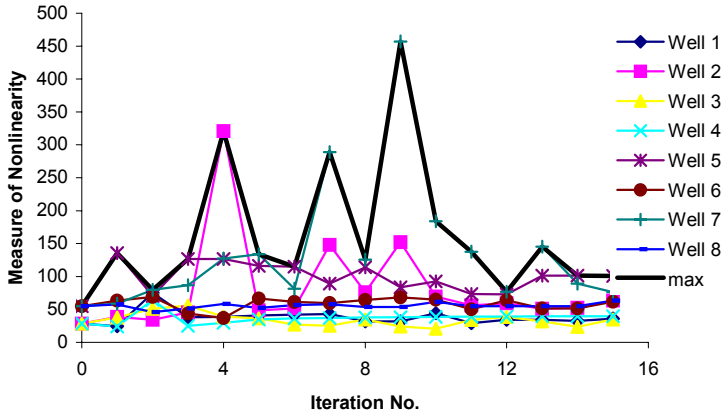

c

Figure 2.7 Measure of nonlinearity for (a) travel-time inversion, (b) generalized travel-time inversion, and (c) amplitude inversion.

2.3 Mathematical Formulation: Sensitivity Computations and Measures of Nonlinearity

We now discuss the mathematical details related to sensitivity computation and measure of nonlinearity for travel-time, generalized travel-time, and amplitude inversion. Although the approach is generally applicable, we will use a streamline simulator here because of the advantages in sensitivity computations. The sensitivities quantify change in production response because of a small change in reservoir properties. They are an integral part of most inverse modeling methods. We also need the sensitivities to quantify nonlinearities in the various inverse methods examined in this study. Several approaches can be used to compute sensitivity coefficients of model parameters. Most of these methods fall into one of the three categories: perturbation method, direct method, and adjoint state method[7,30,35] and can be computationally demanding, particularly for large-scale field applications. However, for streamline models, it is possible to analytically derive a relationship between perturbations in reservoir properties, such as permeability or porosity, and changes in observations such as water-cut and tracer response. Streamline-based sensitivity computation is very fast and involves quantities computed by a single streamline simulation. Hence, we will limit our discussion to streamline models only.

We use the theory of Bates and Watts[32] to measure the nonlinearity in production-data integration. Bates and Watts[32] separate the nonlinearity measures into parameter-effect curvature and intrinsic curvature; thus, they decompose the second-order derivative F_{kk} into one component parallel to the tangent plane defined by F_k for all directions and another component normal to that plane. Here, we do not separate the intrinsic curvature and parameter effect curvature; neither do we consider the direction in the parameter space, because it is not practical to do so for our problem. However, the theory we applied is essentially the same as that of Bates and Watts.[32]

2.3.1 Sensitivity and Nonlinearity of Travel-Time

Streamline methods decouple flow and transport by a coordinate transformation from the physical space to the time-of-flight along streamlines[36]. The time-of-flight is defined as

$$\tau = \int_{\psi} s(x)dr, \tag{2.1}$$

where the integral is along the streamline trajectory, Ψ, and s is the slowness defined as the reciprocal of the interstitial velocity,

$$s = \frac{1}{|v|} = \frac{\phi}{k\lambda_{rt}|\nabla P|}. \tag{2.2}$$

The first-order derivative of slowness with respect to permeability is

$$\frac{\partial s}{\partial k} = -\frac{s}{k} \tag{2.3}$$

and the second-order derivative of slowness is

$$\frac{\partial^2 s}{\partial k^2} = \frac{s}{k^2}. \tag{2.4}$$

If we assume that the streamlines do not shift because of small perturbations in reservoir properties, we can then relate the change in travel time $\delta\tau$ to the change in slowness by

$$\begin{aligned} \delta\tau &= \int_{\Psi} \delta s(x)dr \\ &= \int_{\Psi}\left[-\frac{s(x)}{k(x)}\delta k(x) + \frac{s(x)}{\phi(x)}\delta\phi(x)\right]dr \end{aligned}. \tag{2.5}$$

The travel-time sensitivity along a single streamline at a producer with respect to permeability for a gridblock at location *x* is given by integrating Eq. 2.3 from the inlet to the outlet of the streamline Ψ within the gridblock:

$$\frac{\partial\tau(\psi)}{\partial k(x)} = \int_{inlet}^{outlet}\left[-\frac{s(x)}{k(x)}\right]dr(\psi). \tag{2.6}$$

The overall travel-time sensitivity is then obtained by summing the sensitivities over all streamlines contributing to the arrival time of a particular concentration (for example, the peak concentration):

$$\frac{\partial \tau}{\partial k(x)} = \sum_{all\ \psi} \frac{\partial \tau(\psi)}{\partial k(x)} \quad . \tag{2.7}$$

The second-order derivative of travel time along a single streamline is obtained by integrating Eq. 2.4,

$$\frac{\partial^2 \tau(\psi)}{\partial k^2(x)} = \int_{inlet}^{outlet} \frac{s(x)}{k^2(x)} dr(\psi) \quad , \tag{2.8}$$

and then integrating over all streamlines contributing to a producer,

$$\frac{\partial^2 \tau}{\partial k^2(x)} = \sum_{\Psi} \frac{\partial^2 \tau(\psi)}{\partial k^2(x)} \quad . \tag{2.9}$$

The components of the tangent vector F_k and acceleration vector F_{kk} can now be obtained from Eqs. 2.7 and 2.9:

$$\boldsymbol{F}_k = \left(\frac{\partial \tau}{\partial k_1}, \frac{\partial \tau}{\partial k_2}, \cdots, \frac{\partial \tau}{\partial k_{n_b}} \right)^T ; \tag{2.10}$$

$$\boldsymbol{F}_{kk} = \left(\frac{\partial^2 \tau}{\partial k_1^2}, \frac{\partial^2 \tau}{\partial k_2^2}, \cdots, \frac{\partial^2 \tau}{\partial k_{n_b}^2} \right)^T \quad . \tag{2.11}$$

The 2-norms are used to calculate the vector norms,

$$\left\| \boldsymbol{F}_k \right\| = \left(\sum_{j=1}^{n_b} \left(\frac{\partial \tau}{\partial k_j} \right)^2 \right)^{1/2} \quad , \tag{2.12}$$

$$\left\| \boldsymbol{F}_{kk} \right\| = \left(\sum_{j=1}^{n_b} \left(\frac{\partial^2 \tau}{\partial k_j^2} \right)^2 \right)^{1/2} \quad . \tag{2.13}$$

Now we can calculate the nonlinearity measure of travel-time inversion κ_{tt} according to the theory of Bates and Watts[32] by

$$\kappa_{tt} = \left\| \boldsymbol{F}_{kk} \right\| / \left\| \boldsymbol{F}_k \right\|^2 \quad . \tag{2.14}$$

2.3.2 Sensitivity and Nonlinearity of Amplitude

Tracer transport can be described by the following convection-diffusion equation,

$$\phi\frac{\partial C(x,t)}{\partial t}=\nabla\cdot\left[D(x)\cdot\nabla C(x,t)\right]-u\cdot\nabla C(x,t) \quad (2.15)$$

Ignoring the dispersion term, Eq. 2.15 can be rewritten as

$$\phi\frac{\partial C(x,t)}{\partial t}+u\cdot\nabla C(x,t)=0 \quad (2.16)$$

Applying a transformation to the time-of-flight coordinate, the tracer transport equation along a streamline can be expressed as[36]

$$\frac{\partial C(\tau,t)}{\partial t}+\frac{\partial C(\tau,t)}{\partial \tau}=0 \quad (2.17)$$

For a unit-impulse concentration at (τ, t) = (0,0), the solution is[36]

$$C(x,t)=\delta\left(t-\tau(x)\right), \quad (2.18)$$

where δ is the Dirac-delta function. If the input is C_0, then

$$C(x,t)=C_0(t-\tau) \quad (2.19)$$

Summing the contributions of all streamlines reaching a producer, we get the tracer response at a producer as

$$C(t)=\int_{all\ \psi} C_0(t-\tau)d\psi \quad (2.20)$$

From Eq. 2.19, tracer response at the producer along a single streamline is

$$C(t)=C_0\left(t-\int_{\Psi} s(x)dr\right), \quad (2.21)$$

where we have used the definition of time of flight from Eq. 2.1.

Now, consider a small perturbation in reservoir properties, say permeability. The resulting changes in slowness and concentrations can be written as

$$s(x)=s^0(x)+\delta s(x); \quad (2.22)$$

$$C(t)=C^0(t)+\delta C(t), \quad (2.23)$$

where s^0 and C^0 are initial slowness distribution in the reservoir and the associated tracer response, respectively. Applying Eqs. 2.21 and 2.22, the change in concentration response can be expressed as

$$\begin{aligned}\delta C(t) &= C(t) - C^0(t) \\ &= C_0\left(t - \int_{\Psi}\left[s^0(x) + \delta s(x)\right]dr\right) - C_0\left(t - \int_{\Psi_0} s^0(x)dr\right)\end{aligned} \quad . \tag{2.24}$$

Using a Taylor series expansion and assuming $\Psi = \Psi_0$ (stationary streamlines), we get

$$\begin{aligned}&C_0\left(t - \int_{\Psi}\left[s^0(x) + \delta s(x)\right]dr\right) = C_0\left(t - \int_{\Psi_0} s^0(x)dr - \int_{\Psi_0}\delta s(x)dr\right) \\ &\approx C_0\left(t - \int_{\Psi_0} s^0(x)dr\right) + \left[\left(t - \int_{\Psi_0} s^0(x)dr - \int_{\Psi_0}\delta s(x)dr\right)\right. \\ &\left. - \left(t - \int_{\Psi_0} s^0(x)dr\right)\right] C_0'\left(t - \int_{\Psi_0} s^0(x)dr\right) \\ &= C_0\left(t - \int_{\Psi_0} s^0(x)dr\right) - \int_{\Psi_0}\delta s(x)dr \cdot C_0'\left(t - \int_{\Psi_0} s^0(x)dr\right)\end{aligned} \quad . \tag{2.25}$$

Hence the perturbation in $C(t)$ and $s(x)$ are related by

$$\delta C(t) = -C_0'\left(t - \int_{\Psi_0} s^0(x)dr\right)\int_{\Psi_0}\delta s(x)dr \quad . \tag{2.26}$$

The tracer-concentration sensitivity along a single streamline Ψ is then

$$\begin{aligned}\frac{\partial C(t)}{\partial k(x)} &= -C_0'\left(t - \int_{\Psi} s^0(x)dr\right)\int_{\Psi}\frac{\partial s(x)}{\partial k(x)}dr \\ &= -C_0'\left(t - \int_{\Psi} s^0(x)dr\right)\int_{\Psi}\left[-\frac{s(x)}{k(x)}\right]dr \\ &= -C_0'\left(t - \int_{\Psi} s^0(x)dr\right)\frac{\partial \tau(\Psi)}{\partial k(x)}\end{aligned} \quad . \tag{2.27}$$

The second-order derivative of the tracer concentration with respect to permeability is

$$\begin{aligned}\frac{\partial^2 C(t)}{\partial k^2(x)} &= -C_0'\left(t-\int_\Psi s^0(x)dr\right)\int_\Psi \frac{\partial^2 s(x)}{\partial k^2(x)}dr \\ &= -C_0'\left(t-\int_\Psi s^0(x)dr\right)\int_\Psi \frac{s(x)}{k^2(x)}dr \\ &= -C_0'\left(t-\int_\Psi s^0(x)dr\right)\frac{\partial^2 \tau(\Psi)}{\partial k^2(x)}\end{aligned} . \tag{2.28}$$

As before, we need to sum over all streamlines reaching a producer to get the final first-order and second-order derivatives of the concentration response at the producer.

Now, we need to evaluate the tangent vector $\boldsymbol{F}_k$, the acceleration vector $\boldsymbol{F}_{kk}$, and measure of nonlinearity κ at different observation times. The vectors and norms are expressed as follows:

$$\boldsymbol{F}_k(t_i) = \left(\frac{\partial C(t_i)}{\partial k_1}, \frac{\partial C(t_i)}{\partial k_2}, \cdots, \frac{\partial C(t_i)}{\partial k_{n_b}}\right)^T , \tag{2.29}$$

$$\boldsymbol{F}_{kk}(t_i) = \left(\frac{\partial^2 C(t_i)}{\partial k_1^2}, \frac{\partial^2 C(t_i)}{\partial k_2^2}, \cdots, \frac{\partial^2 C(t_i)}{\partial k_{n_b}^2}\right)^T ; \tag{2.30}$$

$$\left\|\boldsymbol{F}_k(t_i)\right\| = \left(\sum_{j=1}^{n_b}\left(\frac{\partial C(t_i)}{\partial k_j}\right)^2\right)^{1/2} , \tag{2.31}$$

$$\left\|\boldsymbol{F}_{kk}(t_i)\right\| = \left(\sum_{j=1}^{n_b}\left(\frac{\partial^2 C(t_i)}{\partial k_j^2}\right)^2\right)^{1/2} . \tag{2.32}$$

By definition, the measure of nonlinearity at observation time t_i is

$$\kappa(t_i) = \left\|\boldsymbol{F}_{kk}(t_i)\right\| \Big/ \left\|\boldsymbol{F}_k(t_i)\right\|^2 \tag{2.33}$$

The final measure of nonlinearity for amplitude inversion κ_{am} is given by the maximum over all observed data,

$$\kappa_{am} = \max\left[\kappa(t_1), \kappa(t_2), \cdots, \kappa(t_{n_o})\right] . \tag{2.34}$$

2.3.3 Sensitivity and Nonlinearity of Generalized Travel Time

In generalized travel-time inversion, we define the misfit between the calculated and observed tracer concentrations in terms of the following correlation function[26,28]:

$$f(x,\tau) = \int dt \frac{C(x,t+\tau)_o}{A_o} C(x,t)_c \quad , \tag{2.35}$$

where A is the maximum amplitude of tracer concentration and τ is the shift time between calculated and observed tracer concentrations. We seek a τ that shifts the calculated tracer response so that it best matches the observed tracer response.

The criterion for the "best" match is defined as the travel-time residual $\Delta\tau$ that maximizes the correlation function above, that is,

$$f(x,\Delta\tau) = \max\{f(x,\tau) \mid \tau \in [-T,T]\} \quad , \tag{2.36}$$

where T is the estimated maximum travel-time difference between the observed and calculated tracer responses. Therefore, the derivative of $f(x,\tau)$ with respect to τ should be zero at $\Delta\tau$ unless the maximum is at an endpoint T or $-T$,

$$\begin{aligned} \dot{f}_{\Delta\tau} &= [\frac{\partial f(x,\tau)}{\partial \tau}]_{\tau=\Delta\tau} \\ &= \frac{1}{A}\int dt \frac{\partial C(t+\Delta\tau)_o}{\partial t} C(t)_c \frac{\partial t}{\partial \tau} \\ &= \frac{1}{A}\int dt \frac{\partial C(t+\Delta\tau)_o}{\partial t} C(t)_c = 0 \end{aligned} \quad . \tag{2.37}$$

Note that $\partial t / \partial \tau = 1$ in this derivation. Eq. 2.37 is the function that is used to compute the sensitivity of the generalized travel time.

Using Eq. 2.37 and the rule for the derivative of an implicit function, we get

$$\frac{\partial \Delta\tau}{\partial k(x)} = -\frac{\frac{\partial(\dot{f}_{\Delta\tau})}{\partial k(x)}}{\frac{\partial(\dot{f}_{\Delta\tau})}{\partial \Delta\tau}} \quad . \tag{2.38}$$

Taking the derivatives of $\dot{f}_{\Delta\tau}$ with respect to $k(x)$ and $\Delta\tau$, we have

$$\frac{\partial(\dot{f}_{\Delta\tau})}{\partial k(x)} = \frac{1}{A}\int dt \frac{\partial C(t+\Delta\tau)_o}{\partial t}\frac{\partial C(t)_c}{\partial k(x)}$$
$$= \frac{1}{A}\int dt \frac{\partial C(t+\Delta\tau)_o}{\partial t}\frac{\partial C(t)_c}{\partial t}\frac{\partial t}{\partial \tau}\frac{\partial \tau}{\partial k(x)}$$
$$= \frac{1}{A}\int dt \frac{\partial C(t+\Delta\tau)_o}{\partial t}\frac{\partial C(t)_c}{\partial t}\frac{\partial \tau}{\partial k(x)} \quad . \tag{2.39}$$

and

$$\frac{\partial \dot{f}_{\Delta\tau}}{\partial \Delta\tau} = \frac{\int dt \cdot E}{A} \quad , \tag{2.40}$$

where

$$E = \frac{\partial C(t+\Delta\tau)_o}{\partial t}\frac{\partial C(t)_c}{\partial \Delta\tau} + C(t)_c \frac{\partial[\frac{\partial C(t+\Delta\tau)_o}{\partial t}]}{\partial \Delta\tau}$$
$$= \frac{\partial C(t+\Delta\tau)_o}{\partial t}\frac{\partial C(t)_c}{\partial t}\frac{\partial t}{\partial \Delta\tau} + C(t)_c \frac{\partial^2 C(t+\Delta\tau)_o}{\partial t^2}\frac{\partial t}{\partial \Delta\tau}$$
$$= \frac{\partial C(t+\Delta\tau)_o}{\partial t}\frac{\partial C(t)_c}{\partial t} + C(t)_c \frac{\partial^2 C(t+\Delta\tau)_o}{\partial t^2} \quad . \tag{2.41}$$

In the previous derivation, we have applied the relationship $\frac{\partial t}{\partial \Delta\tau} = \frac{\partial t}{\partial \tau} = 1$ at $\tau = \Delta\tau$.

Substitution of Eqs. 2.39 through 2.41 into Eq. 2.38 gives

$$\frac{\partial \Delta\tau}{\partial k(x)}$$
$$= \frac{\int dt[\frac{\partial C(t+\Delta\tau)_o}{\partial t}\frac{\partial C(t)_c}{\partial t}\frac{\partial \tau}{\partial k(x)}]}{\int dt[\frac{\partial C(t+\Delta\tau)_o}{\partial t}\frac{\partial C(t)_c}{\partial t} + C(t)_c \frac{\partial^2 C(t+\Delta\tau)_o}{\partial t^2}]} \quad . \tag{2.42}$$

The second-order derivative of generalized travel-time with respect to permeability is then

$$\frac{\partial^2 \Delta\tau}{\partial k^2(x)}$$
$$= \frac{\int dt[\frac{\partial C(t+\Delta\tau)_o}{\partial t}\frac{\partial C(t)_c}{\partial t}\frac{\partial^2 \tau}{\partial k^2(x)}]}{\int dt[\frac{\partial C(t+\Delta\tau)_o}{\partial t}\frac{\partial C(t)_c}{\partial t} + C(t)_c \frac{\partial^2 C(t+\Delta\tau)_o}{\partial t^2}]} \quad , \tag{2.43}$$

where $\frac{\partial^2 \tau}{\partial k^2}$ is calculated by Eq. 2.8.

Finally, to calculate measures of nonlinearity, the components of the tangent vector F_k and acceleration vector F_{kk} are obtained from Eqs. 2.42 and 2.43 as follows:

$$F_k = \left(\frac{\partial \Delta\tau}{\partial k_1}, \frac{\partial \Delta\tau}{\partial k_2}, \cdots, \frac{\partial \Delta\tau}{\partial k_{n_b}} \right)^T ; \tag{2.44}$$

$$F_{kk} = \left(\frac{\partial^2 \Delta\tau}{\partial k_1^2}, \frac{\partial^2 \Delta\tau}{\partial k_2^2}, \cdots, \frac{\partial^2 \Delta\tau}{\partial k_{n_b}^2} \right)^T . \tag{2.45}$$

The 2-norms of the vectors are calculated by

$$\|\boldsymbol{F}_k\| = \left(\sum_{j=1}^{n_b} \left(\frac{\partial \Delta\tau}{\partial k_j} \right)^2 \right)^{1/2} ; \tag{2.46}$$

$$\|\boldsymbol{F}_{kk}\| = \left(\sum_{j=1}^{n_b} \left(\frac{\partial^2 \Delta\tau}{\partial k_j^2} \right)^2 \right)^{1/2} . \tag{2.47}$$

The measure of nonlinearity for the generalized travel-time inversion is evaluated using Eqs. 2.46 and 2.47:

$$\kappa_{gt} = \|\boldsymbol{F}_{kk}\| \big/ \|\boldsymbol{F}_k\|^2 . \tag{2.48}$$

2.3.4 Sensitivity Computations: A ¼ Five-Spot Example

We illustrate sensitivity computations for the three methods using the tracer response in a heterogeneous quarter five-spot pattern **(Fig. 2.8). Fig. 2.9a** is the sensitivity distribution for the peak travel-time, and Fig. 2.9b is the sensitivity distribution for the generalized travel-time. **Figs. 2.10a** through 10c show the sensitivity distribution for the amplitude before, at, and after peak time, respectively. From Figs. 2.9 and 2.10, we can see that the sensitivity distribution between the wells for travel-time inversion is more uniform than that for amplitude inversion. Also, the magnitude of the amplitude sensitivity is much smaller than that of the travel-time sensitivity. This smaller sensitivity contributes to the high nonlinearity of amplitude inversion, because the

nonlinearity is evaluated by $||\boldsymbol{F}_{kk}||/||\boldsymbol{F}_k||^2$, where $\boldsymbol{F}_k$ is the sensitivity vector. Such relationship between nonlinearity and sensitivity for inverse modeling has also been observed by Grimstad and Mannseth.[33,34]

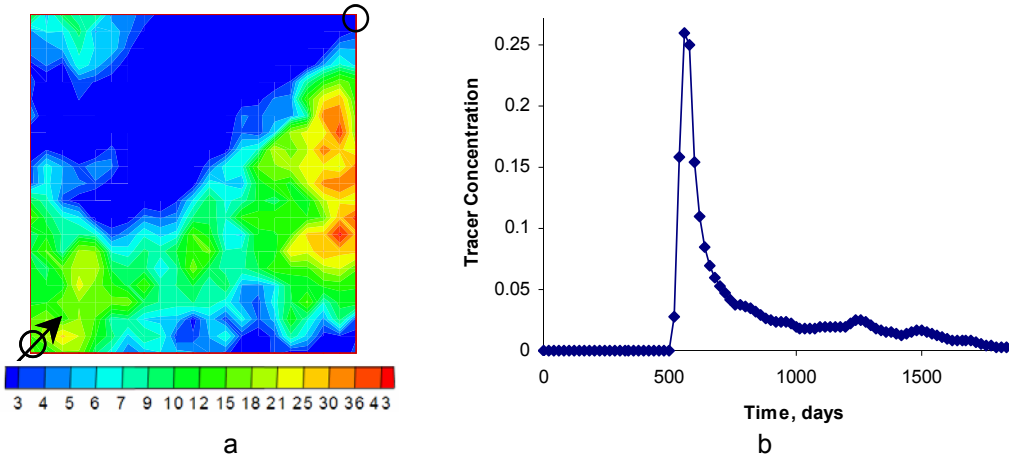

Figure 2.8 Tracer response for a ¼ five-spot heterogeneous case.

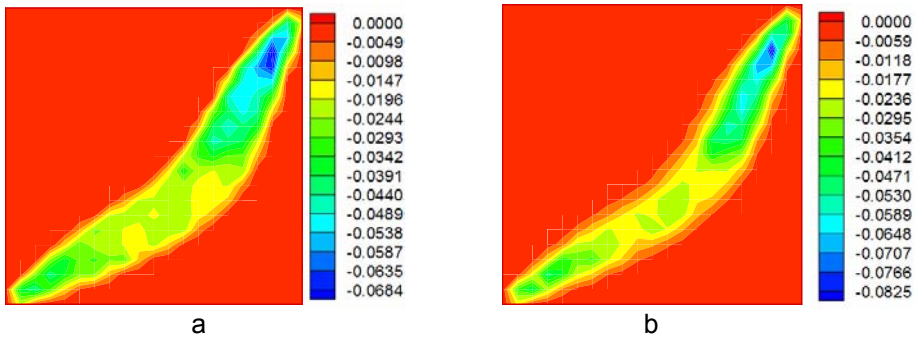

Figure 2.9 Sensitivity for (a) travel-time and (b) generalized travel-time inversion.

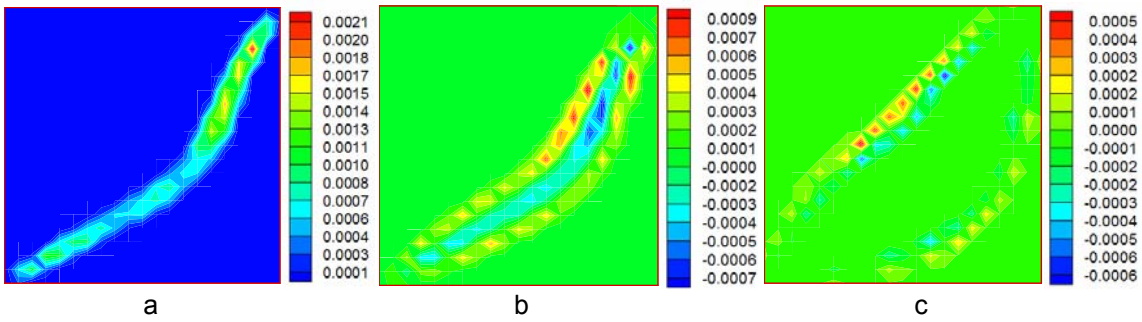

Figure 2.10 Sensitivity distribution for amplitude inversion (a) before peak time, (b) at peak time, and (c) after peak time.

2.4 Data Inversion

Our goal is to reconcile high-resolution geologic models to field-production history, for example tracer response. This typically involves the solution of an underdetermined inverse problem. The mathematical formulation behind such streamline-based inverse problems has been discussed elsewhere.[13,21,22] Briefly, in our approach we start with a prior static model that already incorporates geologic, well-log, and seismic data. We then minimize a penalized misfit function consisting of the following three terms:

$$\|\delta \boldsymbol{d} - \boldsymbol{S}\delta \boldsymbol{R}\| + \beta_1 \|\delta \boldsymbol{R}\| + \beta_2 \|\boldsymbol{L}\delta \boldsymbol{R}\| . \qquad (2.49)$$

In Eq. 2.49, $\delta \boldsymbol{d}$ is the vector of data residuals at the wells, while $\boldsymbol{S}$ is the sensitivity matrix containing the sensitivities of the observed data with respect to the reservoir parameters. Also, $\delta \boldsymbol{R}$ corresponds to the change in the reservoir property, and $\boldsymbol{L}$ is a second-spatial-difference operator. The first term ensures that the difference between the observed and calculated production response is minimized. The second term, called a norm constraint, penalizes deviations from the initial model. This helps preserve geologic realism because our initial or prior model already incorporates available geologic and static information related to the reservoir. Finally, the third term, a roughness penalty, simply recognizes the fact that production data are an integrated

response and are thus best suited to resolve large-scale structures rather than small-scale property variations.

The minimum in Eq. 2.49 can be obtained by an iterative least-squares solution to the augmented linear system

$$\begin{pmatrix} \boldsymbol{S} \\ \beta_1 \boldsymbol{I} \\ \beta_2 \boldsymbol{L} \end{pmatrix} \delta \boldsymbol{R} = \begin{pmatrix} \delta \boldsymbol{d} \\ \boldsymbol{0} \\ \boldsymbol{0} \end{pmatrix}. \tag{2.50}$$

The weights β_1 and β_2 determine the relative strengths of the prior model and the roughness term. The selection of these weights can be somewhat subjective, although there are guidelines in the literature.[37] In general, the inversion results will be sensitive to the choice of these weights.

In Eq. 2.50, $\delta \boldsymbol{d}$ is replaced by $\delta \boldsymbol{\tau}$ for travel-time inversion, $\delta \boldsymbol{C}$ for amplitude inversion, and $\delta \Delta \boldsymbol{\tau}$ for generalized travel-time inversion. The sensitivity matrix S is also replaced by the corresponding expression.

Note that one of the major advantages of travel-time and the generalized travel-time approach is that the size of the sensitivity matrix S is dependent only on the number of wells regardless of the number of data points. This leads to considerable savings in computation time. We use an iterative sparse matrix solver, LSQR, for solving this augmented linear system efficiently.[38] The LSQR algorithm is well suited for highly ill-conditioned systems and has been widely used for large-scale tomographic problems in seismology.

2.5 Applications

2.5.1 A Two-Phase Example With Infill Drilling

So far, we have focused on single-phase tracer flow. We now consider a two-phase waterflood example with changing streamlines.[26] The flood pattern is a nine-spot. We start with one central injector and four side producers. Four corner-producers are

introduced at 300 days. Pressure and streamlines are updated every 100 days. **Fig. 2.11a** shows the reference permeability and the well pattern. The reference permeability is the same as the one used for the tracer example. The water-cut responses from the eight producers are shown in **Fig. 2.12a**. Also superimposed in Fig. 2.12a are the water-cut responses from the initial model, a homogeneous permeability field conditioned at the well locations.

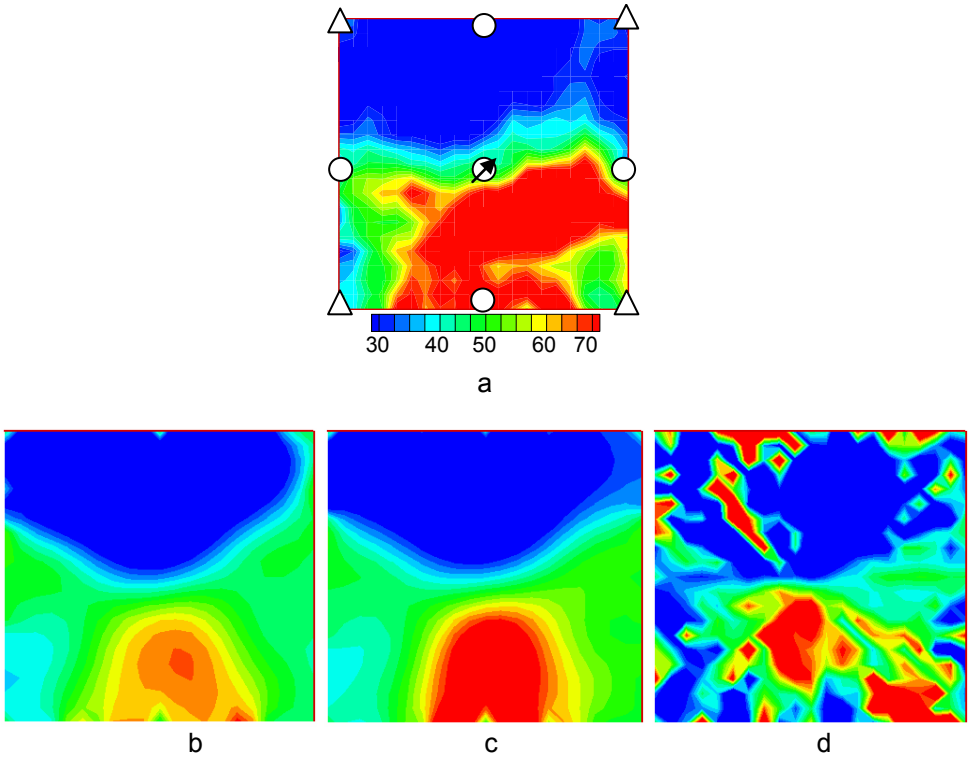

Figure 2.11 A two-phase example with infill drilling: (a) reference permeability model, triangle for infill wells in the mid-term of production, (b) estimated permeability by travel-time inversion, (c) estimated permeability by generalized travel-time inversion, and (d) estimated permeability by amplitude inversion.

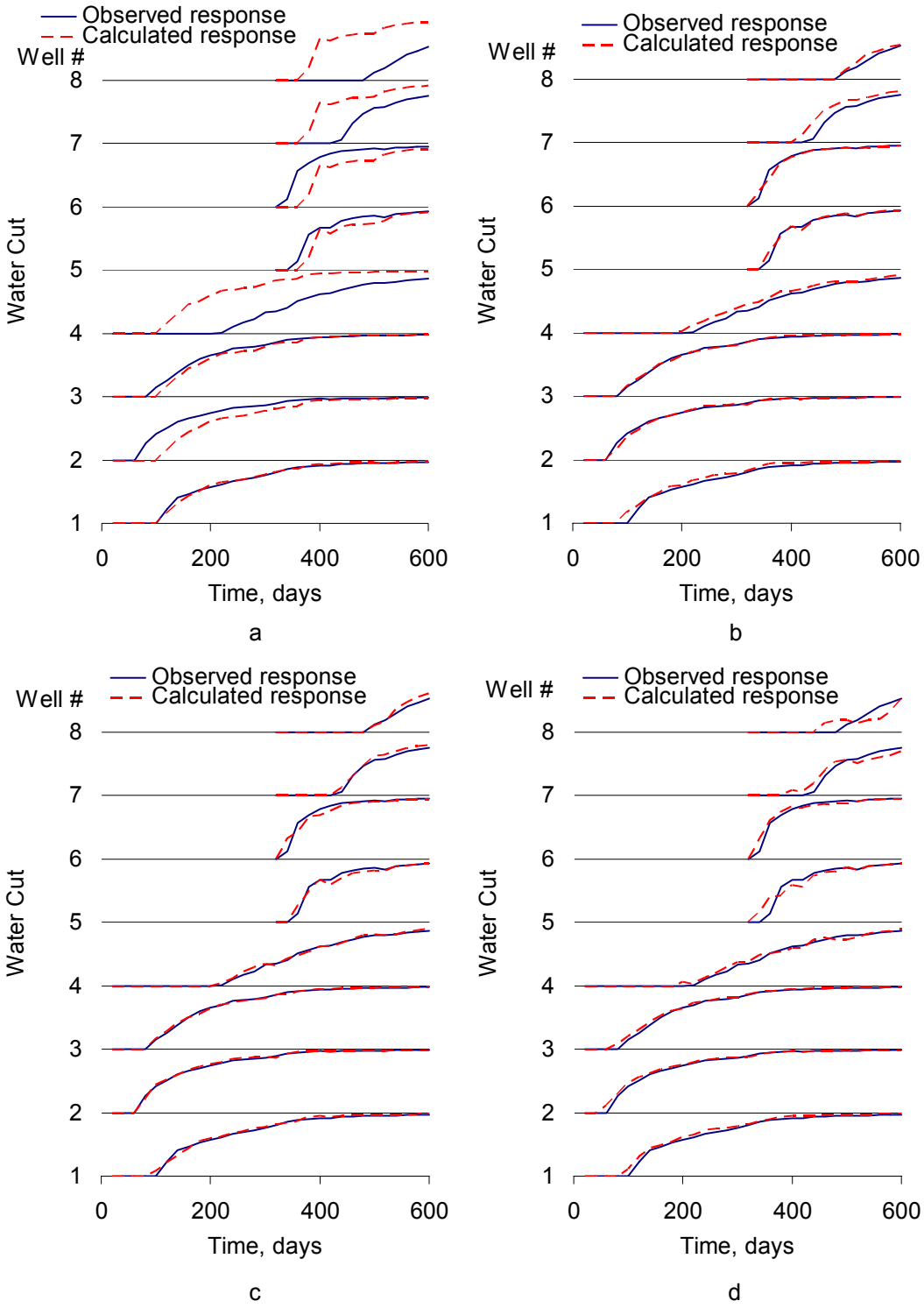

Figure 2.12 Water-cut response (a) for uniform initial permeability, (b) after peak arrival-time inversion, (c) after generalized travel-time inversion, and (d) after direct amplitude inversion.

Figs. 2.12b through 2.12d show the water-cut match by travel-time inversion, generalized travel-time inversion, and amplitude inversion, respectively. Clearly, the match by generalized travel-time inversion is the best, followed by travel-time inversion. Amplitude match did not work for Well 8.

Fig. 2.11b is the estimated permeability field after travel-time match. On comparing with Fig. 2.11a, we can see that the low-permeability areas are reproduced well; however, the high-permeability contrast to the south is not detected properly. Fig. 2.11c shows the permeability field derived by generalized travel-time inversion. It reproduces not only the low-permeability areas but also the high-permeability regions. Fig. 2.11d shows the estimated permeability field after the amplitude inversion. Clearly, the results show signs of instability, as discussed before.

Fig. 2.13 shows the measure of nonlinearity for the three approaches. We can see that both the travel-time and the generalized travel-time have a similar magnitude of nonlinearity. In contrast, the amplitude inversion is three to four orders of magnitude more nonlinear than the travel-time inversion. This is partly the reason for the failure of the amplitude inversion. Our experience with amplitude inversion indicates that the results tend to be more sensitive to the choice of inversion parameters (β_1, β_2 in Eq. 2.49). For homogeneous or smooth starting models, we can obtain a reasonable solution by careful choice of inversion parameters. But for models with significant heterogeneity, especially for field applications, direct amplitude inversion often fails.

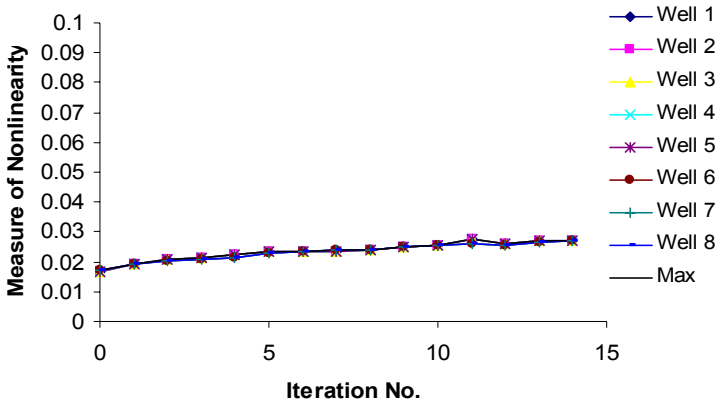

a

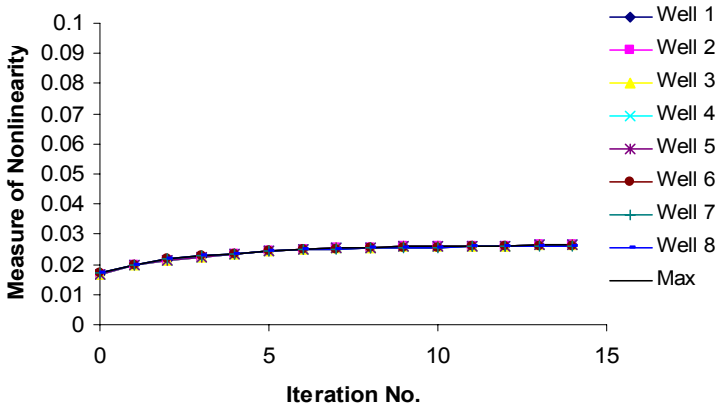

b

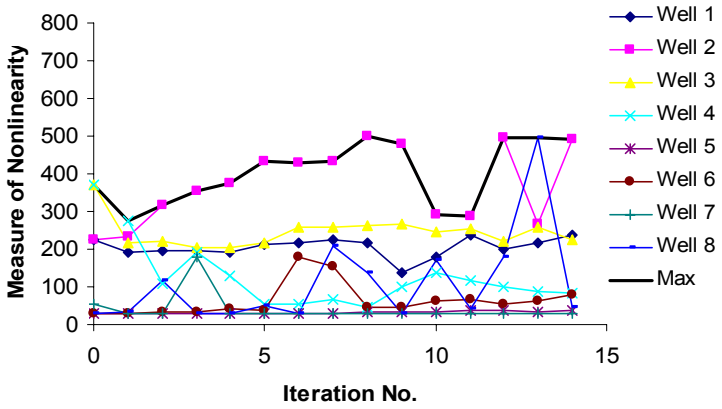

c

Figure 2.13 Measure of nonlinearity for the two-phase, infill example: (a) travel-time inversion, (b) generalized travel-time inversion, and (c) amplitude inversion.

2.5.2 Field Application: The Ranger Field, Texas

A multiwell, mulitracer, interwell tracer injection study was carried out in the McCleskey sandstone of the Ranger field, Texas. The first description of this data set was published by Lichtenberger.[40] The dataset was also described later by Allison *et al*.[41] The 320-acre area of interest includes 13 producers and four injectors, injecting seven different tracers. The seven tracers injected included five conservative tracers consisting of four decaying (Tritium, Cobalt-57, Cobalt-58, and Cobalt-60), one chemical (sodium thiocyanate, NaSCN), and two partitioning tracers (tertiary butyl alcohol, TBA, and isopropyl alcohol, IPA).

All tracers were injected in small slugs on the same day except for TBA, which was injected in a small slug 20 days later. Tracer sampling continued for 826 days after injection of the first set of tracers. The tracer injection pattern is shown in **Fig. 2.14.** Detailed information for injection locations and the amounts of each tracer injected can be found elsewhere.[41,42]

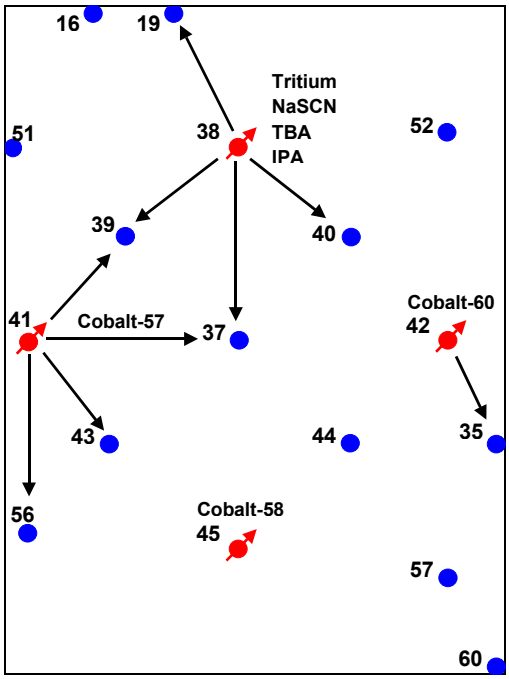

Figure 2.14 Tracer injection pattern: the Ranger field case.

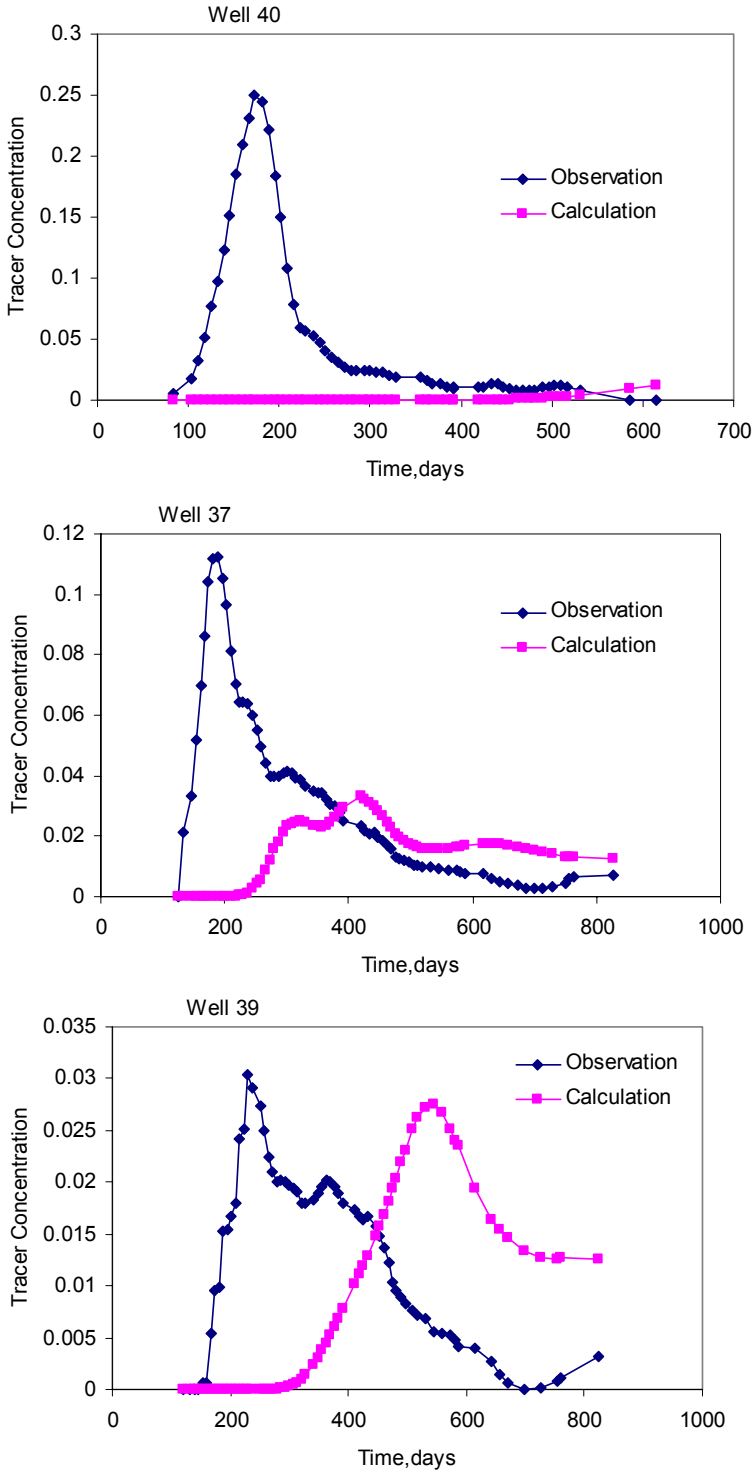

Figure 2.15 NaSCN tracer response for the initial permeability field at Well 40, Well 37, and Well 39.

We can use the conservative tracers (Tritium and NaSCN) to obtain permeability distribution in the study area. However, the Tritium response may be affected by a chromatographic delay because of tritium exchange with immobile hydrogen.[40] We selected NaSCN as the conservative tracer for permeability inversion. Totally, 5,655 lbs of NaSCN was injected into Well 38 and four wells (Wells 19, 37, 39, and 40) showed tracer response as indicated in Fig. 2.14. The observed tracer responses in Wells 37, 39, and 40 are shown in **Fig. 2.15,** along with the calculated response from the initial permeability model. The data from Well 19 was not used because of its low production rate (<20 B/D).

Choice of an Initial Model. During inverse modeling, a proper selection of the initial model can be critical to ensure a plausible solution. Such an initial model should incorporate all available prior information. For our simulation studies, we use a 31×45×6 grid which corresponds to 100×100-foot gridblocks areally, and 2 to 4-foot gridblocks vertically. A total of 141 core samples were available for analysis. We did not have well- and depth-specific data, but rather a summary of the core data for all wells. The core data indicated a fair degree of permeability heterogeneity in the reservoir but only slight variation in porosity. For the initial model, we used a uniform value of porosity and a heterogeneous permeability field generated using Sequential Gaussian Simulation[1] based on well data **(Fig. 2.16).** We assume that $k_x = k_y$, $k_z = 0.1k_x$ and only k_x is altered during inversion.

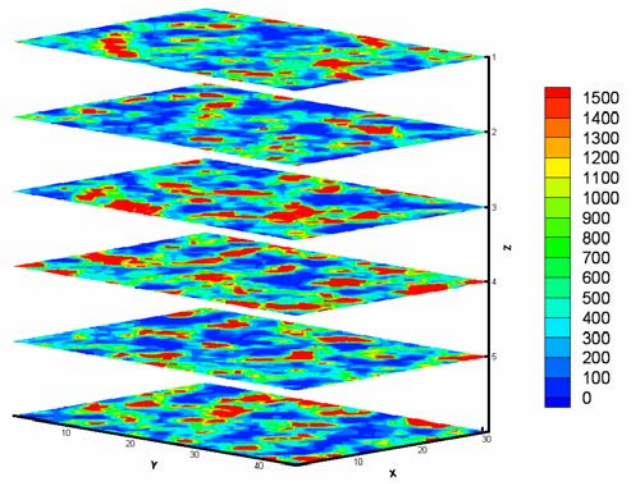

Figure 2.16 Initial permeability distribution for the Ranger field case.

Estimating Permeability. We matched the NaSCN data to obtain the permeability distribution (k_x) in the study area using the three different approaches: travel-time inversion, generalized travel-time inversion, and amplitude inversion. Fig. 2.15 shows the NaSCN responses from a streamline simulator using the initial permeability field. Also, superimposed are the observed NaSCN concentrations. Clearly, there is a large difference between the calculated and observed NaSCN response. **Fig. 2.17** shows the NaSCN concentration match after travel-time inversion. The peak arrival times are now in agreement with the observed data. The tracer concentration amplitudes show improvement but the overall match is still not satisfactory. **Fig. 2.18** is the NaSCN concentration match after the generalized travel-time inversion. From Fig. 2.18, we can see that not only are the peak-arrival times well matched, but the calculated concentration amplitudes are also in close agreement with the observed data. This shows that generalized travel-time inversion is an effective one-step inversion process. **Fig. 2.19** displays the NaSCN concentration match after direct amplitude inversion. Clearly, the calculated responses have changed very little from the initial responses. The results indicate that amplitude inversion may not be as effective as the travel-time inversion, particularly when the initial model is far from the solution. Generalized travel-time inversion stands out as the best among the three inversion methods.

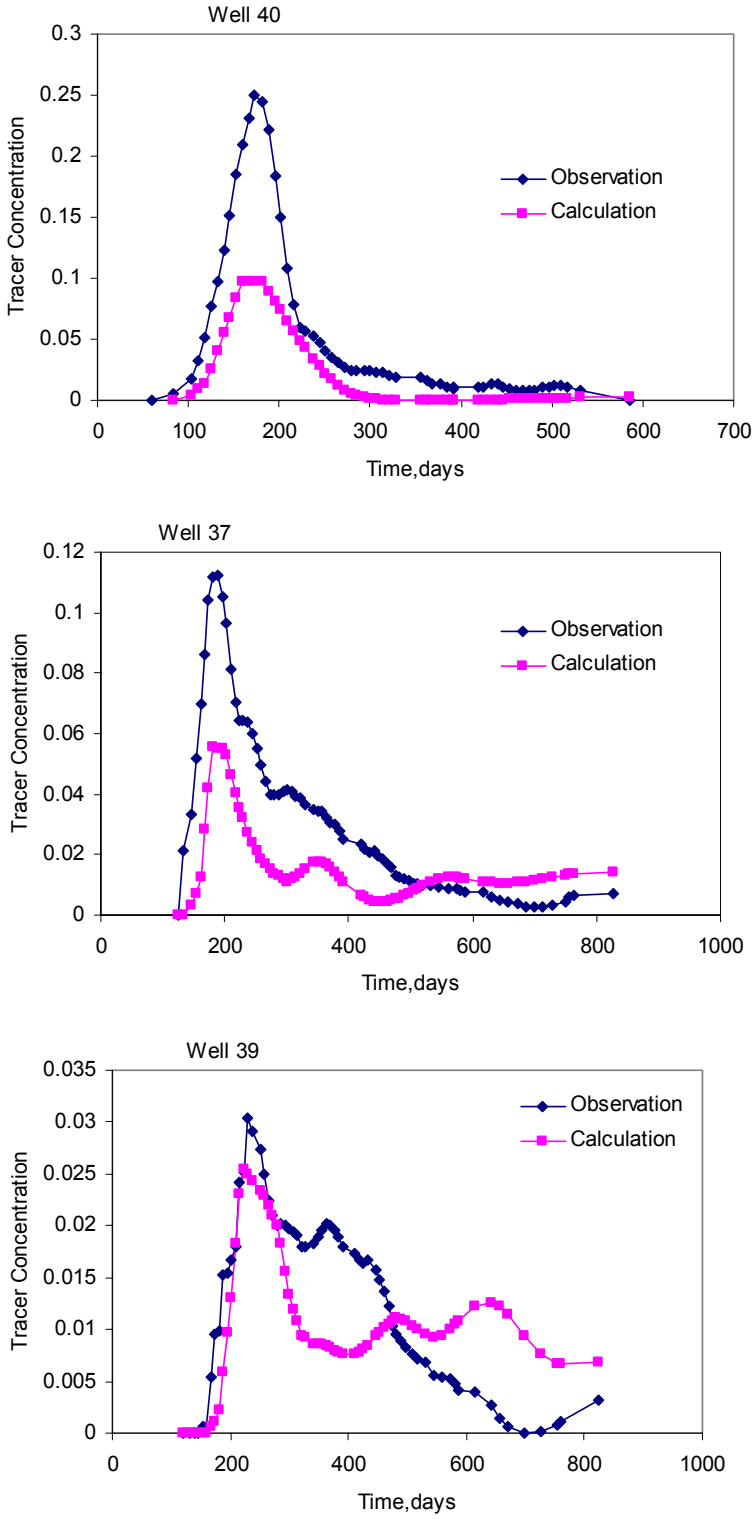

Figure 2.17 NaSCN tracer response after travel-time inversion at Well 40, Well 37, and Well 39.

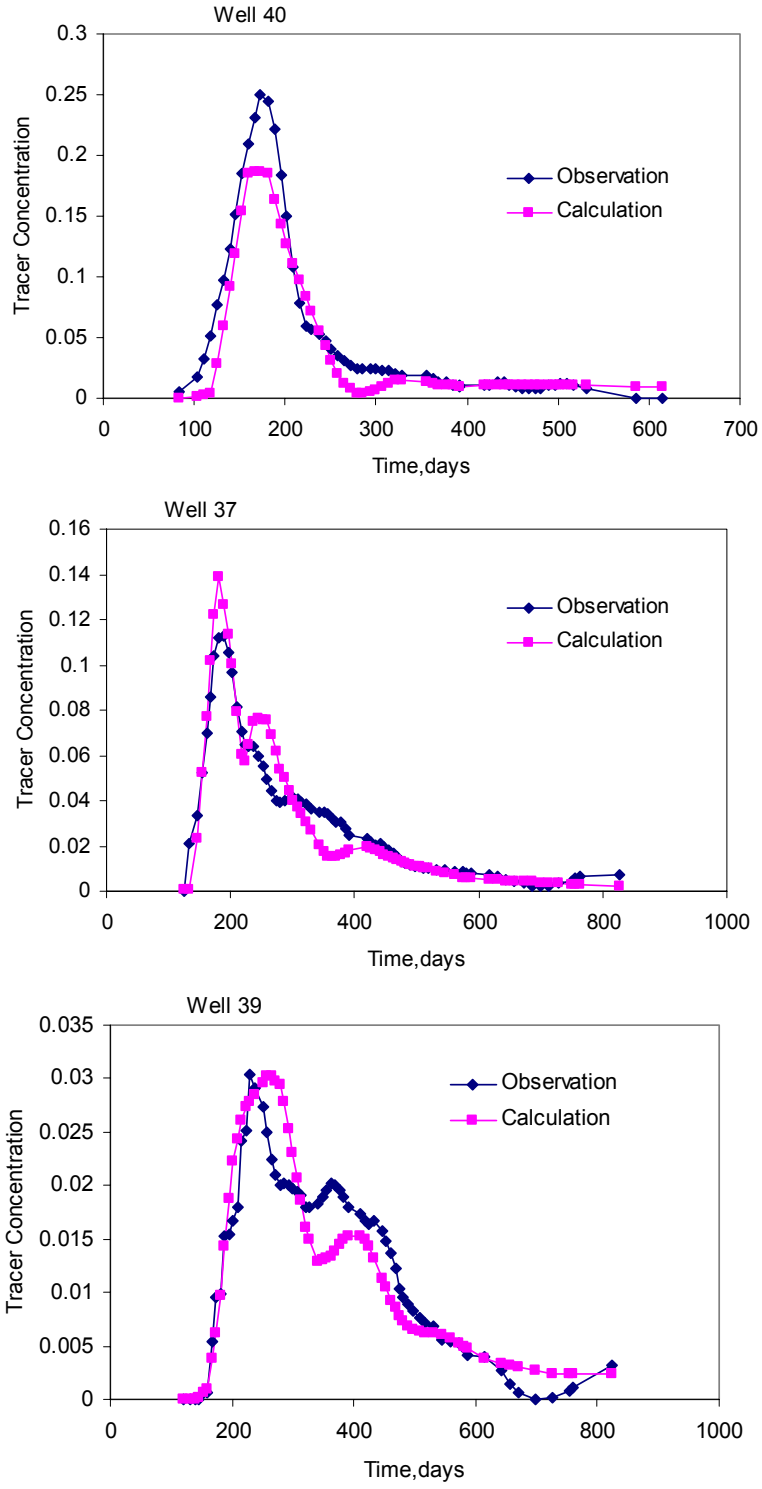

Figure 2.18 NaSCN tracer response after generalized travel-time inversion at Well 40, Well 37, and Well 39.

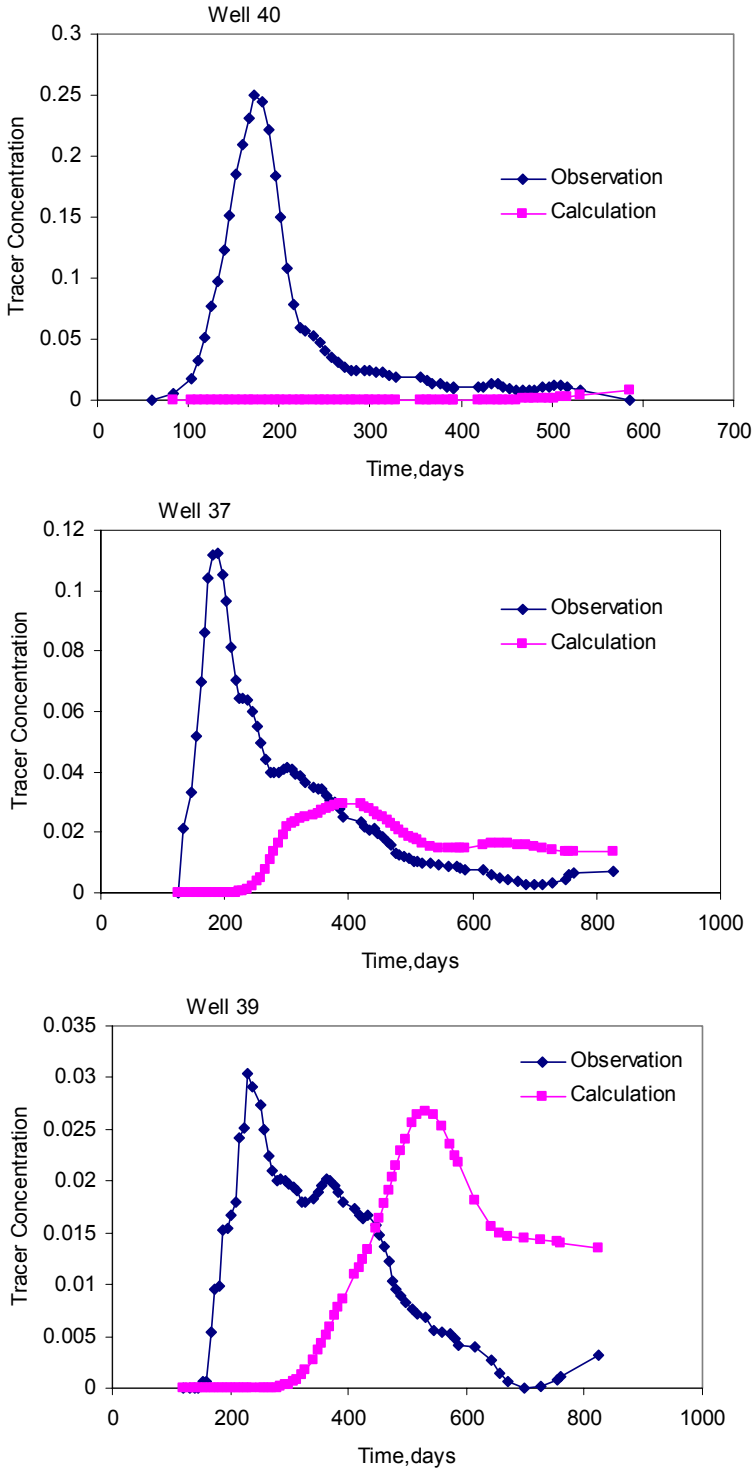

Figure 2.19 NaSCN tracer response after direct amplitude inversion at Well 40, Well 37, and Well 39.

Fig. 2.20 summarizes nonlinearity for the three inversion methods. The measure of nonlinearity for the field example is given by the maximum amongst the three producers. Amplitude inversion displays the highest measure of nonlinearity, approximately 200 to 250, while travel-time inversion is quasilinear, with a nonlinearity of approximately 0.2 to 0.4. The generalized travel-time inversion is between these two cases in terms of nonlinearity measure. However, it is one order of magnitude larger than the travel-time inversion, while two orders of magnitude smaller than that of the amplitude inversion. Generalized travel-time inversion keeps most of the favorable features of travel-time inversion and has a much better tracer-concentration amplitude match than travel-time inversion. The severe nonlinearity of the amplitude inversion is partly responsible for its poor performance for the field case.

Fig. 2.21 shows the permeability fields derived by travel-time inversion and generalized travel-time inversion. **Fig. 2.22** shows the permeability change after travel-time inversion and generalized travel-time inversion. In **Fig. 2.23,** we show that there is a general agreement between our final model and the permeability distribution reported by Allison *et al.*[41] by a manual history matching of the tracer data. The most significant change by Allison *et al.* was introduction of a high-permeability streak in the original permeability model between Wells 38 and 40. Our results from generalized travel-time inversion also indicate the presence of higher permeability between Wells 38 and 40 in the corresponding layer (Fig. 2.23) However, our results did not require the additional changes near the boundary obtained by Allison *et al.*

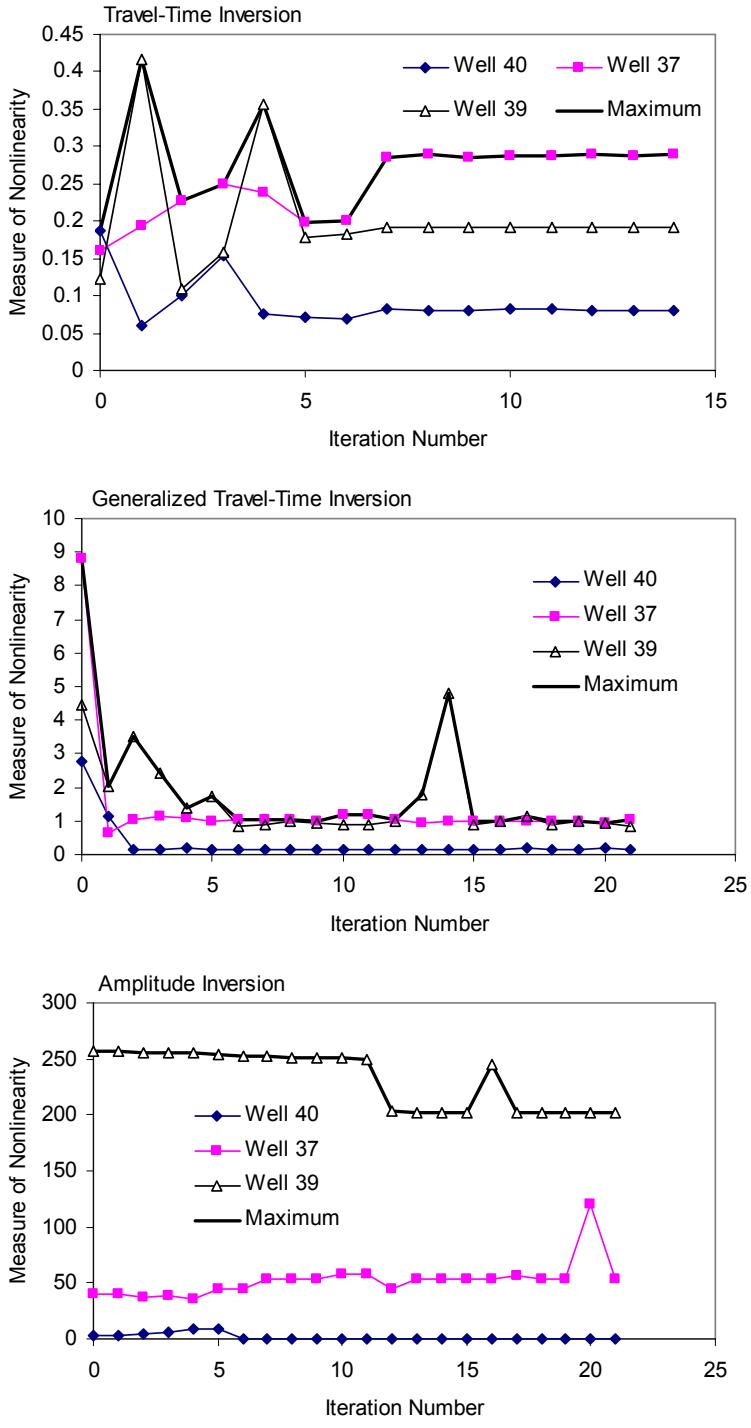

Figure 2.20 Measure of nonlinearity for travel-time inversion, generalized travel-time inversion, and amplitude inversion.

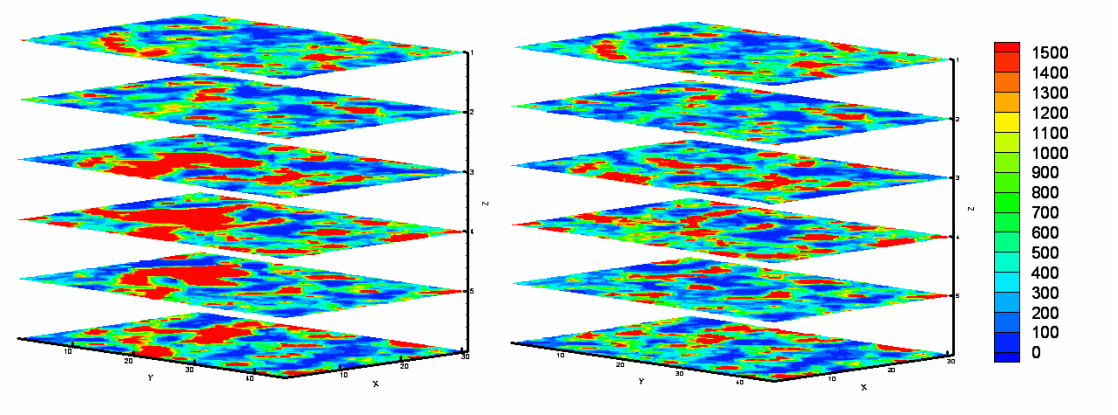

a b

Figure 2.21 Derived permeability field after NaSCN concentration match by (a)generalized travel-time inversion and (b) travel-time inversion.

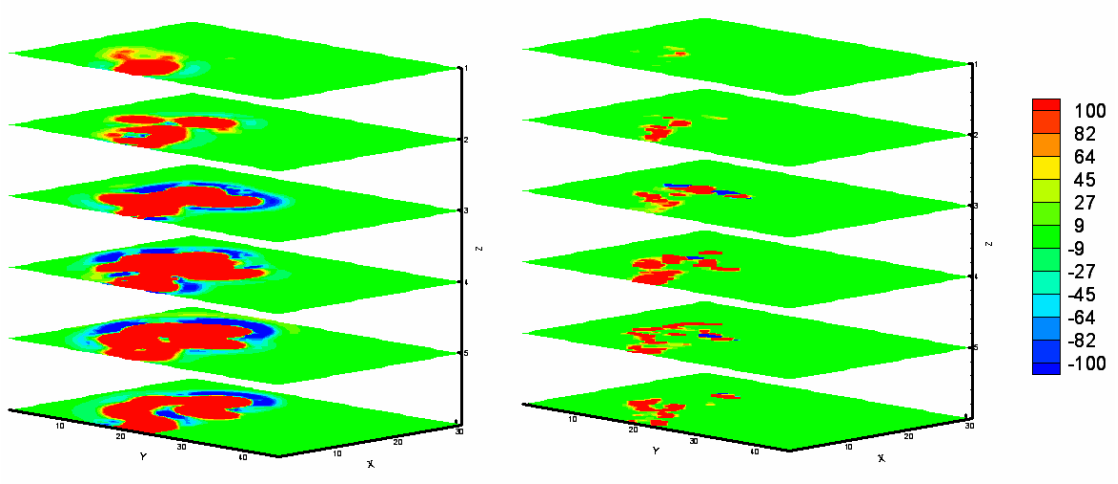

a b

Figure 2.22 Permeability change after (a) generalized travel-time match and (b) travel-time match.

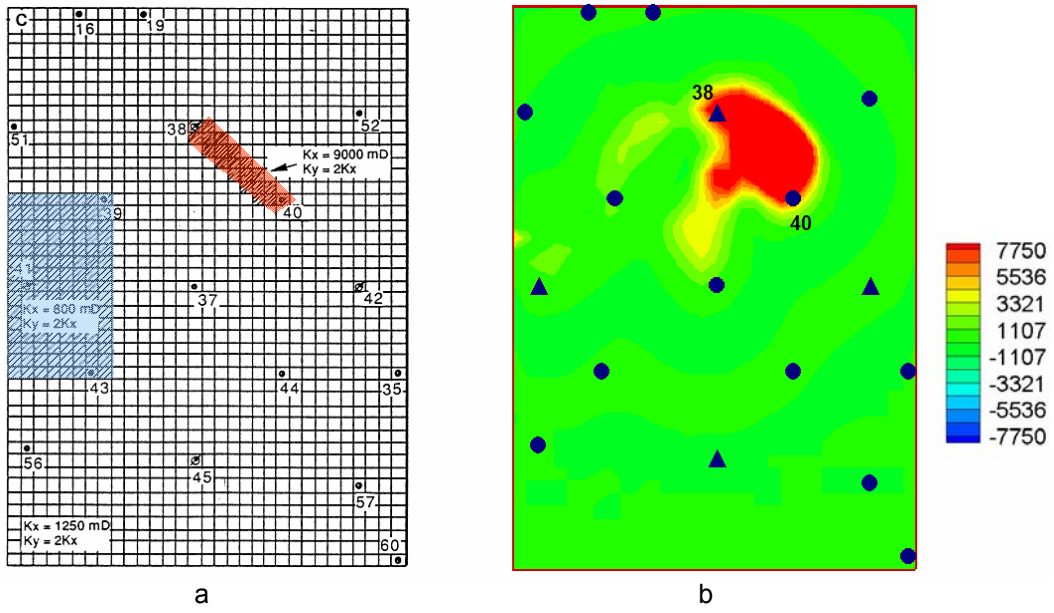

Figure 2.23 (a) Permeability multipliers from the manual history match in Layer 3, by Allison et al., and (b) permeability change from generalized travel-time inversion in the corresponding layer.

2.6 Chapter Summary

We have presented three approaches to production-data integration and examined their relative merits using quantitative measures of nonlinearity. These are travel-time, generalized travel-time, and the commonly used amplitude inversion. The travel-time inversion of production data is robust and computationally efficient. Unlike conventional amplitude matching that can be highly nonlinear, the travel-time inversion has quasilinear properties. This makes the method particularly attractive for field-scale applications where the prior geologic model might be far from the solution. The generalized travel-time inversion appears to retain most of the desirable features of the travel-time inversion and also accomplishes the amplitude match. Some specific findings from this study can be summarized as follows:

1. We have quantitatively investigated the nonlinearities associated with travel-time

and amplitude inversion for production data integration. The nonlinearity is expressed in terms of a simple and intuitive geometric measure of curvature as proposed by Bates and Watts[16] and later used by Grimstad and Mannseth.[17]

2. The nonlinearity in travel-time inversion is found to be orders of magnitude smaller than the conventional amplitude inversion. As a result, the travel-time inversion has better convergence properties and is less likely to be trapped in local minimum.
3. Travel-time sensitivity is more uniform between the wells. In contrast, the amplitude sensitivity can be localized near the wells. The higher magnitude of the travel-time sensitivity also contributes to its quasilinearity and improved convergence properties.
4. The generalized travel-time inversion effectively combines travel time and amplitude inversion while retaining most of the desirable properties of the travel-time inversion. For the field example studied here, the generalized travel-time inversion outperformed both travel-time and amplitude inversion.

CHAPTER III

ASSISTED VS. AUTOMATIC HISTORY MATCHING USING STREAMLINE MODELS*

Reconciling high-resolution geologic models to production history is a very time-consuming aspect in reservoir modeling. Current practice still involves a tedious history-matching process that is highly subjective and often employs ad-hoc property multipliers. Recently streamline models have shown significant promise in improving the history matching process. In particular, the streamline-based 'assisted history-matching' utilizes the streamline trajectories to identify and limit changes only to the regions contributing to the well production history. It is now a well-established procedure and has been applied successfully to numerous field cases.

In this chapter, we enhance the streamline-based assisted history matching in two important aspects that can significantly improve its efficiency and effectiveness. First, we utilize streamline-derived analytic sensitivities to determine the spatial distribution and magnitude of the changes needed to improve the history match. Second, we use a 'generalized travel time inversion (GTTI)' for model updating via an iterative minimization procedure. Using this approach, we can account for the full coupling of the streamlines rather than changing individual or bundles of streamlines at a time. The approach is more akin to automatic history matching; however, by intervening at every step in the iterative model updating, we can retain control over the process as in assisted history matching. Our approach leads to significant savings in time and manpower during field-scale history matching.

---

*Part of this chapter is reprinted with permission from "Field Experiences With Assisted and Automatic History Matching Using Streamline Models" by Cheng, H., Wen, X.-H., Datta-Gupta, A., and Milliken, W.J., 2004. paper SPE 89857 presented at the 2004 SPE Annual Technical Conference and Exhibition, Houston, September 26–29.

We demonstrate the power of our method using two field examples with model sizes ranging from 10^5 to 10^6 grid blocks and with over one hundred wells. The reservoir models include faults, aquifer support and several horizontal/high angle wells. History matching was performed using both assisted history matching and the GTTI. Whereas the general trends in permeability changes were similar for both the methods, the GTTI seemed to significantly improve the water cut history matching on a well-by-well basis within a few iterations. Our experience indicates that the GTTI can also be used very effectively to improve the quality of history match derived from the assisted history matching. The changes to the reservoir model from GTTI were found reasonable with no artificial discontinuities or apparent loss of geologic realism.

3.1 Introduction

Traditionally, history matching is performed manually on the upscaled reservoir model and frequently uses local or regional multipliers to reservoir properties. By adjusting the regions and multipliers, a history match could be achieved using mostly trial and error. The trial-and-error involves considerable subjective judgment and personal bias and most importantly may create artificial discontinuities inside the reservoir, potentially destroying the correlation built into the initial geologic model.

A more systematic approach to history matching, called Assisted History Matching (AHM) uses streamlines to build upon and improve traditional history matching techniques.[4-6] The AHM is also a manual approach. However, changes to the model can be limited to the streamlines contributing to the production history of the well of interest and the amount of changes can be computed using some simple semi-analytical methods. The approach is a significant improvement over the traditional manual history matching but still could be time consuming, particularly when there are a large number of wells. This is complicated by the coupled nature of the flow equations which makes matching

individual wells difficult without impacting other wells also. Finally, if we limit changes along streamlines only, it can introduce 'tube like' artifacts into the geologic model.

Geostatistically-based automatic history matching (production data integration) has been an active area of research and a number of techniques have been reported in the literature in the past decade. The main goal here is to match well production data by modifying the initial model in such a way that it preserves the underlying geostatistical features built into the initial model. Yeh[7] and Wen *et al.*[8] provided a review of these inverse techniques. Both finite difference and streamline fluid flow modeling can be used in automated history matching.[9] Typically, an inverse technique is needed for production data integration, and requires multiple solutions of the flow equations within a nonlinear optimization procedure.[10-12] And this brings a hurdle to the practical applications. Streamline based inverse techniques have shown great potential in this regard[13-18] and they only require a single solution of the flow equations per minimization iteration.[13-14] The sensitivities of production data with respect to reservoir properties can be computed analytically using a single forward simulation. This renders substantial time-saving.

Much of the ideas of AHM are actually embedded in the streamline-based sensitivity computations. The sensitivities define the relationship between reservoir properties and production response. Specifically, they quantify how, for example, the water-cut history at a well will change if we change permeability at any location in the reservoir model. Using the sensitivities, we can significantly speed-up the assisted history matching process and compute the amount of changes for reservoir properties through optimization. Instead of matching wells individually, we can handle the coupled problem directly and update the geologic model to match all the wells simultaneously. The approach is more akin to automatic history matching; however, by intervening at every step in the iterative model updating, we can retain control over the process as in assisted history matching.

In this chapter, we enhance the streamline-based assisted history matching in two important aspects that can significantly improve its efficiency and effectiveness. First,

we utilize streamline-derived analytic sensitivities to determine the spatial distribution and magnitude of the changes needed to improve the history-match. These sensitivities are then incorporated into an optimization algorithm to update the reservoir model during flow simulation. Secondly, a "generalized travel-time inversion (GTTI)"[24,26] is used for inverse modeling. The GTTI is robust because of its quasi-linear properties resulting in rapid convergence even if the prior model is far from the solution. We demonstrate our approach using two field examples with over 100 wells and more than 30 years of production history.

3.2 Background and Illustrative Examples

3.2.1 Assisted History Matching

Assisted history matching utilizes unique information-content in streamlines in terms of injector-producer relationship to facilitate history matching.[4-5] The main steps in assisted history matching are: (i) Flow simulation to generate production response. Either streamline or finite-difference simulators can be used for this purpose; (ii) Streamline generation based on the finite-difference velocity field. This step is not necessary for streamline simulators as streamlines are already available; (iii) Use of streamlines to assign grid blocks or regions to each producer; (iv) Computing the mismatch between the observed and computed production response at each well using streamlines; (v) Updating grid block or region properties manually to improve the history match on a well-by-well basis. The use of streamlines leads to simple and unambiguous changes in the model. Also, the changes are minimized to preserve the geology. An outline of the procedure of assisted history matching is given in a flow chart in **Fig. 3.1**.

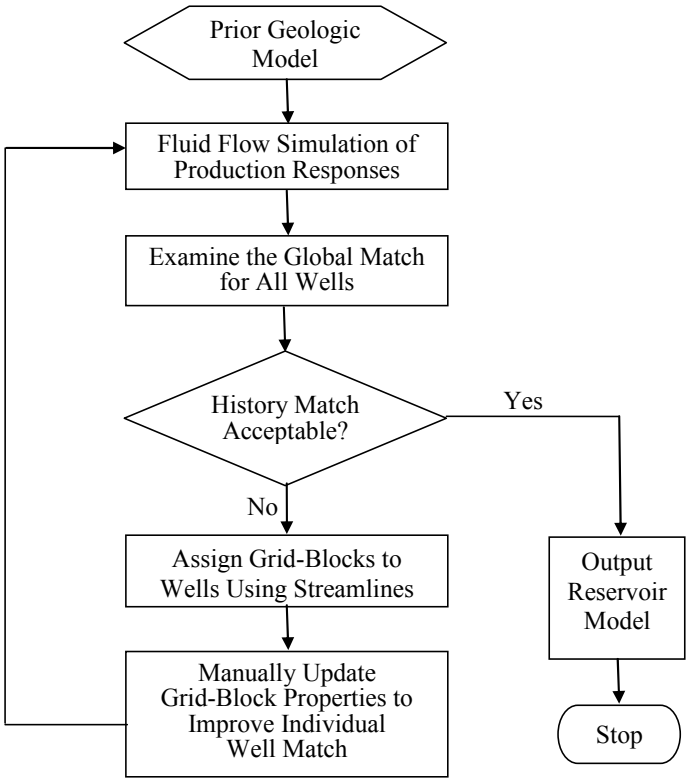

Figure 3.1 Flowchart for assisted history matching.

Illustration of the Procedure. **Fig. 3.2** shows a 2D reference permeability field (50×50 grid with cell size 10 feet × 10 feet) generated using Sequential Gaussian Simulation[1] and the corresponding fractional-flow data at four producing wells in 5-spot pattern. The variogram of the reference field is spherical with range of 100 feet and 20 feet in the direction of 45 degree and 135 degree, respectively. We generated an initial model using the same geostatistical method with the same histogram and variogram as for the reference field. The initial permeability and the water cut responses from the four corner wells are shown in **Fig. 3.3**. Note that this initial model visually is quite close to the reference model. The flow responses, however, are quite different from the reference model. **Fig. 3.4** shows the streamlines for the initial model. Now in order to match the reference water cut, streamlines are used to help assigning cells to wells and grouping the cells. From streamlines, we know which cells to change to history match a particular

well. Besides, we know which streamlines contribute to early breakthrough (A), middle stage (B), and later stage (C) water cut. Streamline helps grouping cells that need to be modified. We can change cells covered by streamlines marked ‘A’ to match early breakthrough, and change those associated with ‘B’ and ‘C’ to match middle and later stage water cut.

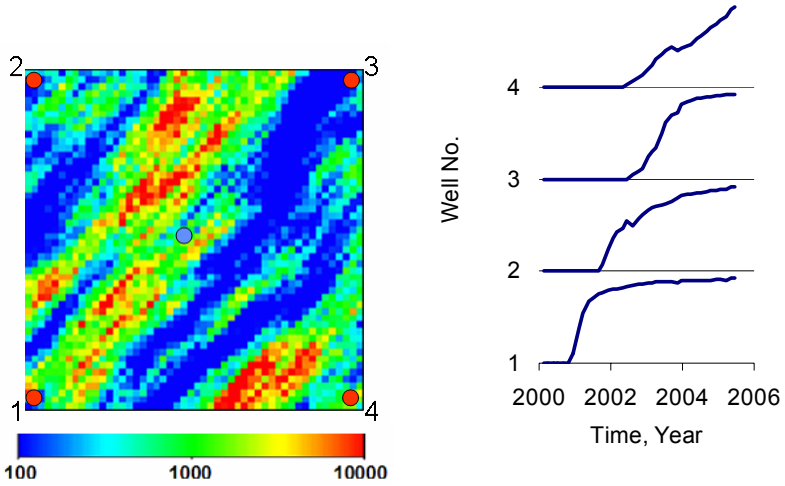

Figure 3.2 Reference permeability field and water cut responses.

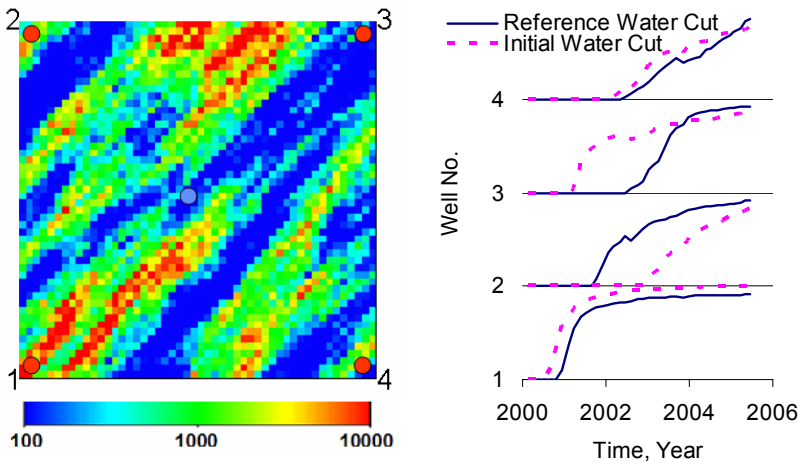

Figure 3.3 Initial permeability field and water cut responses.

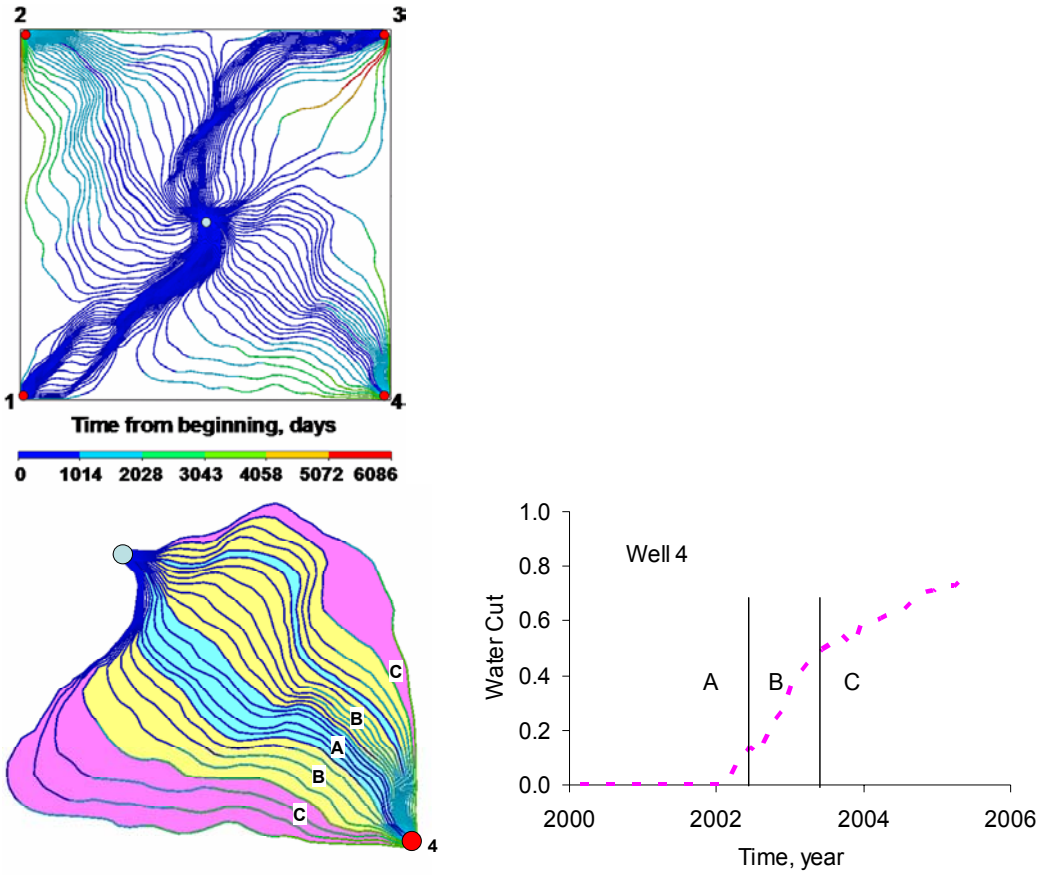

Figure 3.4 Illustration of streamline-based assisted history matching water-cut response.

The assisted history matching can accelerate the history matching process significantly. However, the approach is still more or less manual and requires some trial and error. Individual well matching can sometimes deteriorate matches in other wells because of the coupled nature of the flow field. Finally, limiting the changes to streamlines can introduce artifacts in the geologic model unless the changes are kept to a minimum. Recently, a number of approaches have been reported to improve the efficiency of the AHM method. These include the use of tracer-like flow assumption to compute the modifications of reservoir properties within the well regions delineated by streamlines that can match multiple phase production history,[17,43] and the integration of streamline information at different levels with geostatistics.[16,44] These approaches, however, do not directly use the sensitivity coefficients derived from the streamline

simulation to quantify the changes. Therefore, the improvement in efficiency is marginal at best.

3.2.2 Streamline-Based Automatic History Matching

This approach utilizes streamline-derived sensitivities to update geologic models.[9,13,14,26] The major steps are: (i) Streamline-based flow simulation to compute production response at the wells; (ii) Quantification of the mismatch between observed and computed production response; (iii) Streamline-based analytic sensitivity computation of the production response with respect to reservoir parameters; (iv) Updating reservoir properties to match the production history via inverse modeling using streamline-derived sensitivities. An outline of the procedure of streamline-based automatic history matching is given in a flow chart in **Fig. 3.5**.

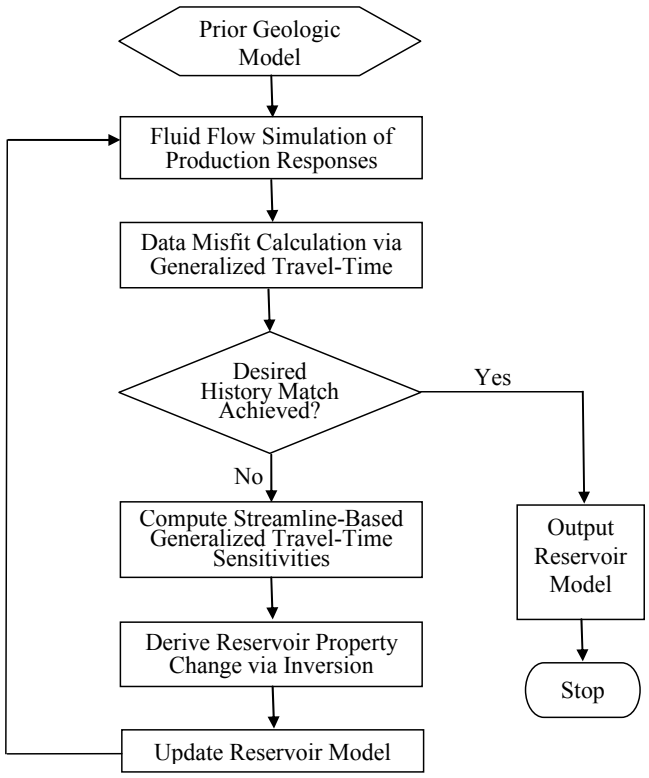

Figure 3.5 Flowchart for automatic history matching.

Illustration of the Procedure. To illustrate the procedure, we use the same synthetic example used for assisted history matching. We have used a commercial 3D streamline simulator, FrontSim[51] (Version 2003a), for modeling two-phase flow in the reservoir. Production data misfit is represented by a 'generalized travel time' at each producing well. A "generalized travel time" or "travel-time shift" is computed by systematically shifting the computed production response towards the observed data until the cross-correlation between the two curves is maximized.[24,26] This is illustrated in **Fig. 3.6** and is discussed further later. The sensitivities calculated for automatic history matching are shown in **Fig. 3.7**. These sensitivities are calculated along the streamlines analytically using time of flight and fractional flow information. Unlike assisted history matching, there is no need for manual intervention to look at the streamlines to determine where to change the models. Also, with the sensitivity information, we can apply different modifications determined from optimization to different locations. Figs. 3.7d and 7e show that sensitivities are calculated along the streamlines. The largest sensitivities in magnitude (dark-blue region) correspond to early breakthrough, and the medium (light-blue to green) and small (yellow) sensitivities correspond to middle stage and later stage water cut. Also the whole region covered by the sensitivities will be changed systematically and automatically by generalized travel-time inversion. **Fig. 3.8** shows that the water-cut responses are in good agreement with the reference, and the updated permeability model maintains the general features of the initial model. As desired, the permeability was increased around Well 2 while decreased around Well 3 to match the history (**Fig. 3.9**, also refer to Fig. 3.3 for the initial model). The decrease of objective function (shift time) with the iteration number, as well as the associated water-cut misfit, is shown in **Fig. 3.10**. The shift time objective function reduces from 670 days to 20 days in 20 iterations, and it reduces quickly in the first few iterations.

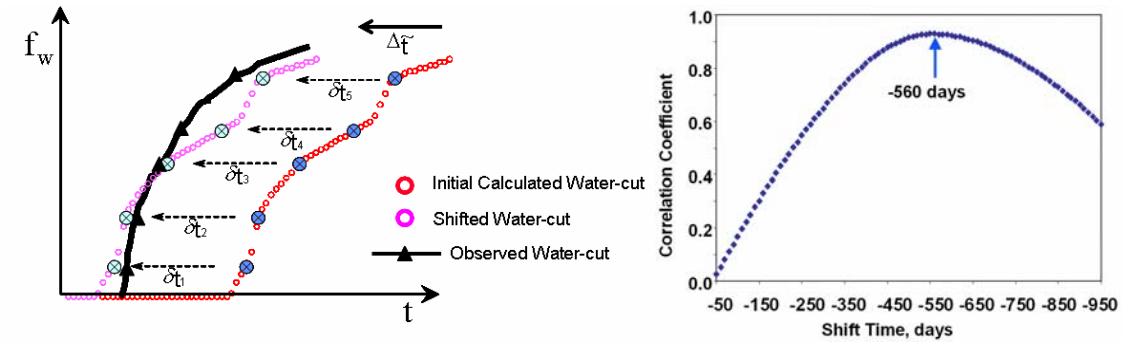

Figure 3.6 Illustration of generalized travel time misfit, correlation function, and generalized travel time sensitivity calculation.

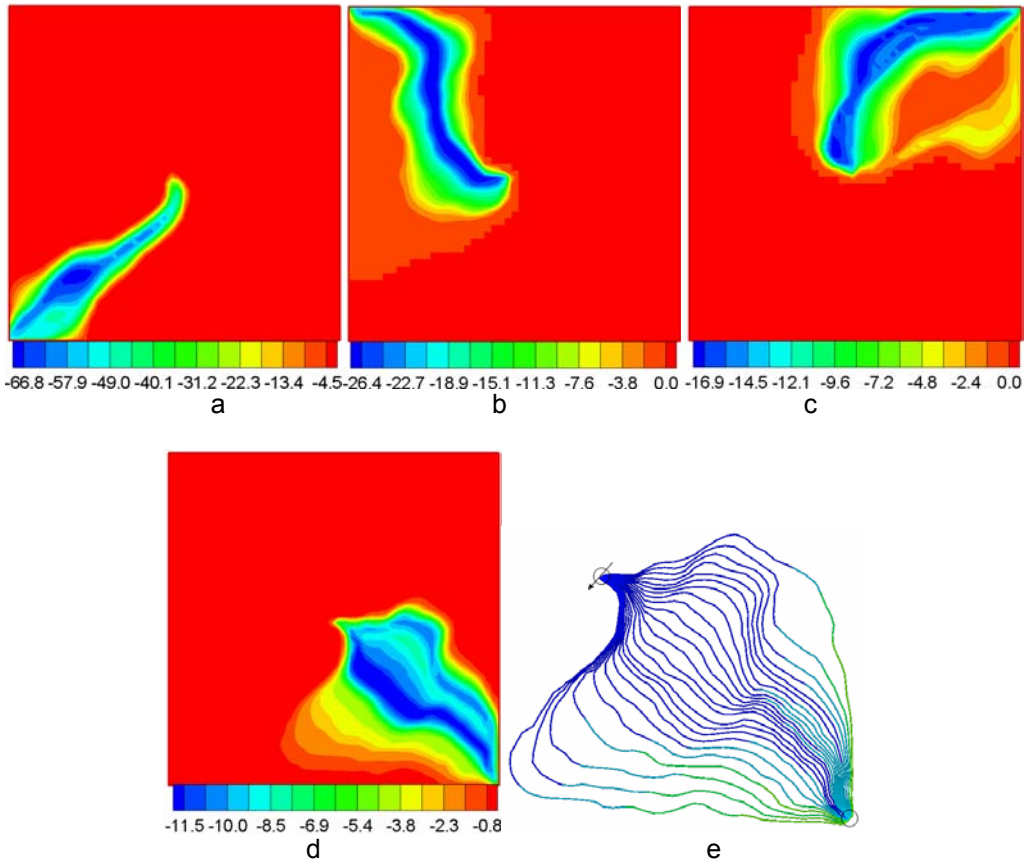

Figure 3.7 Generalized travel time sensitivities for (a) Well 1, (b) Well 2, (c) Well 3, (d) Well 4, and (e) streamlines associated with Well 4.

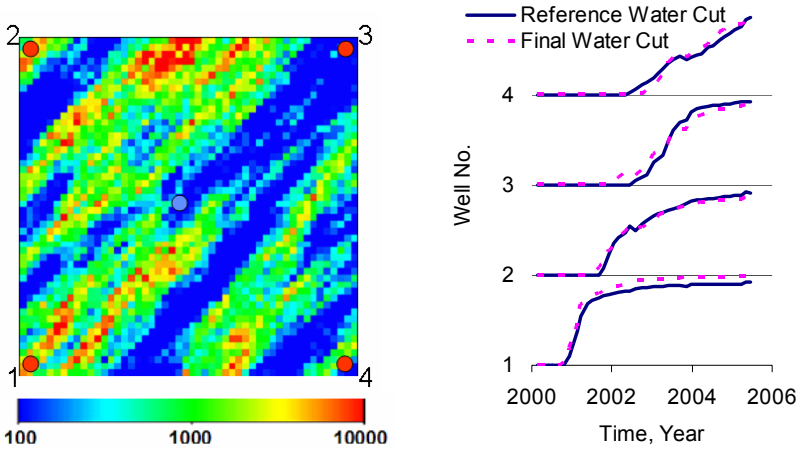

Figure 3.8 Updated permeability field and water cut matches.

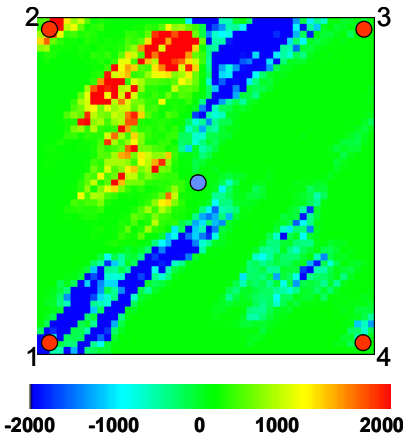

Figure 3.9 Permeability changes.

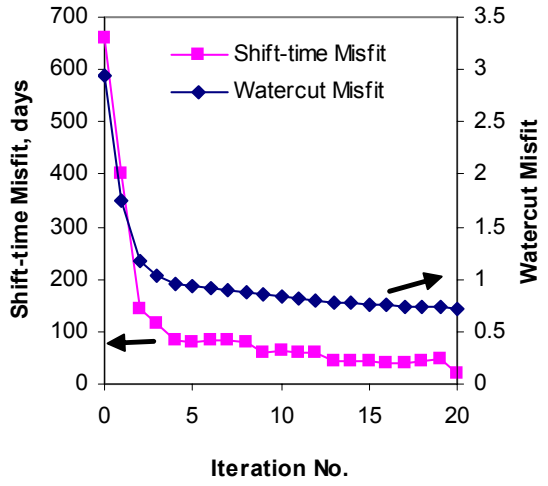

Figure 3.10 Misfit reduction.

Multiple Realizations. An important advantage of the streamline-based inversion is its computational efficiency. This makes dynamic conditioning of multimillion-cell models feasible using the streamline approach. In addition, we are able to generate multiple realizations to assess uncertainty in performance forecasting, for example, using the randomized maximum likelihood method.[45] Using multiple realizations and an ensemble average map, we can also reveal large-scale spatial trends common to all realizations. To illustrate this, we generated 100 initial models and history matched all of them to the reference production data in 4 wells using the streamline-based inversion. Initial realizations are generated by unconditional Gaussian simulation with the same histogram and variogram as for the reference field.

The water-cut responses from all initial and updated realizations are shown in **Figs. 3.11** and **3.12**. Clearly, after inversion, the calculated water-cut responses all moved much closer to the reference responses (Fig. 3.12). Note that in the randomized maximum likelihood method we match "realizations" of the observed production history rather than the history itself; hence, we see the spread in the water-cut responses in the updated models. For 100 realizations, it took only 150 minutes in a PC (Intel Xeon 3.06 GHz processor). The mean and variance of the 100 realizations is shown in **Fig. 3.13**.

The final ensemble mean field captured most of the low permeability region and some of the high permeability region (Fig. 3.13a), while the variance field (Fig. 3.13b) displays the uncertainty among the updated models.

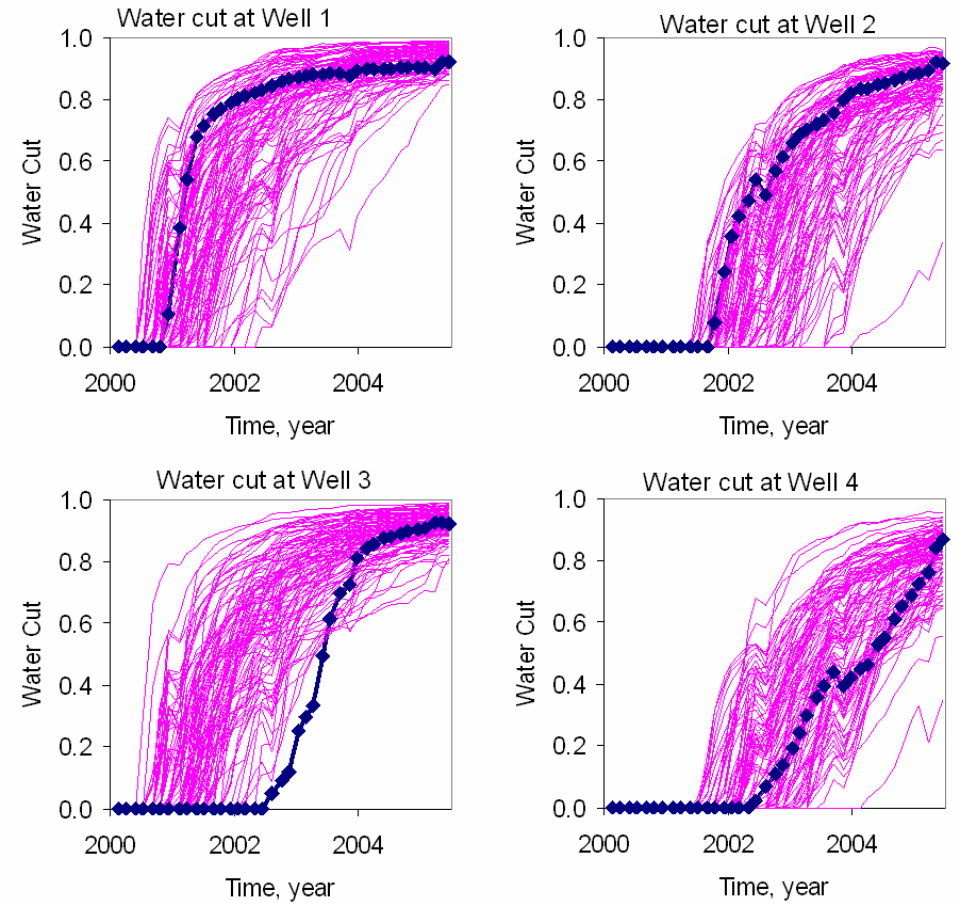

Figure 3.11 Water cuts of four producers from 100 initial realizations together with the results from the reference field (blue squares).

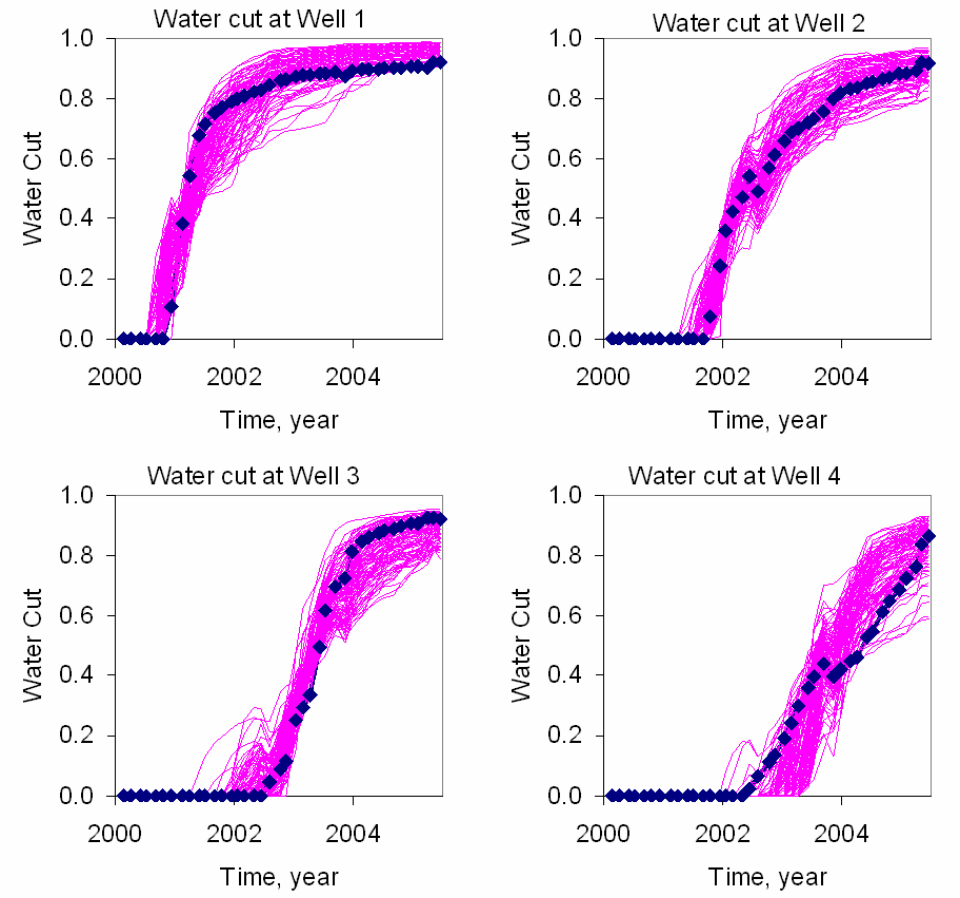

Figure 3.12 Water cuts of four producers from 100 updated realizations together with the results from the reference field (blue squares).

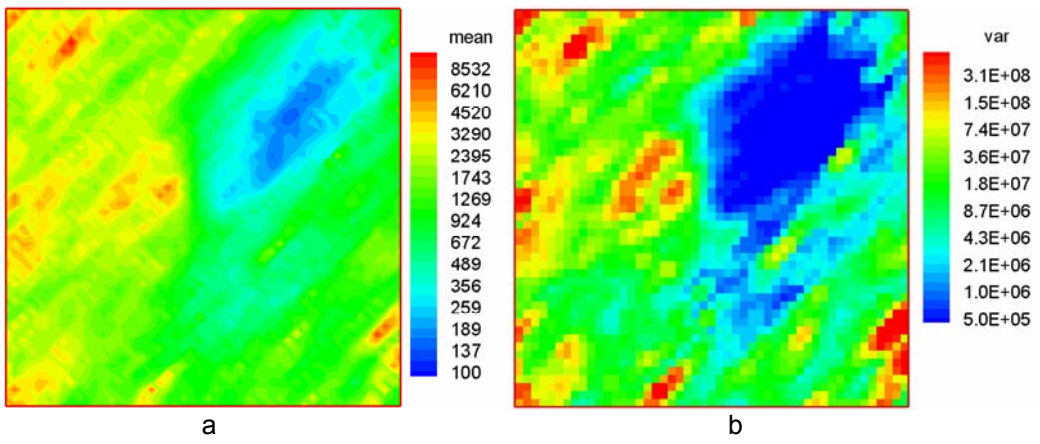

Figure 3.13 (a) Ensemble mean of the 100 final estimated permeability fields and (b) uncertainty in terms of the variance.

3.3 Streamline-Based Automatic History Matching: Mathematical Formulation

Several previous publications describe streamline-based sensitivity computations and generalized travel time inversion.[9,13,14,18,26] In this section, we briefly outline the mathematical background behind the approach.

3.3.1 Forward Modeling: Streamline Simulation

Streamline simulators approximate 3D fluid flow calculations by a sum of 1D calculations along streamlines. The choice of streamline direction for 1D calculations makes the approach extremely effective for modeling convection-dominated flows in the reservoir.[27] This is typically the case when heterogeneity is the predominant factor controlling oil recovery, for example in waterflooding. The streamline approach for modeling multidimensional, multiphase flow basically comprises of five major steps:[21,47] (i) Tracing streamlines in 3D based on a numerical solution of the pressure and velocity equations; (ii) Recasting the transport (saturation) equations in terms of streamline time of flight which is the travel time of a tracer along the streamline; (iii) Solution of the saturation equation along streamlines; (iv) Periodic updating of streamlines to account for changing field conditions such as infill drilling and rate changes; (v) Use of operator splitting to account for transverse fluxes such as gravity.

The computational advantage of the streamline methods can be attributed to four principal reasons: (i) Streamlines may need to be updated only infrequently; (ii) The transport equations along streamlines can often be solved analytically; (iii) The 1D numerical solutions along streamlines are not constrained by the underlying grid stability criteria, thus allowing for larger timesteps; (iv) For displacements dominated by heterogeneity, the CPU time often scales nearly linearly with the number of gridblocks, making it the preferred method for fine-scale geologic simulations. Furthermore, the self-similarity of the solution along streamlines may allow us to compute the solution only once and map it to the time of interest. Other advantages are sub-grid resolution and reduced numerical artifacts such as artificial diffusion and grid orientation effects, since

the streamline grid used to solve the transport equations is effectively decoupled from the underlying static grid.

3.3.2 Generalized Travel Time and Sensitivity Calculations

As shown in **Fig. 3.6**, we define the generalized travel time as the optimal time shift $\Delta\tilde{t}$ that maximizes the following correlation function:

$$R^2(\Delta t_j) = 1 - \frac{\sum\left[y_j^{obs}(t_i + \Delta t_j) - y_j^{cal}(t_i)\right]^2}{\sum\left[y_j^{obs}(t_i) - \overline{y_j^{obs}}\right]^2}, \tag{3.1}$$

where y is the flow responses we wish to match, e.g., water cut at producing wells, j is producer index and i is observation data index. The overall production data misfit can now be expressed in terms of a generalized travel-time misfit at all wells as $\sum_{j=1}^{N_w}\left(\Delta\tilde{t}_j\right)^2$, with N_w being the total number of producing wells. Our objective is to minimize this generalized travel time misfit, and we need the sensitivities for minimization.

Sensitivity Computations. In GTTI, we shift the entire fractional flow curve by a constant time. Thus, every data point in the fractional-flow curve has the same shift time, $\delta t_1 = \delta t_2 = \cdots = \Delta\tilde{t}$ (Fig. 6). So we can sum up and average the travel time sensitivities of all data points to obtain a rather simple expression for the sensitivity of the generalized travel time with respect to reservoir parameters m as follows[26]

$$\frac{\partial\Delta\tilde{t}_j}{\partial m} = -\frac{\sum_{i=1}^{N_{dj}}\left(\partial t_{i,j}/\partial m\right)}{N_{dj}}. \tag{3.2}$$

It now reduces to the sensitivity of the arrival times at the producing well, $\partial t_{i,j}/\partial m$. These sensitivities can be easily obtained in terms of the sensitivities of the streamline time of flight,[26]

$$\frac{\partial t}{\partial m} = \frac{\dfrac{\partial \tau}{\partial m}}{\dfrac{\partial f_w}{\partial S_w}}. \tag{3.3}$$

In the above expression, the fractional-flow derivatives are computed at the saturation of the outlet node of the streamline. The time-of-flight sensitivities can be obtained analytically in terms of simple integrals along streamline. For example, the time-of-flight sensitivity with respect to permeability will be given by[13]

$$\frac{\partial \tau}{\partial k(\mathbf{x})} = \int_{\Sigma} \frac{\partial s(\mathbf{x})}{\partial k(\mathbf{x})} dx = -\int_{\Sigma} \frac{s(\mathbf{x})}{k(\mathbf{x})} dx, \tag{3.4}$$

where the integrals are evaluated along the streamline trajectory, and the 'slowness' which is the reciprocal of interstitial velocity, is given by

$$s(\boldsymbol{x}) = \frac{\phi(\boldsymbol{x})}{\lambda_{rt} k(\boldsymbol{x}) \left|\nabla P(\boldsymbol{x})\right|}. \tag{3.5}$$

Note that the quantities in the sensitivity expressions are either contained in the initial reservoir model or are available after the forward simulation run.

3.3.3 Data Integration

Our goal is to reconcile high-resolution geologic models to field production history. This typically involves the solution of an underdetermined inverse problem. The mathematical formulation behind such streamline-based inverse problems has been discussed elsewhere.[13,21] Both the deterministic and stochastic approaches have been used with equal success.[49] In the deterministic approach pursued here, we start with a prior static model that already incorporates geologic, well log, and seismic data. We then minimize a penalized misfit function consisting of the following three terms,

$$\left\| \Delta\tilde{\boldsymbol{t}} - \boldsymbol{G}\delta\boldsymbol{m} \right\| + \beta_1 \left\| \delta\boldsymbol{m} \right\| + \beta_2 \left\| \boldsymbol{L}\delta\boldsymbol{m} \right\|. \tag{3.6}$$

In Eq. 3.6, $\Delta\tilde{\boldsymbol{t}}$ is the vector of generalized travel-time shift at the wells; $\boldsymbol{G}$ is the sensitivity matrix containing the sensitivities of the generalized travel time with respect to the reservoir parameters. Also, $\delta\boldsymbol{m}$ correspond to the change in the reservoir property

and $\boldsymbol{L}$ is a second spatial difference operator that is a measure of roughness and is analogous to imposing a prior variogram or covariance constraint. The first term ensures that the difference between the observed and calculated production response is minimized. The second term, called a 'norm constraint', penalizes deviations from the initial model. This helps preserve geologic realism because our initial or prior model already incorporates available geologic and static information related to the reservoir. Finally, the third term, a roughness penalty, simply recognizes the fact that production data are an integrated response and are thus, best suited to resolve large-scale structures rather than small-scale property variations. The minimum in Eq. 3.6 can be obtained by an iterative least-squares solution to the augmented linear system

$$\begin{pmatrix} \boldsymbol{G} \\ \beta_1 \boldsymbol{I} \\ \beta_2 \boldsymbol{L} \end{pmatrix} \delta \boldsymbol{m} = \begin{pmatrix} \Delta \tilde{\boldsymbol{t}} \\ \boldsymbol{0} \\ \boldsymbol{0} \end{pmatrix}. \tag{3.7}$$

The weights β_1 and β_2 determine the relative strengths of the prior model and the roughness term. In general, the inversion results will be sensitive to the choice of these weights.

When the data and the prior model statistics are specified, for example, the data errors and model parameter covariance (variogram), we can adopt a Bayesian formulation that leads to the minimization of the following function,

$$\frac{1}{2}\left(\boldsymbol{m}-\boldsymbol{m}_p\right)^T \boldsymbol{C}_M^{-1}\left(\boldsymbol{m}-\boldsymbol{m}_p\right)+\frac{1}{2}\left[\Delta \tilde{\boldsymbol{t}}\right]^T \boldsymbol{C}_D^{-1}\left[\Delta \tilde{\boldsymbol{t}}\right]. \tag{3.8}$$

The minimum in Eq. 3.8 can be obtained by an iterative least-squares solution to the linear system[49]

$$\begin{bmatrix} \boldsymbol{C}_D^{-1/2}\boldsymbol{G} \\ \boldsymbol{C}_M^{-1/2} \end{bmatrix} \delta \boldsymbol{m} = \begin{bmatrix} \boldsymbol{C}_D^{-1/2}\left(\Delta \tilde{\boldsymbol{t}}\right) \\ \boldsymbol{C}_M^{-1/2}\left(\boldsymbol{m}_p-\boldsymbol{m}\right) \end{bmatrix}. \tag{3.9}$$

where $\boldsymbol{C}_D$ and $\boldsymbol{C}_M$ are the data error covariance and the prior model parameter covariance respectively, and $\boldsymbol{m}_p$ is the prior term. Eq. 3.9 represents a system of equations that is analogous to the deterministic formulation in Eq. 3.7. We use an iterative sparse matrix

solver, LSQR, for solving these augmented linear systems in Eqs. 3.7 and 3.9. The LSQR algorithm is well suited for highly ill-conditioned systems and has been widely used for large-scale tomographic problems in seismology.[38]

It is important to realize that automatic history matching does not necessarily imply that the user has to lose control over the process. Instead, it is recommended that the user intervene after every iteration of the process to determine the plausibility of the changes and accept or reject or modify the changes. From this point of view, the only difference from assisted history matching is the use of the sensitivities and the non-linear optimization technique to determine the spatial location and the extent of changes to the prior model.

3.4 Field Examples

We now discuss applications of streamline-based assisted and automatic history matching to two field examples. We illustrate the use of automatic history matching both for conditioning static geologic models to production data and also as a "finisher/post-processor" to assisted history matching to further improve the matches.

3.4.1 Field Example 1

The first model we studied is a cutout section from a large sandstone reservoir containing over 1.5 MMMSTB of oil.[5] The reservoir is characterized by three principal depositional settings, incised channel fill, regional marine shale, and tidal delta complex. The sector we considered has an average porosity of 20% (**Fig. 3.14**) with median permeability of about 1000 md. The grid dimensions are 30×46×39 (53,820 cells). The model has two faults, an aquifer, and four different relative permeability zones. The oil is a 36º API gravity oil with a viscosity of 0.3 cp at reservoir conditions. The field has been produced for approximately 50 years by primary depletion and phased waterflooding. The simulation model starts at Year 1965 and ends at Year 2001.

Recovery to Year 2001 is approximately 35% OOIP with a field-wide water cut of approximately 93%. Altogether there are 130 wells in the simulation and history matching process. Only water-cut history was used to update the permeability model.

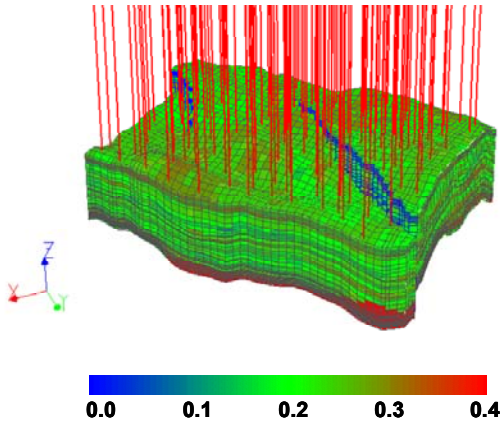

Figure 3.14 Porosity distribution and well locations for field example 1.

For automatic history matching, we will use two different starting models. In the first case, the initial model is up-scaled directly from the static fine-scale geostatistical model using flow-based upscaling method.[50] This initial model was used in both assisted and automatic history matching. In the second case, the initial model is the updated permeability model after assisted history matching.[5] Our goal in this second case is to use automatic history matching to further improve the results of assisted history matching.

We choose horizontal permeability as our model parameter in the inversion. Vertical permeability is also changed during the inversion by preserving the ratio of horizontal and vertical permeability. Porosity in the model was not altered because its variation was relatively minor compared to permeability.

Assisted vs. Automatic History Matching. **Fig. 3.15** shows the field-wide water-cut performance for the initial geologic model, the updated model by automatic history

matching, as well as the result from assisted history matching. We can see that the initial model shows large deviations from the field production history. The results from automatic history matching exhibit significant improvement in the water-cut match. For this case, the matches from the automatic history matching appear to be better than that of assisted history matching, particularly in the early period.

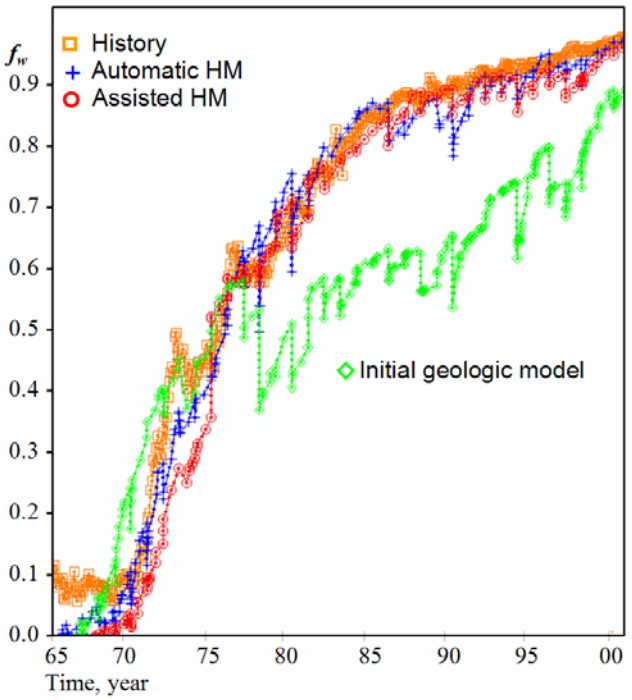

Figure 3.15 Field-wide water-cut performance for BBCK model.

The water-cut match for a few typical wells from amongst the 130 wells is given in **Fig. 3.16**. For validation purposes, we matched only part of the history data for some wells and used the updated model to predict the production performance for the rest of the period. For example, for Well 128 we matched the data only to Year 1989. Clearly, the prediction for the rest of time period shows marked improvement compared to the initial model.

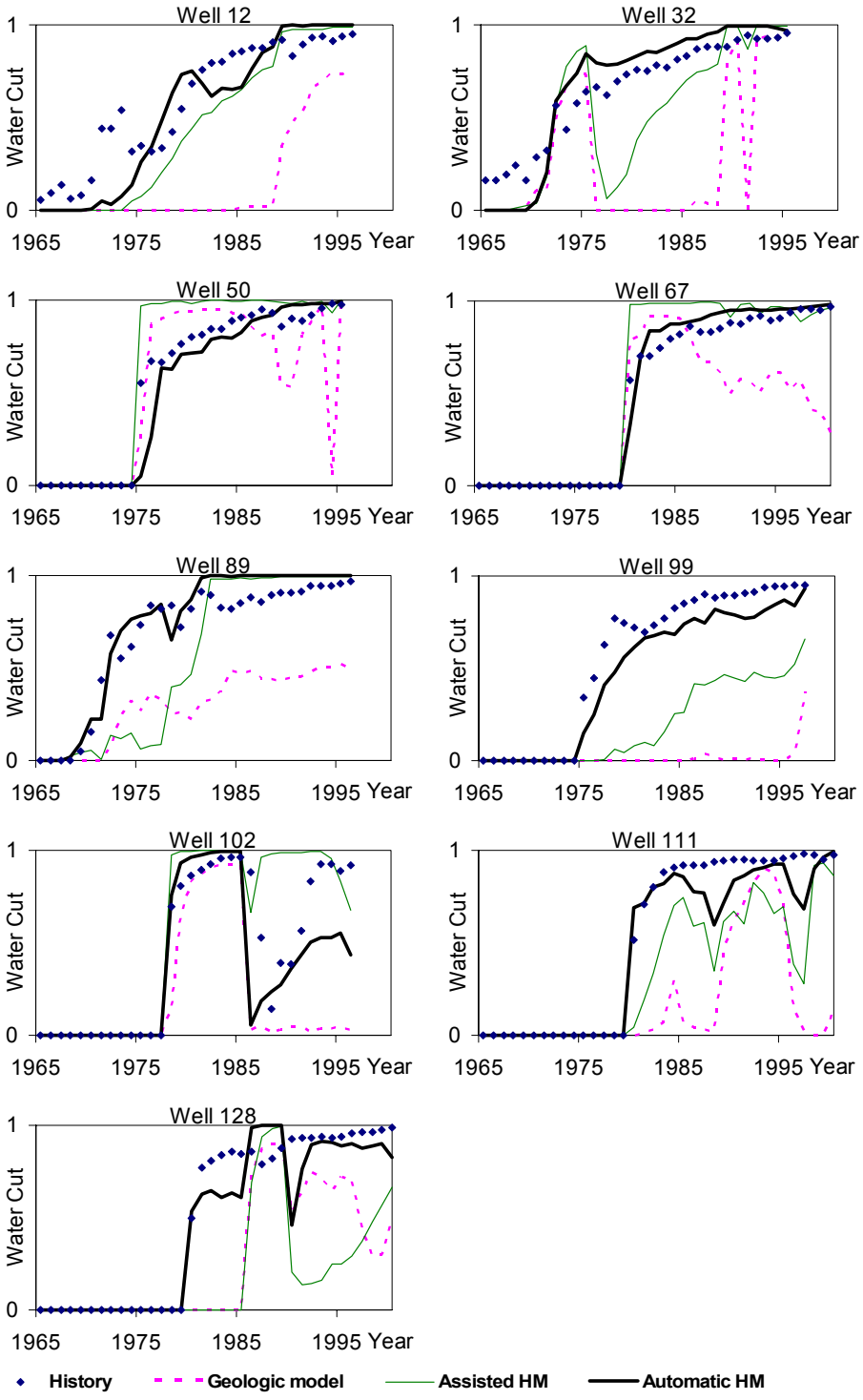

Figure 3.16 Comparison of water cut match by automatic and assisted history matching.

The permeability models before and after automatic history matching are shown in **Fig. 3.17**. The inverted model has increased heterogeneity by increasing the permeability contrast and variance. In some areas, the permeabilities are increased and in other areas decreased. Overall, the final updated model by automatic history matching preserved most of the prior geologic features while improving the history match.

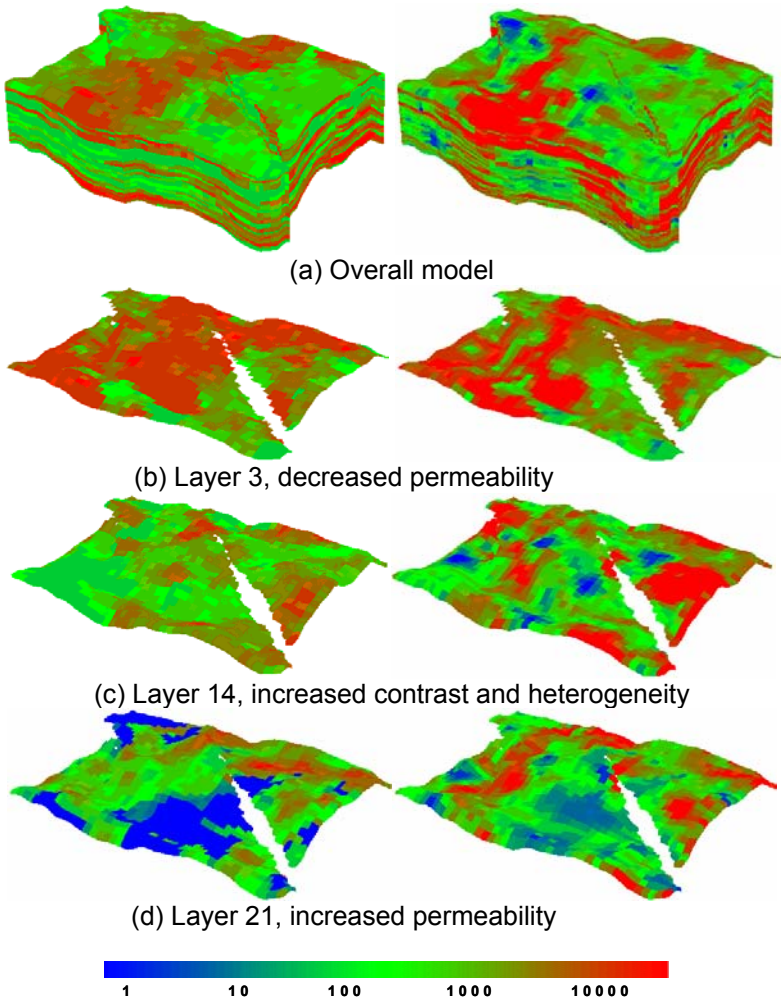

Figure 3.17 Horizontal permeability distribution of initial static geologic model (left side of each group) and the final inverted model by automatic history matching starting from the initial static model.

It should be noted that production data smoothing is an important step during generalized travel-time inversion with field data. The field production history data are frequently erratic with numerous fluctuations. Very often, the time step sizes used in the streamline simulation are larger than the intervals of observed data. Thus, the short-term fluctuations in the production data are not captured by simulation. We averaged the production data before inversion over pre-specified interval using the simulation time steps as guidelines. This helps the inversion to capture the general trend of the production history and not to be trapped by small details. Data smoothing also facilitates the calculation of the shift time during generalized travel-time calculations.

As mentioned before, the automatic history matching using streamline-derived sensitivities is very computationally efficient. For this case, it took about 5 hours for IBM Regatta workstation for 8 inversion iterations and less than one week, including the setup time, for the entire history match. Assisted history matching for the same field case will generally take much longer, of the order of a few months depending upon the experience level of the user.

Automatic History Matching as 'Post Processor' to Assisted History Matching. Here we utilize automatic history matching to further improve upon the geologic model derived from assisted history matching. The field-wide water-cut match after assisted history matching is already quite close to the history data (**Fig. 3.18**). After automatic history matching, it is further improved, particularly in the early time (see the enlarged figure of early time section on the right of Fig. 3.18).

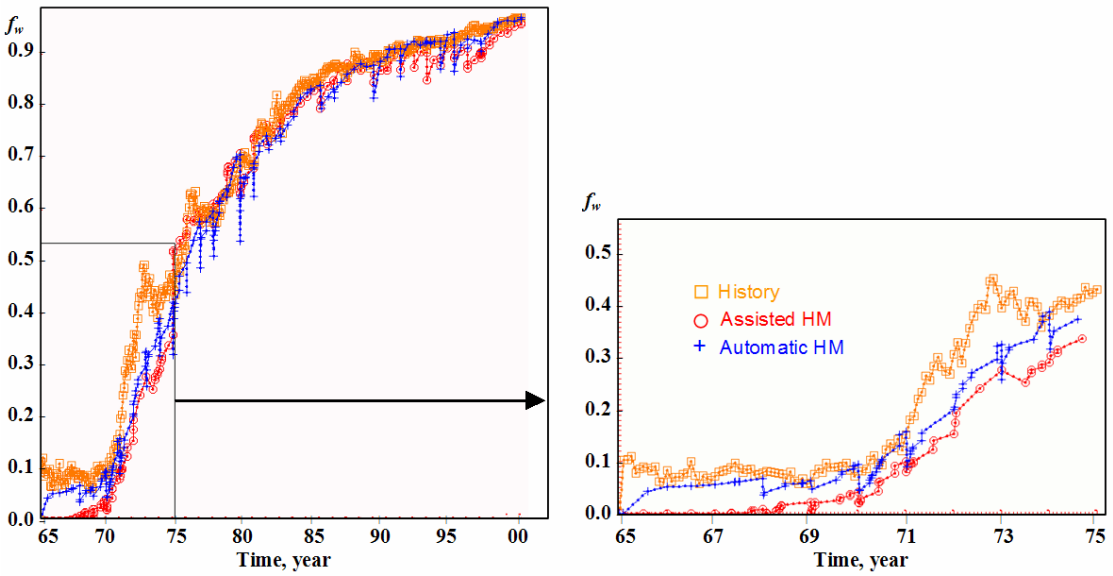

Figure 3.18 Field-wide water-cut performancefor Example 1.

For individual well-by-well water-cut matches, most wells show further significant improvement over assisted history matching (see **Fig. 3.19** for some typical wells from 130 wells). For example, the water cuts in some wells (e.g., Wells 50, 67) are shifted right to match the history, while some are shifted left (e.g., Wells 12, 89, 99) to match the history. The most significant improvement is observed for Well 99. For very few wells (3 wells), the water cut in the updated model is slightly worse than the initial model. After eight iterations, the objective function was reduced by half, and the water-cut misfit was reduced by 20 to 30 percent. Each inversion iteration consists of one forward (FrontSim[51]) simulation (about 30 minutes) and one LSQR solution (about 8 minutes). The entire history match process took about 5 hours for eight iterations in IBM Regatta workstation.

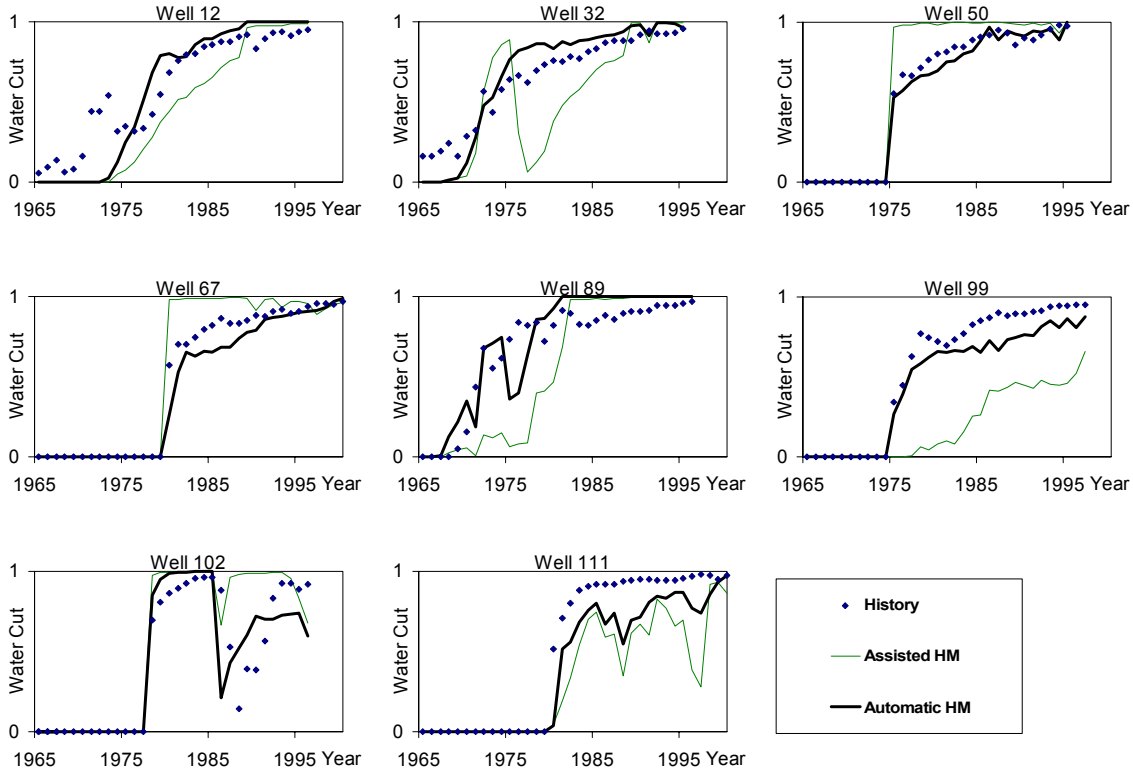

Figure 3.19 Automatic history matching improved water-cut match upon assisted history matching for most of 130 wells.

Fig. 3.20 shows the permeability models before and after automatic history matching. From a visual inspection we see that most of the features in the initial model are preserved in the updated model. However, comparing on a layer-by-layer basis, we can find some detailed changes in the model. We show a number of layers where the main changes occur.

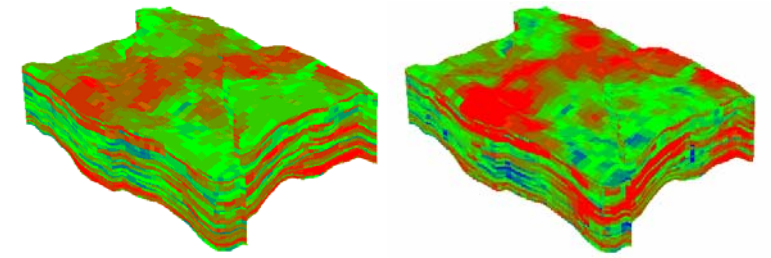

(a) Overall model

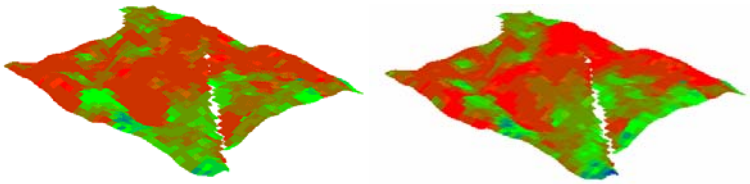

(b) Layer 3, little change, most of the layers have little change

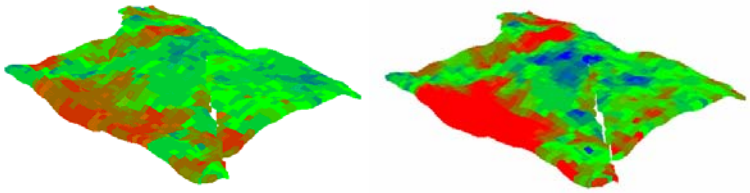

(c) Layer 8, increased contrast

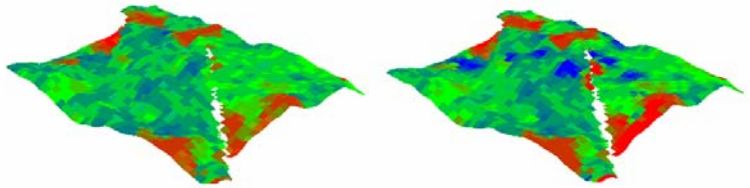

(d) Layer 13, increased permeability along fault (also in Layer 11-22)

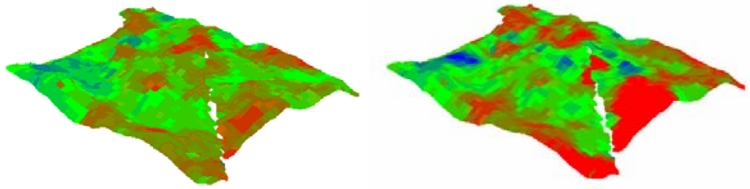

(e) Layer 14, increased permeability

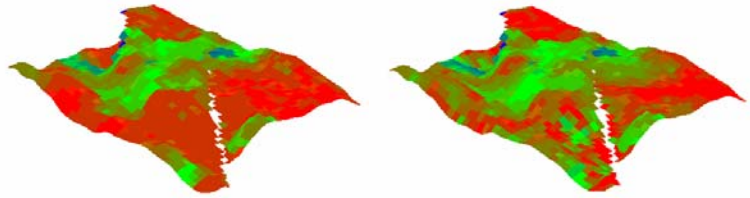

(f) Layer 34, decreased permeability

Figure 3.20 Horizontal permeability distribution for assisted history matched model (left side of each group) and automatic history matched model starting from the assisted history matched model for Example 1.

Fig. 3.21 shows the permeability histogram for four different cases: (i) the initial static geologic model, (ii) the updated model via automatic history matching starting from the initial geologic model, (iii) the updated model via assisted history matching starting from the initial geologic model, and (iv) the updated model via automatic history matching starting from assisted history-matched model.

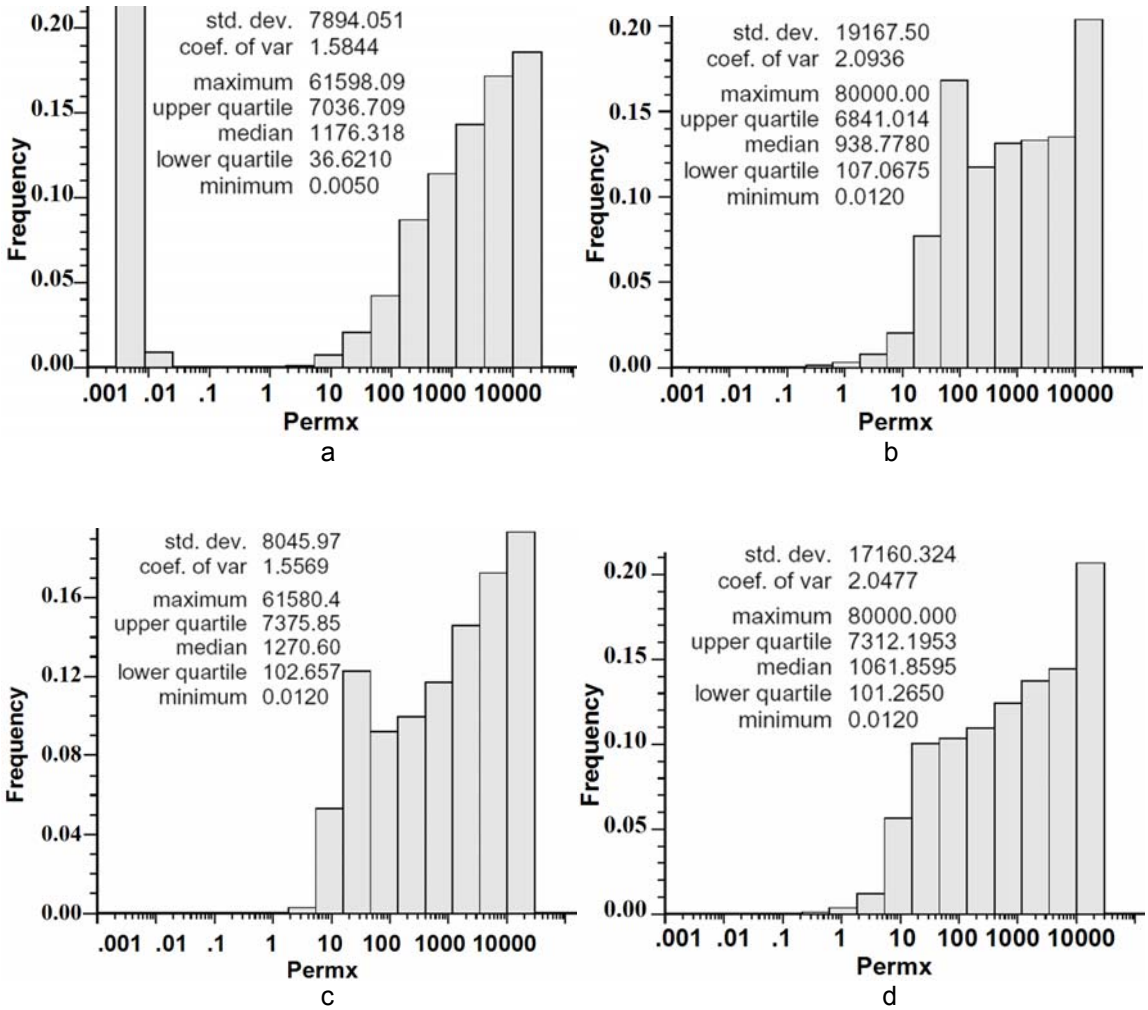

Figure 3.21 Horizontal permeability histogram for (a)static geologic model, (b) final inverted model starting from static model, (c)assisted history matched model, and (d) final inverted model starting from assisted history matched model.

We can see from Fig. 3.21 that the automatic history matching leads to a similar permeability statistics regardless of whether we started from the initial model or the updated model after assisted history matching. We can see that the low permeability at the initial geological model have been removed, indicating the need to increase permeability at the low permeability regions to match the production data. Interestingly, the histograms of the permeability models from assisted history matching and automatic history matching show very similar features. This further demonstrates that the similarity in principle between the streamline-based assisted and automatic history matching.

3.4.2 Field Example 2

This second example is a geologically complex sandstone reservoir consisting of several different facies. The reservoir lies between an underlying shale and an overlying shallow marine shale-siltstone. The reservoir itself is a structural trap (**Fig. 3.22**). The erratic distribution of sandstones and intervening shales indicate that the depositional environment was transitional and most likely associated with or part of a deltaic environment. The simulation model has 156 wells, 200×65×40 grid blocks (520,000 cells), and 28 years of production history.[5] Among the 156 wells, 83 producers which had significant water-cut response were used for production data integration purpose. There are inactive cells in the model (dark blue area in Fig. 3.22), and aquifer support was modeled by large porosity values along the periphery. Five different relative permeability zones are used. The reservoir was under primary depletion for an extended period of time, followed by peripheral water-injection.

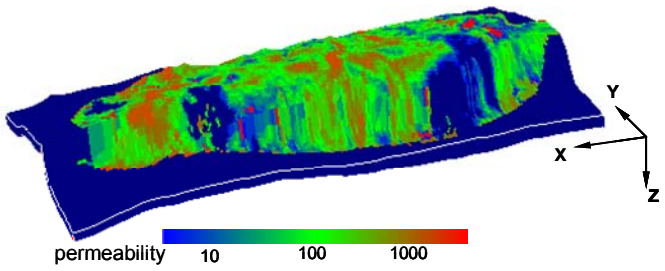

Figure 3.22 Initial static geologic model for Example 2.

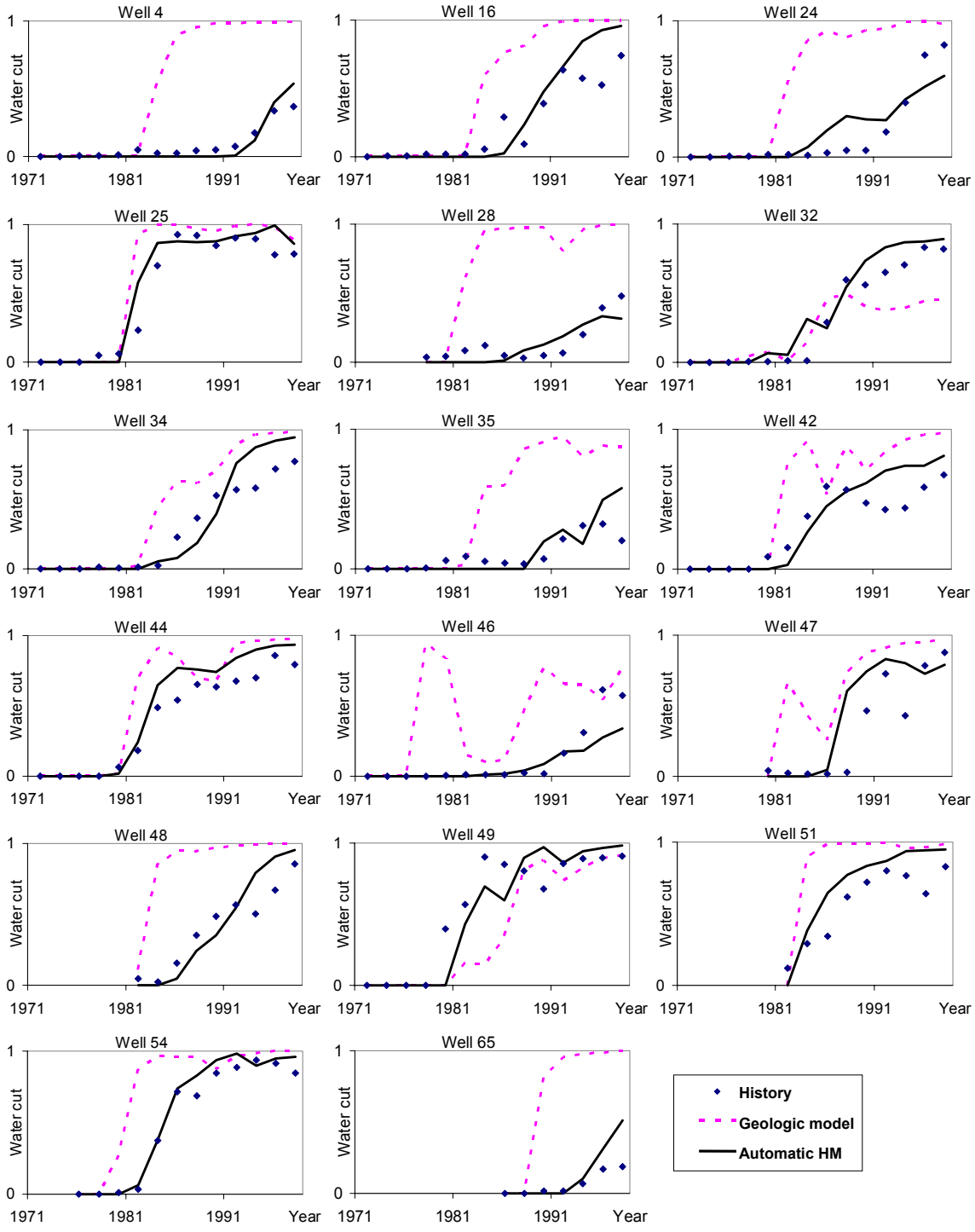

Figure 3.23 Water cut match by automatic history matching for 20 typical wells among 83 wells for Example 2.

The water-cut responses from the initial permeability model significantly deviate from the history. After 10 iterations by automatic history matching, most of the wells exhibit a much better history match. Some typical wells are shown in **Fig. 3.23**. After inversion, both shift-time misfit and water-cut misfit were reduced by about half (**Fig. 3.24**).

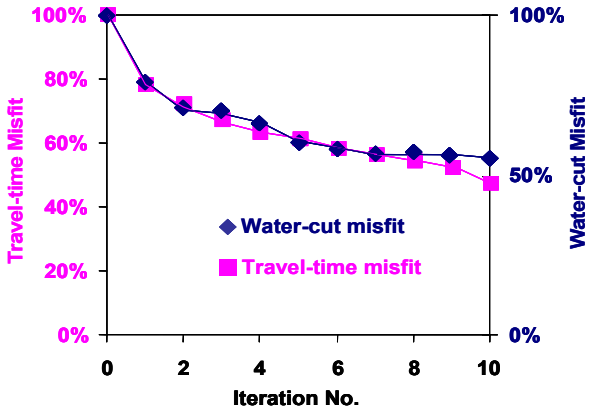

Figure 3.24 Water cut and shift time misfit reduction for Example 2 by automatic history matching.

Fig. 3.25 compares the permeability before and after the history match. For most of the 40 layers, the changes are hard to discern by visual comparison (Fig. 3.25c). This is primarily because the streamline-based sensitivities help target the changes to regions of maximum impact. Although some layers show obvious change, the general trend of the static geologic model is retained. We can see that in some areas, permeabilities are reduced (e.g., Fig. 3.25a), while for some regions, permeabilities are increased (e.g., Fig. 3.25b). We also observed that some high permeability channels are created (e.g., Figs. 3. 25b,d), while some low permeability barriers are formed (e.g., Fig. 3.25d). It is reasonable for automatic history matching to form high permeability channel and low permeability barrier for a deltaic depositional environment.

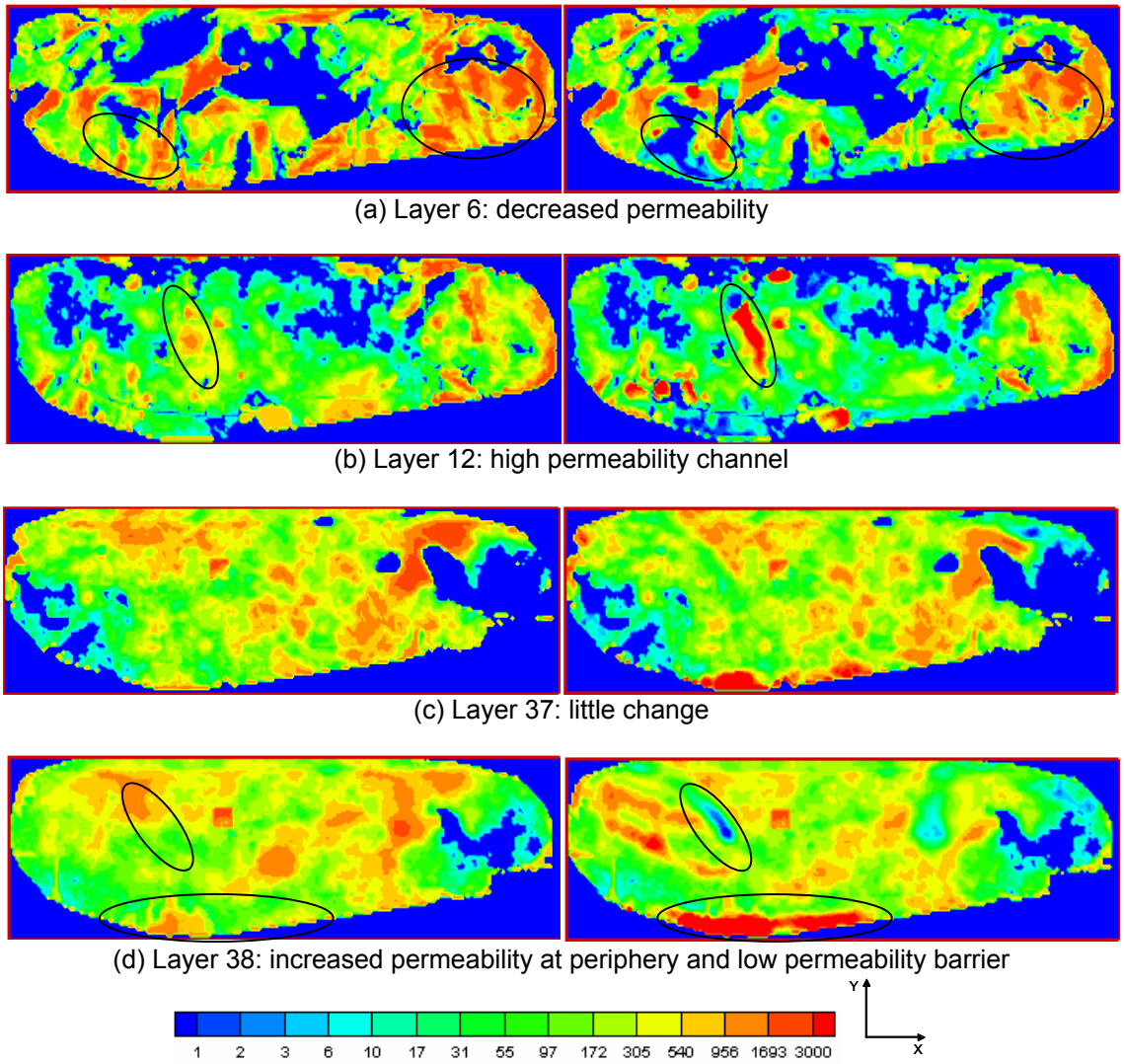

(a) Layer 6: decreased permeability

(b) Layer 12: high permeability channel

(c) Layer 37: little change

(d) Layer 38: increased permeability at periphery and low permeability barrier

Figure 3.25 Horizontal permeability distribution before (left side of each group) and after automatic history matching for Example 2.

Also from the histogram comparison (**Fig. 3.26**), we can see that the heterogeneity is increased in the updated model. This is reasonable considering the erratic distribution of sandstones and intervening shales and the depositional environment. Both the low values and the high values are further extended, and the artifacts from high permeability cut-off in the initial model seem to have disappeared in the updated model.

For this example, it took about 17 hours for IBM Regatta workstation with 10 inversion iterations and less than one week including the setup time for the entire history matching process.

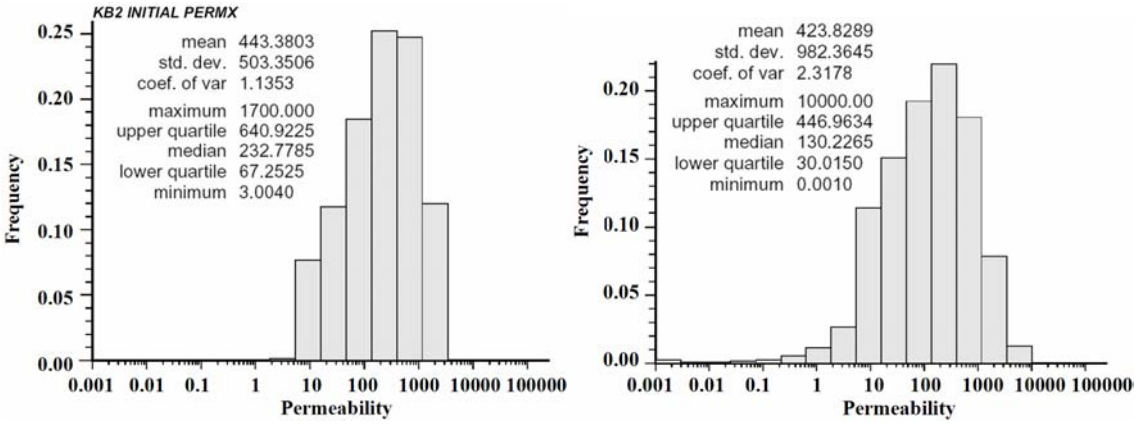

Figure 3.26 Horizontal permeability histogram before(left) and after(right) automatic history matching for Example 2.

3.5 Chapter Summary

In this chapter we highlight the similarities between streamline-based assisted and automatic history matching. We enhance the streamline-based assisted history matching in two important aspects that can significantly improve its efficiency and effectiveness. First, we utilize streamline-derived analytic sensitivities to relate the changes in reservoir properties to the production response. These sensitivities can be computed analytically and contain much more information than that used in the assisted history matching. Second, we utilize the sensitivities in an optimization procedure to determine the spatial distribution and magnitude of the changes in reservoir parameters needed to improve the history-match. By intervening at each iteration during the optimization process, we can retain control over the history matching process as in assisted history matching. This allows us to accept, reject, or modify changes during the automatic history matching

process. We have demonstrated the power and utility of our approach using two large field examples. Some specific conclusions of this chapter can be summarized as follows:

1. Use of streamline-derived sensitivities can significantly improve the efficiency of assisted history matching. In particular, the sensitivities can be utilized to directly obtain the changes in reservoir properties necessary to improve the history match in a more objective way. This eliminates the time-consuming and subjective manual adjustment of parameters in the assisted history matching process. By intervening at every stage of the iterative process, we can retain control over the history matching process to preserve plausibility and geologic realism.
2. Streamline-based sensitivities and inversion allow us to take into account the full coupling of the streamlines in the reservoir rather than changing individual wells or streamline bundles at a time. This not only significantly increases the efficiency, but also preserves geologic continuity and minimizes the chances of introducing non-physical artifacts during the history matching process.
3. The power and utility of streamline-based inversion is demonstrated using two field examples with model sizes ranging from 10^5 to 10^6 grid blocks and with over one hundred wells. In both the cases, the streamline-based automatic history matching led to better individual well matches as well as field-wide matches compared to assisted history matching and with no apparent loss of geologic realism. We have shown that the automatic history matching can be used both for conditioning geologic models and also to further improve the models derived from the assisted history matching.
4. The use of sensitivities during assisted history matching can lead to significant savings in computation time and manpower. For the field examples presented here, the automatic history matching took days compared to months for assisted history matching. This makes it possible to generate multiple history-matched models to perform uncertainty analysis.

CHAPTER IV

HISTORY MATCHING OF FINITE-DIFFERENCE MODELS USING STREAMLINE-DERIVED SENSITIVITIES*

We propose a novel approach to history matching finite-difference models that combines the advantage of the streamline models with the versatility of finite-difference simulation. Current streamline models are limited in their ability to incorporate complex physical processes and cross-streamline mechanisms in a computationally efficient manner. A unique feature of streamline models is their ability to efficiently compute the sensitivity of the production data with respect to reservoir parameters using a single flow simulation. These sensitivities define the relationship between changes in production response because of small changes in reservoir parameters and thus, form the basis for many history matching algorithms. In our approach, we utilize the streamline-derived sensitivities to facilitate history matching during finite-difference simulation. First, the velocity field from the finite-difference model is used to compute streamline trajectories, time of flight and parameter sensitivities. The sensitivities are then utilized in an inversion algorithm to update the reservoir model during finite-difference simulation.

The use of finite-difference model allows us to account for detailed process physics and compressibility effects. Although the streamline-derived sensitivities are only approximate, they do not seem to noticeably impact the quality of the match or efficiency of the approach. For history matching, we use 'a generalized travel-time inversion' that is shown to be extremely robust because of its quasi-linear properties and converges in only a few iterations. The approach is very fast and avoids much of the

---

*Part of this chapter is reprinted with permission from "Fast History Matching of Finite-Difference Models Using Streamline-Derived Sensitivities" by Cheng, H., Khargoria, A., He, Z., and Datta-Gupta, A., 2004. Paper SPE 89447 presented at the SPE/DOE fourteenth symposium on Improved Oil Recovery, Tulsa, OK, April 17-21, 2004.

subjective judgments and time-consuming trial-and-errors associated with manual history matching. We demonstrate the power and utility of our approach using a synthetic example and two field examples. The first one is from a CO_2 pilot area in the Goldsmith San Andreas Unit, a dolomite formation in west Texas with over 20 years of waterflood production history. The second example is from a giant middle-eastern reservoir and involves history matching a multimillion cell geologic model with 16 injectors and 70 producers. The final model preserved all of the prior geologic constraints while matching 30 years of production history.

4.1 Introduction

Recently, the streamline approach has provided an extremely efficient means for computing parameter sensitivities. With the streamline method, the sensitivities can be computed analytically using a single flow simulation.[13,26] Because the sensitivity calculations involve evaluation of 1-D integrals along streamlines, the method scales very well with respect to model size or the number of parameters. Although the streamline models have been extremely successful in bridging the gap between geologic modeling and flow simulation, they are currently limited in their ability to incorporate complex physical processes and cross-streamline mechanisms in a computationally efficient manner.[27] Thus, an efficient and robust approach to production data integration using finite-difference models will be particularly useful in characterizing reservoirs dominated by mechanisms such as compressibility and gravity effects, transverse dispersion and other complex physical mechanisms.

In this chapter we propose a novel approach to history matching finite-difference models that combines the advantage of the streamline models with the versatility of finite-difference simulation. We first generate streamlines using the velocity field derived from a finite-difference simulator. The streamlines are then used to compute the parameter sensitivities for updating the reservoir model. The updated model is then used

in the finite-difference simulation to predict reservoir performance and the process is repeated until a satisfactory history match is obtained. For history matching, we use 'a generalized travel-time inversion' that is shown to be extremely robust because of its quasi-linear properties and converges in only a few iterations. The approach is very fast and avoids much of the subjective judgments and time-consuming trial-and-errors associated with manual history matching. It is based upon proven techniques from geophysical inversion and is designed to preserve geologic realism during history matching. We have illustrated the power and practical feasibility of the method using synthetic and field examples.

4.2 Approach

An outline of the procedure in our proposed approach is given in a flow chart in **Fig. 4.1**. Briefly, the major steps are as follows:

4.2.1 Flow Simulation Using Finite-Difference Simulator

We have utilized a commercial finite-difference simulator (viz. ECLIPSE[52]) for modeling fluid flow in the reservoir. The two-phase black oil model used here is completely general and includes comprehensive physical mechanisms such as compressibility, gravity effects and other cross-streamline fluxes such as mobility effects, rate changes, infill drilling etc.

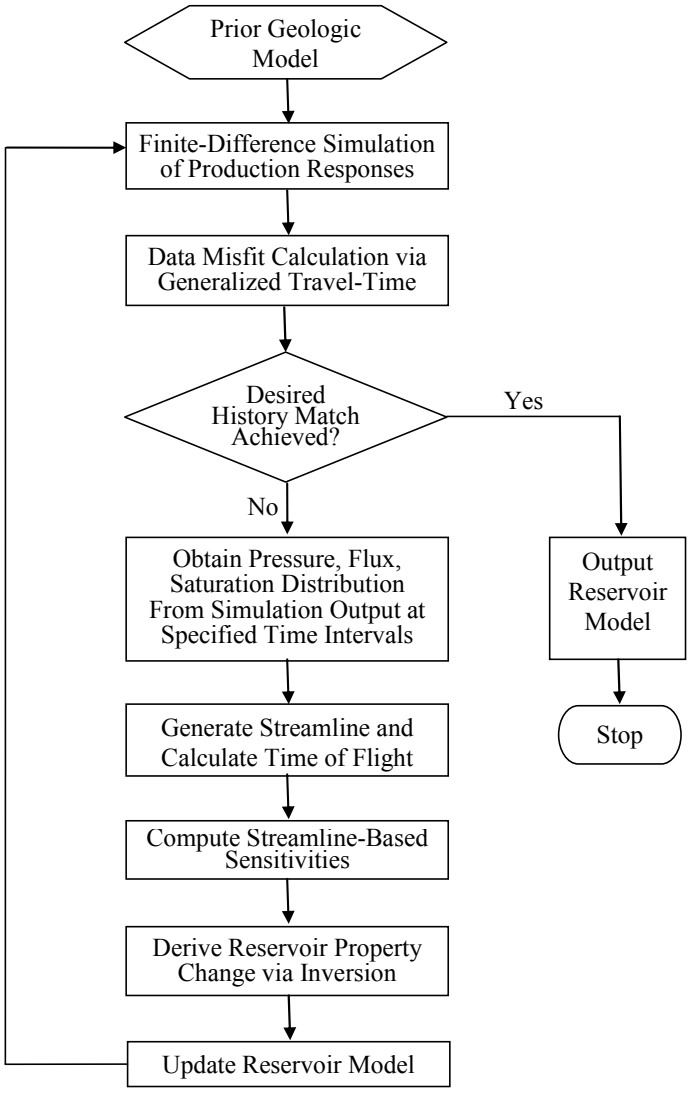

Figure 4.1 Flowchart for history matching finite-difference models using streamline-derived sensitivities.

4.2.2 Generalized Travel-Time Computations

Production data misfit is represented by a 'generalized travel-time' at each producing well. The 'generalized travel-time' is computed by systematically shifting the computed production response towards the observed data until the cross-correlation between the

two is maximized. This is illustrated in **Fig. 4.2** and is discussed further later. By defining a generalized travel time, we effectively reduce the data mismatch at a well into a single 'travel time shift' and thus, are able to retain many of the desirable properties of travel time inversion.[19]

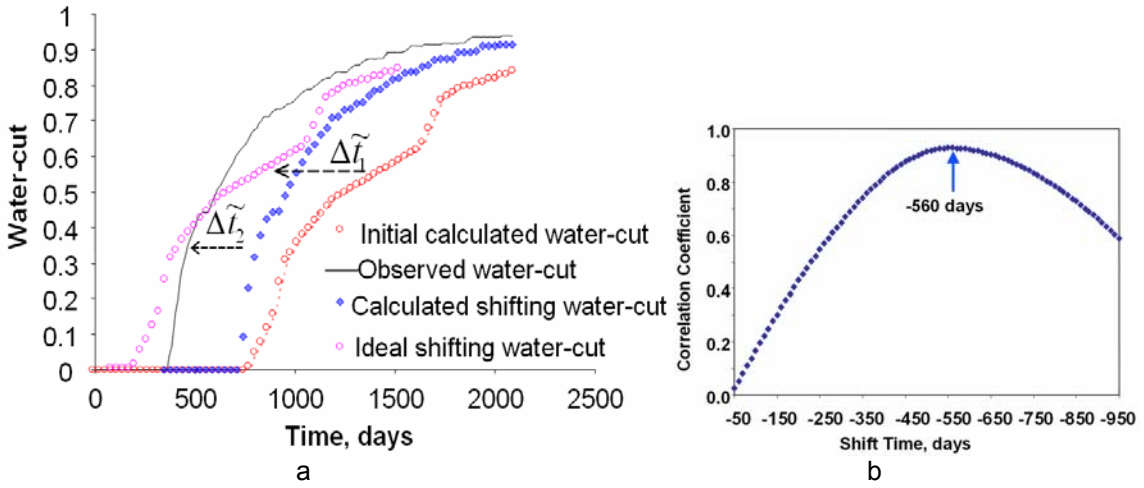

Figure 4.2 Illustration of generalized travel-time inversion: (a) history-matching by systematically shifting the calculated water-cut to the observed history, (b) best shift-time which maximizes the correlation function.

4.2.3 Streamline-Based Sensitivity Computations

The fluid fluxes obtained from the finite-difference simulator are utilized to trace streamline trajectories and calculate time of flight. These calculations can account for complex geology and faulted systems.[53,54] The time of flight is then utilized to compute the sensitivity of the generalized travel-time with respect to reservoir parameters as discussed later. Note that the sensitivity computations require a single flow simulation regardless of the number of parameters.

4.2.4 Model Updating via Generalized Travel-Time Inversion

This step involves computing the changes in the model parameters via a least-squared minimization technique that utilizes the streamline-derived sensitivity coefficients. Additional constraints are imposed to penalize deviation from a prior model to preserve geologic realism and also, to restrict permeability changes to large-scale trends consistent with the low resolution of the production data.[13]

Note that the streamline-based sensitivity computations are completely general and can account for changing conditions such as infill drilling and rate changes via streamline updating. However, these sensitivities are only approximations in the presence of compressibility and cross-streamline mechanisms. A basic premise of our approach is that these approximate sensitivities are adequate for inverse modeling. All our results indicate that this is a reasonable assumption. We store the pressure and flux information from finite-difference simulation for each streamline update for the entire simulation run. Thus, only one finite-difference simulation is required for each model update. The process is repeated until a satisfactory history match is obtained.

4.2.5 Illustration of the Procedure: A Synthetic Example

Before discussing the mathematical formulation we will first illustrate the procedure using a simple example. This involves history matching water-cut response from a 5-spot pattern with infill drilling. **Fig. 4.3a** shows the reference permeability field and well locations. The mesh size used is 21×21×1. The reference permeability distribution consists of a low-permeability trend towards north and a high-permeability trend towards south. Four infill wells (Wells 5-8) were introduced at 600 days of production. The water-cut responses from ECLIPSE for the eight producers using the reference permeability field are shown in **Fig. 4.4**. We treat this as the observed data. Next, starting from a homogeneous initial permeability model (Fig. 4.3b) we match the water-cut response via the generalized travel-time inversion. The permeability for each grid block is treated as an adjustable parameter for this example (a total of 441 parameters). The initial and final water-cut matches are shown in Figs. 4.4a and 4.4b. The final

permeability distribution is shown in Fig. 4.3c. Clearly, the final permeability model captured the large-scale trend of the reference permeability field. The permeability multipliers resulting from the history matching are shown in Fig. 4.3d. The production data integration process is very efficient and takes only a few iterations to converge (**Fig. 4.5**). The CPU time required for this case is less than 4 minutes for 16 iterations in a PC (Intel Xeon 3.06 GHz Processor).

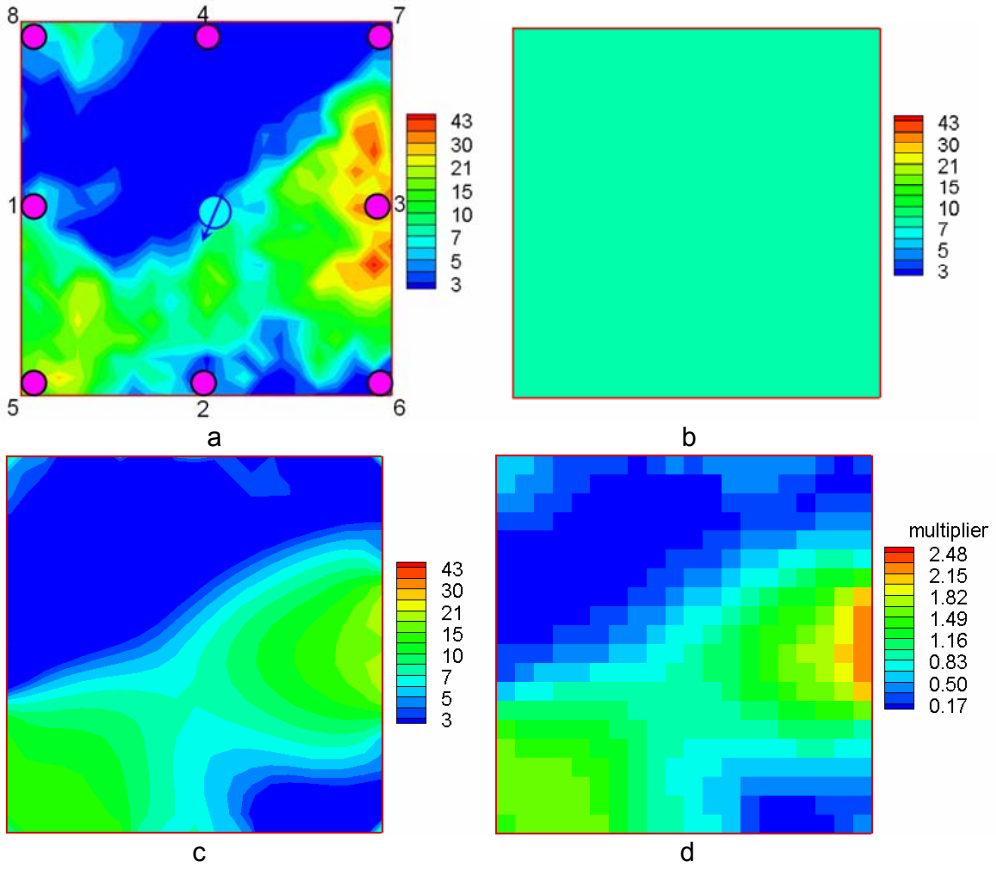

Figure 4.3 Permeability distribution for the synthetic 9-spot case: (a) reference permeability field, (b) homogeneous initial permeability, (c) final permeability distribution after inversion, and (d) permeability multiplier obtained from history matching.

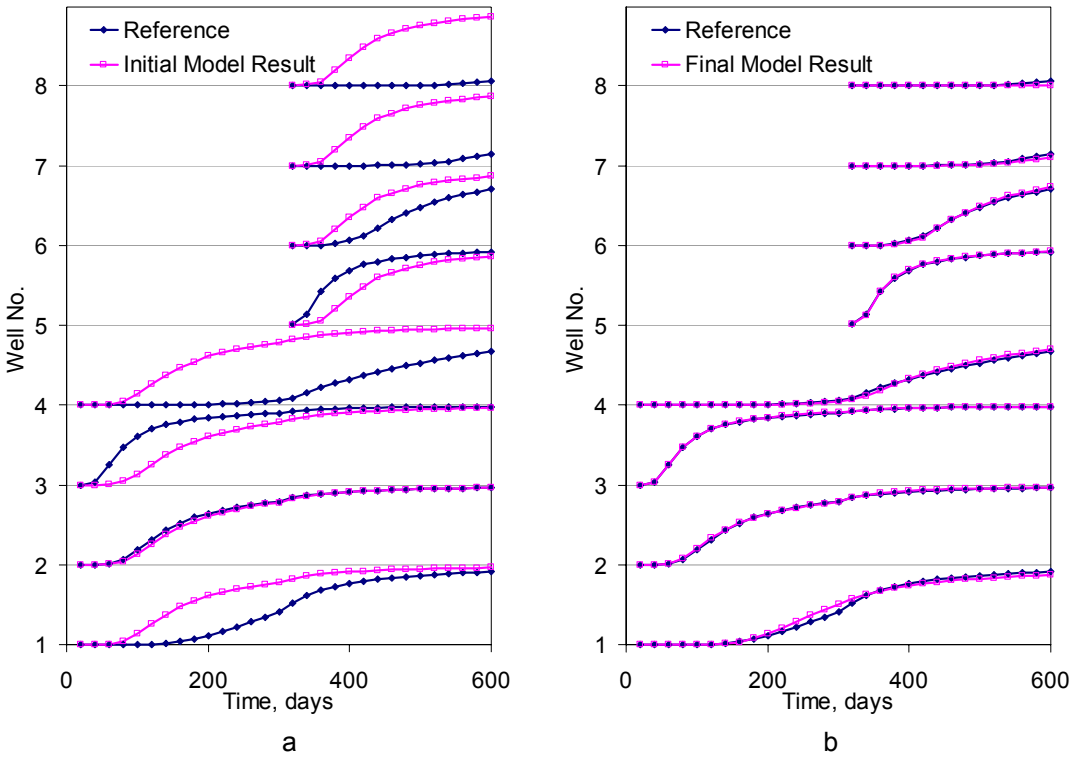

Figure 4.4 Water-cut match for the synthetic 9-spot case by (a) initial homogeneous permeability model and (b) final inverted permeability model.

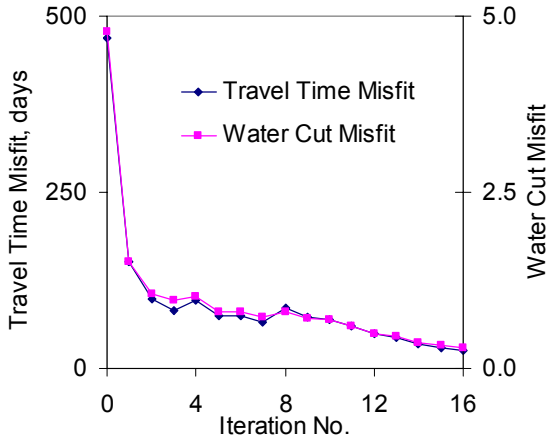

Figure 4.5 Travel-time and water-cut misfit reduction for the synthetic example.

4.3 Mathematical Background: Generalized Travel-Time Inversion and Sensitivity Computations

In this section we discuss the mathematical details related to streamline-based sensitivity computations and generalized travel-time inversion. Much of the work has been presented in our earlier papers.[13,26] We provide a summary for completeness.

4.3.1 Streamline-Based Sensitivity Calculation

The sensitivity calculations assume two-phase incompressible flow. However, we utilize these sensitivities for model updating during black-oil finite-difference simulation. The basic premise here is that the approximate sensitivities, for most purposes, are adequate for inverse modeling.

Two-phase incompressible flow equation in the streamline time of flight coordinate is given by Eq. 4.1.

$$\frac{\partial S_w}{\partial t} + \frac{\partial f_w}{\partial \tau} = 0 \,. \tag{4.1}$$

In Eq. 4.1, the time of flight can be defined in terms of 'slowness', s(x)

$$\tau = \int_{\psi} s(\boldsymbol{x}) dr \,, \tag{4.2}$$

and the 'slowness' which is the reciprocal of interstitial velocity, is given by

$$s(\boldsymbol{x}) = \frac{\phi(\boldsymbol{x})}{\lambda_{rt} k(\boldsymbol{x}) \left| \nabla P(\boldsymbol{x}) \right|} \,. \tag{4.3}$$

We assume that streamlines do not shift significantly because of small perturbations in reservoir properties. For steady velocity fields, this assumption is strictly valid for porosity and quite satisfactory for permeability changes.[36] We can now compute the sensitivity of fractional flow to reservoir parameters through a variation in the streamline time of flight as follows:

$$\delta f_w = \frac{\partial f_w}{\partial \tau} \delta \tau \,. \tag{4.4}$$

The change in the time of flight can be expressed in terms of the slowness change as

$$\delta\tau = \int_{\psi} \delta s(\boldsymbol{x}) dr \,. \tag{4.5}$$

Now, the slowness is a composite response and its variation can be related to changes in reservoir properties as follows

$$\delta s(\boldsymbol{x}) = \frac{\partial s(\boldsymbol{x})}{\partial k} \delta k(\boldsymbol{x}) + \frac{\partial s(\boldsymbol{x})}{\partial \phi} \delta\phi(\boldsymbol{x}) \,, \tag{4.6}$$

where the partial derivatives are

$$\frac{\partial s(\boldsymbol{x})}{\partial k} = \frac{-\phi(\boldsymbol{x})}{\lambda_{rt} k^2(\boldsymbol{x}) \left|\nabla P\right|} = -\frac{s(\boldsymbol{x})}{k(\boldsymbol{x})} \,, \tag{4.7}$$

$$\frac{\partial s(\boldsymbol{x})}{\partial \phi} = \frac{1}{\lambda_{rt} k(\boldsymbol{x}) \left|\nabla P\right|} = \frac{s(\boldsymbol{x})}{\phi(\boldsymbol{x})} \,. \tag{4.8}$$

The time of flight sensitivities can be obtained analytically in terms of simple integrals along streamline. For example, the time of flight sensitivity with respect to permeability will be given by[36]

$$\frac{\partial \tau}{\partial k(\boldsymbol{x})} = \int_{\Sigma} \frac{\partial s(\boldsymbol{x})}{\partial k(\boldsymbol{x})} dx = -\int_{\Sigma} \frac{s(\boldsymbol{x})}{k(\boldsymbol{x})} dx \,, \tag{4.9}$$

where the integrals are evaluated along the streamline trajectory. It is to be noted that the quantities in the sensitivity expressions are either contained in the initial reservoir model or are produced by a single simulation run.

4.3.2 Data Misfit and the Concept of a Generalized Travel-Time

Production data integration typically involves the minimization of a least squares functional representing the difference between the observed data and the calculated response from a simulator. Additional constraints are imposed via a prior geologic model to ensure 'plausibility' of the solution to the inverse problem.[10,12,13,21-23,26,27,56,57]. Production data misfit is most commonly represented as follows

$$J_p = \sum_{j=1}^{N_w} \sum_{i=1}^{N_{dj}} w_{ij} \left(y_j^{cal}(t_i) - y_j^{obs}(t_i) \right)^2, \; for \quad i = 1, \cdots, N_{dj}, \quad j = 1, \cdots, N_w \,. \tag{4.10}$$

In the above equation, $y_j(t_i)$ denotes the production data for well j at time t_i, N_w and N_{dj} stand for the number of production wells and the number of observed data at each well, respectively and w_{ij} represent the data weights. We refer to the minimization in Eq. 10 as an 'amplitude matching'. It is well known that such minimization leads to a highly non-linear inverse problem.[24] The solution to the inverse problem, in general, will be non-unique, can be unstable and often converges to a local minimum. On the other hand, a travel-time inversion whereby the observed and computed production responses are lined-up at the breakthrough time has quasi-linear properties.[31] As a result, the minimization is more robust and is relatively insensitive to the choice of the initial model.

By defining a generalized travel-time, we effectively accomplish an 'amplitude matching' while preserving most of the benefits of a travel-time inversion. In this approach, we seek an optimal time-shift at each well to minimize the production data misfit at the well. This is illustrated in Fig. 2a where the calculated water-cut response is systematically shifted in small time increments towards the observed response, and the data misfit is computed for each time increment. Taking well *j* as an example, the optimal shift will be given by the Δt_j that minimizes the misfit function,

$$J = \sum_{i=1}^{Ndj} \left[y_j^{obs}\left(t_i + \Delta t_j\right) - y_j^{cal}\left(t_i\right) \right]^2 = f(\Delta t_j). \tag{4.11}$$

Or, alternatively maximizes the coefficient of determination given by the following

$$R^2(\Delta t_j) = 1 - \frac{\sum \left[y_j^{obs}(t_i + \Delta t_j) - y_j^{cal}(t_i) \right]^2}{\sum \left[y_j^{obs}(t_i) - \overline{y_j^{obs}} \right]^2}. \tag{4.12}$$

Thus, we define the generalized travel-time as the 'optimal' time-shift $\Delta\tilde{t}_j$ that maximizes the $R^2(\Delta t_j)$ as shown in Fig. 4.2b. It is important to point out that the computation of the optimal time-shift does not require any additional flow simulations. It is carried out as a post-processing at each well after the calculated production response is derived using a flow simulation. The overall production data misfit can now be expressed in terms of a generalized travel-time misfit at all wells as follows

$$E = \sum_{j=1}^{Nw} (\Delta \tilde{t}_j)^2 . \tag{4.13}$$

4.3.3 Sensitivity of the Generalized Travel-Time

Let m represent the vector of reservoir parameters. Now, consider a small perturbation in reservoir properties, $\delta \boldsymbol{m}$, such that it results in a time-shift δt_j for the entire computed production response at well j, that is, every data point of well j has a common time-shift (**Fig. 4.6**). We then have the following relationship for the observed times $((t_{1,j}, \ldots\ldots\ldots, t_{N_{dj},j})$

$$\begin{aligned} \delta t_j &= \delta t_{1,j} = \left[\frac{\partial t_{1,j}}{\partial \boldsymbol{m}} \right]^T \delta \boldsymbol{m} , \\ &\ldots\ldots\ldots\ldots\ldots\ldots\ldots\ldots, \\ \delta t_j &= \delta t_{N_{dj},j} = \left[\frac{\partial t_{N_{dj},j}}{\partial \boldsymbol{m}} \right]^T \delta \boldsymbol{m} . \end{aligned} \tag{4.14}$$

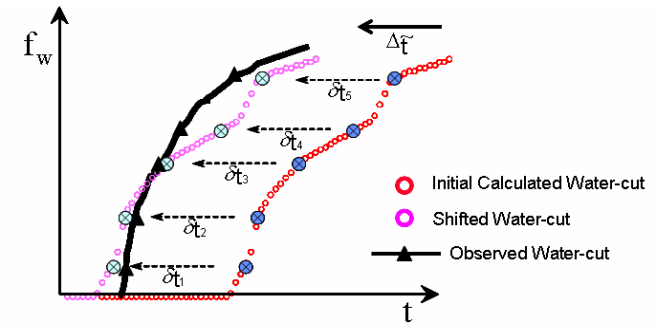

Figure 4.6 Illustration of generalized travel-time sensitivity computation using the same shift-time for every data points.

Summing Eq. 4.14 over all the data points, we can arrive at the following simple expression for the sensitivity of the travel-time shift with respect to the reservoir parameter, m, which represents a component of the vector $\boldsymbol{m}$.

$$\frac{\partial t_j}{\partial m} = \frac{\sum_{i=1}^{N_{dj}} \left(\partial t_{i,j} / \partial m \right)}{N_{dj}}. \tag{4.15}$$

Also, based on the definition of the generalized travel-time, we have the following

$$\frac{\partial \Delta \tilde{t}_j}{\partial m} = -\frac{\partial t_j}{\partial m}. \tag{4.16}$$

The negative sign in Eq. 4.16 reflects the sign convention adopted for defining the generalized travel-time shift which is considered negative if the computed response is to the right of the observed data as shown in Fig. 2a. For example, the travel-time will decrease if permeability increases; however, the 'travel-time shift' will increase.

Combining Eqs. 4.14-16, we obtain a rather simple expression for the sensitivity of the generalized travel-time with respect to reservoir parameters as follows

$$\frac{\partial \Delta \tilde{t}_j}{\partial m} = -\frac{\sum_{i=1}^{N_{dj}} \left(\partial t_{i,j} / \partial m \right)}{N_{dj}}. \tag{4.17}$$

It now remains to calculate to the sensitivity of the arrival times at the producing well, $\partial t_{i,j} / \partial m$. These sensitivities can be easily obtained in terms of the sensitivities of the streamline time of flight, and the result is as follows:

$$\frac{\partial t}{\partial m} = \frac{\dfrac{\partial \tau}{\partial m}}{\dfrac{\partial f_w}{\partial S_w}}. \tag{4.18}$$

In the above expression, the fractional flow derivatives are computed at the saturation of the outlet node of the streamline. The time of flight sensitivities can be obtained analytically as in Eq. 4.9.

There are some important practical issues that are worth mentioning here. First, changing field conditions such as infill drilling and rate changes are accounted for by streamline updating. Second, by utilizing a finite-difference simulators, we are no longer constrained by the limitations of streamline simulation. Third, for wells with no

calculated breakthrough response, the application of generalized travel-time concept is not so obvious although the basic idea remains the same. The shift-time is taken as the difference between the observed breakthrough time and the last observation time. Finally, it is better to shift the calculated curve relative to the observed curve if calculated curve has more non-zero water-cut points than the observed curve; and vice-versa.

4.4 Data Integration

Our goal is to reconcile high-resolution geologic models to field production history. This typically involves the solution of an underdetermined inverse problem. In the deterministic approach pursued here, we start with a prior static model that already incorporates geologic, well log, and seismic data. We then minimize a penalized misfit function consisting of the following three terms,

$$\left\|\Delta\tilde{\boldsymbol{t}} - \boldsymbol{S}\delta\boldsymbol{R}\right\| + \beta_1\left\|\delta\boldsymbol{R}\right\| + \beta_2\left\|\boldsymbol{L}\delta\boldsymbol{R}\right\|. \tag{4.19}$$

An alternative formulation based on the Bayesian inverse theory is given by Vega et al.[49] In Eq. 4.19, $\Delta\tilde{\boldsymbol{t}}$ is the vector of generalized travel time shift at the wells, $\boldsymbol{S}$ is the sensitivity matrix containing the sensitivities of the generalized travel time with respect to the reservoir parameters. Also, $\delta\boldsymbol{R}$ correspond to the change in the reservoir property and L is a second spatial difference operator. The first term ensures that the difference between the observed and calculated production response is minimized. The second term, called a 'norm constraint', penalizes deviations from the initial model. This helps preserve geologic realism because our initial or prior model already incorporates available geologic and static information related to the reservoir. Finally, the third term, a roughness penalty, simply recognizes the fact that production data are an integrated response and are thus, best suited to resolve large-scale structures rather than small-scale property variations.

The minimum in Eq. 4.19 can be obtained by an iterative least-squares solution to the augmented linear system

$$\begin{pmatrix} \boldsymbol{S} \\ \beta_1 \boldsymbol{I} \\ \beta_2 \boldsymbol{L} \end{pmatrix} \delta \boldsymbol{R} = \begin{pmatrix} \Delta \tilde{\boldsymbol{t}} \\ \boldsymbol{0} \\ \boldsymbol{0} \end{pmatrix}. \tag{4.20}$$

The weights β_1 and β_2 determine the relative strengths of the prior model and the roughness term. The selection of these weights can be somewhat subjective although there are guidelines in the literature.[37] In general, the inversion results will be sensitive to the choice of these weights.

Note that one of the major advantages of the generalized travel-time approach is that the size of the sensitivity matrix S is dependent only on the number of wells regardless of the number of data points. This leads to considerable savings in computation time. We use an iterative sparse matrix solver, LSQR, for solving this augmented linear system efficiently.[38] The LSQR algorithm is well suited for highly ill-conditioned systems and has been widely used for large-scale tomographic problems in seismology.[39]

4.5 Field Applications

In this section, we discuss application of the history matching algorithm to two field examples. The first one is from the Goldsmith San Andreas Unit, a dolomite formation in West Texas. We match 20 years of waterflood production history. The second field example is from a giant middle-eastern reservoir with 16 injectors and 70 producers. A total of 30 years of production history with detailed rate, infill well and re-perforation schedule were matched. Compressibility, gravity effects and aquifer support were included during the finite-difference simulation.

4.5.1 Goldsmith Case

This example includes a CO_2 pilot project area (**Fig. 4.7**) in the Goldsmith San Andres Unit (GSAU) in west Texas. The pilot area (**Fig. 4.8**) consists of nine inverted 5-spot patterns covering around 320 acres with average thickness of 100ft and has over 50 years of production history prior to CO_2 project initiation in Dec. 1996.

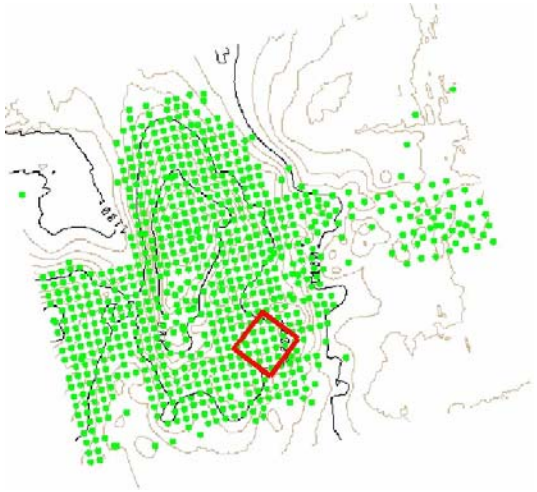

Figure 4.7 CO2 pilot project site, Goldsmith field.

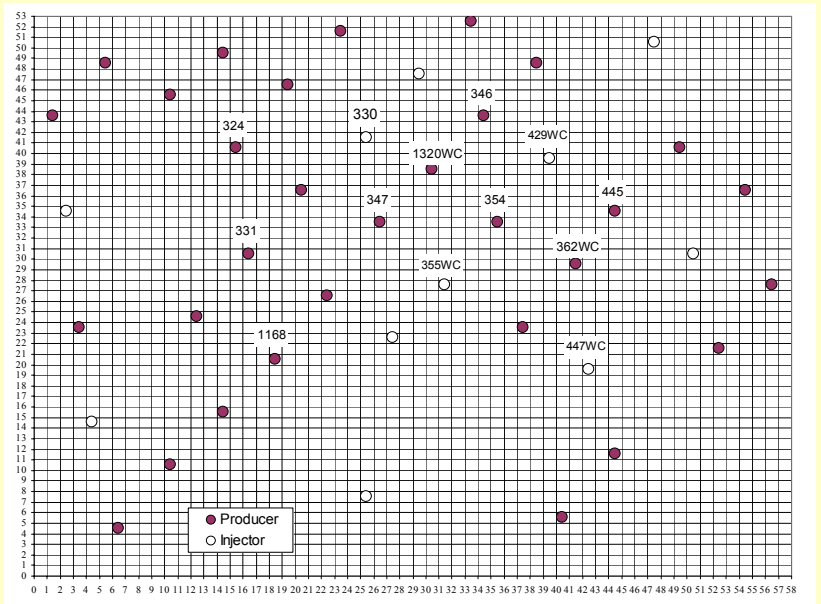

Figure 4.8 Well configuration of the study area.

We performed a history matching for 20 years of waterflood prior to the initiation of CO_2 injection. Because of the practical difficulties in establishing correct boundary conditions for the pilot area, extra wells located outside the pilot area were included in this study. The extended study area included 11 water injectors and 31 producers. Among the producers within the study area, 9 wells showed significant water-cut response before the initiation of the CO_2 injection and are used for history matching. The detailed production rates and the well schedule including infill drilling, well conversions and well shut-in can be found elsewhere.[12] The study area is discretized into 58×53×10 mesh or a total of 30,740 grid cells. The porosity field was obtained by a Sequential Gaussian Co-simulation using well and seismic data. These porosities were not altered during history matching. The initial permeability field was generated based on the porosity-permeability transform (**Fig. 4.9a**). By altering the permeability during inversion, we effectively altered the porosity-permeability transform which was considered 'soft' information for this carbonate reservoir.

We history matched 20 years of production responses for the 9 producers for the period May 1968 to December 1989. The final permeability field and the resulting permeability multipliers are shown in Figs. 4.9b and 4.9c. The permeability multipliers range from 0.05 to 20, a rather wide interval. However, the changes are restricted to small regions determined by the sensitivity calculations.

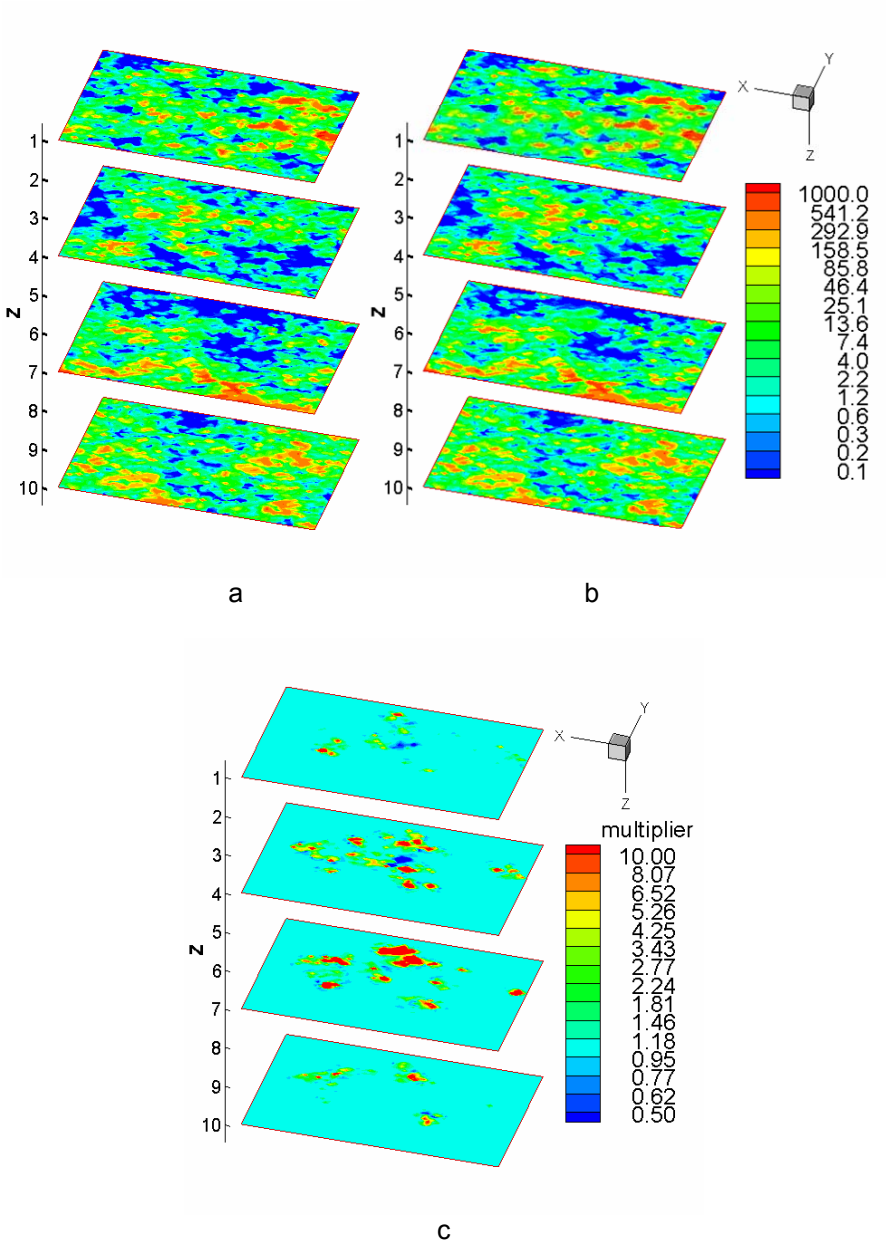

Figure 4.9 Permeability distribution for Goldsmith case: (a) initial permeability field generated via a cloud transform based on the porosity-permeability relationship, (b) final permeability field from history matching, and (c) permeability multiplier generated from history matching.

Fig. 4.10 shows the water-cut match before and after inversion. Although the initial match was already reasonable for several wells, the matches were further improved by the generalized travel-time inversion. For example, the matches for Well 4, 7, and 9 are significantly improved. **Fig. 4.11** shows the misfit versus the number of iterations during the inversion. In 9 iterations, the arrival-time misfit is reduced by over 70 percent and the water-cut misfit is reduced by one-third. **Fig. 4.12** shows misfit of arrival time at 0.2 fractional water cut. For this field example with 31 producers, 11 injectors and 20 years of history matching, the computation time requirement was about 100 minutes in a PC (Intel Xeon 3.06 GHz Processor).

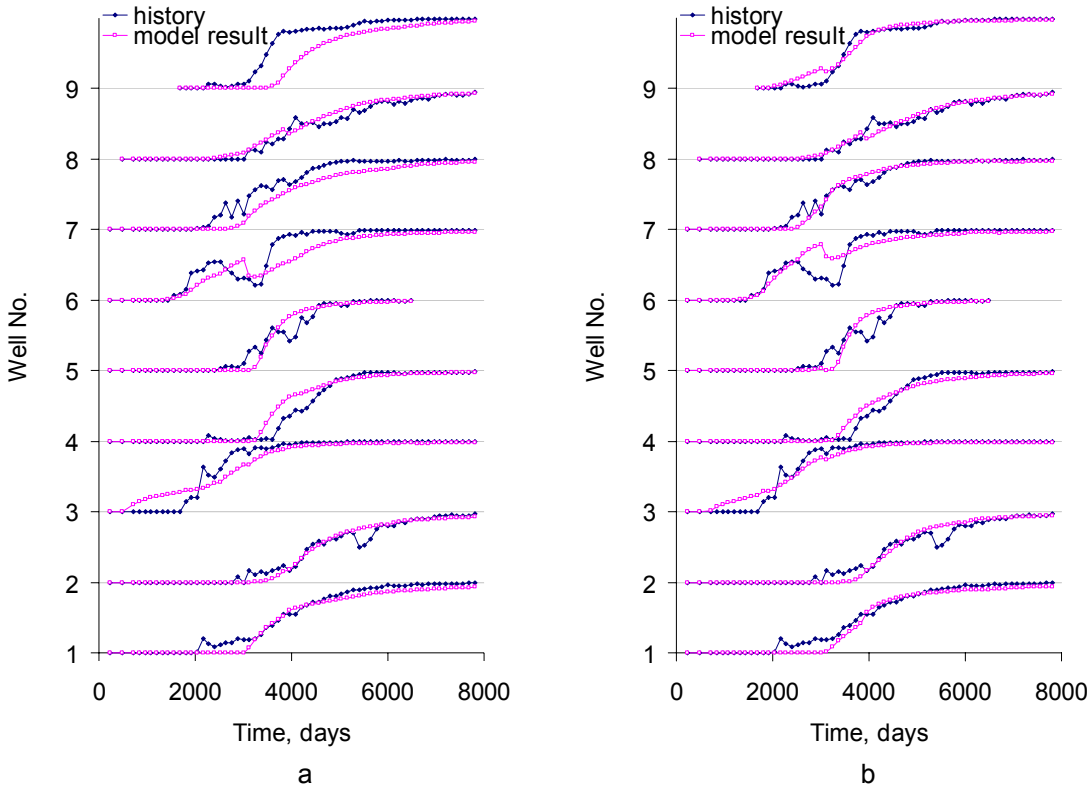

Figure 4.10 Water-cut matching for Goldsmith case: (a) initial water-cut match and (b) final water-cut match obtained from history matching.

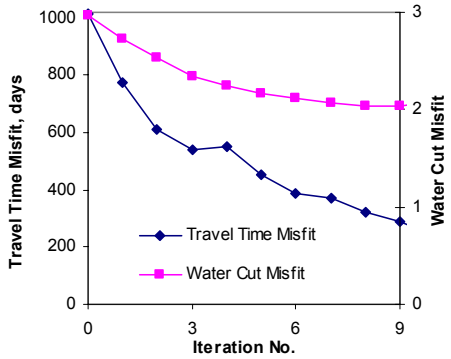

Figure 4.11 Misfit reduction for Goldsmith case.

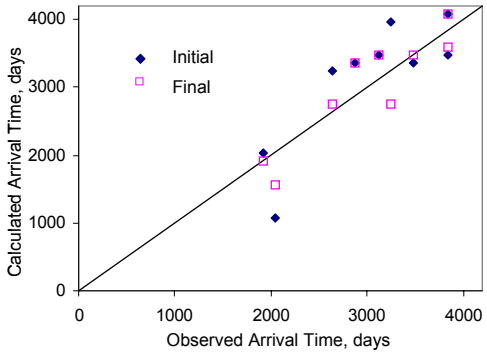

Figure 4.12 Arrival-time comparison for Goldsmith case.

4.5.2 A Giant Middle-Eastern Field Example

The reservoir under consideration is located in the middle-east and ranks 22nd largest in the world. It is a carbonate reservoir with a large north-south anticline measuring 25 km by 15 km and contains extra light crude at an average depth of 8000ft. The field has been under waterflood for the last 30 years. A detailed history matching of the water flood production response using streamline models was presented by Qassab et al.[29] Here we repeat the exercise using a commercial finite-difference simulator and the generalized travel-time inversion.

The initial geologic model was created based on well log derived porosity, facies information and 3-D seismic data. From the facies based porosity model, 3-D

permeability distributions were generated using appropriate core based porosity-permeability transforms. The fine-scale geologic model contained about 1 million cells. We utilized an upscaled model for production data integration. We performed a vertical upscaling of the geologic model to 13 layers based on the geologic markers. Cross-sections of the detailed geologic model and the corresponding upscaled model for both porosity and permeability distributions in the reservoir and the detailed upscaling methods can be found elsewhere.[55] The grid size for the upscaled model is 74×100×13. The initial water saturation in the simulation model was obtained using facies-based J-curves and capillary-gravity equilibrium conditions. Gravity effects were included in the simulation model and had a significant impact on the results, especially on the water-cut responses because of water-slumping. In addition, it was important to include fluid compressibility and aquifer influx to obtain a pressure history consistent with the field observations.

Production data smoothing is an important step during generalized travel-time inversion with field data. The field production history data are frequently erratic with large-scale fluctuations. Very often the time step sizes in simulation are larger than the intervals of observation data. Thus, the fluctuations within short time intervals in the production data are not captured by simulation. We suggest averaging (smoothing) the production data before inversion over pre-specified interval using the simulation time steps as guidelines. This helps the inversion capture the general trend of the production history and not be trapped by small details. Data smoothing also facilitates the calculation of the shift-time during generalized travel-time calculations.

Production Data Integration. Out of the 70 producers in the field (**Fig. 4.13**), 48 wells had water-cut response. Starting with the upscaled model, the grid block permeabilities were changed via the generalized travel-time inversion to match the water-cut histories at the 48 producers. **Fig. 4.14** compares the initial permeability field with the final permeability field derived after inversion. From a visual examination, it is difficult to discern any differences. This is partly a consequence of the ‘norm’ constraint

(Eq. 4.19) during the inversion that attempts to preserve the initial geologic model. Also, the streamline-based sensitivities help target the changes to regions of maximum impact. **Fig. 4.15** shows the permeability multipliers resulting from history matching and indicates the regions where permeabilities have been altered during inversion. In general, permeabilities increased at the northern higher elevation with higher quality reservoir facies. No permeability enhancements were observed in the lower interval that represents low quality reservoir. These changes are consistent with those observed by Qassab et al.[55] and were found to be geologically realistic. **Fig. 4.16** shows the misfit reduction during the inversion. In 9 iterations, the arrival-time misfit has been reduced by half and the water-cut misfit has been reduced by almost one quarter. **Fig. 4.17a** compares the observed and calculated water arrival-times at 0.1 fractional water-cut using the initial static model. After 9 iterations of generalized travel-time inversion, the corresponding arrival-times are shown in Fig. 4.17b. There is a significant reduction in the scatter indicating a close match between the observed and calculated water breakthrough times. The entire history matching took about 9 hours in a PC (Intel Xeon 3.06 GHz Processor).

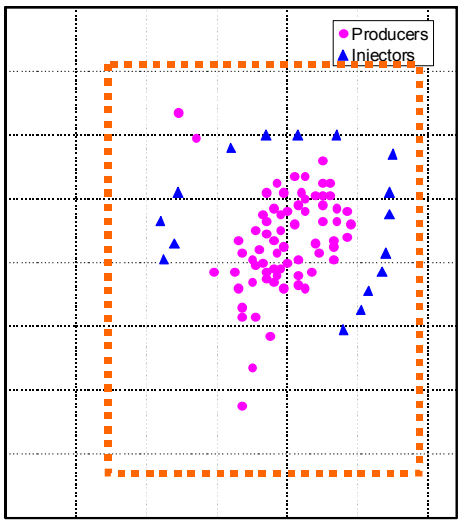

Figure 4.13 Well location map for the giant middle-eastern case. Dotted lines denote simulation area (from SPE 84079).

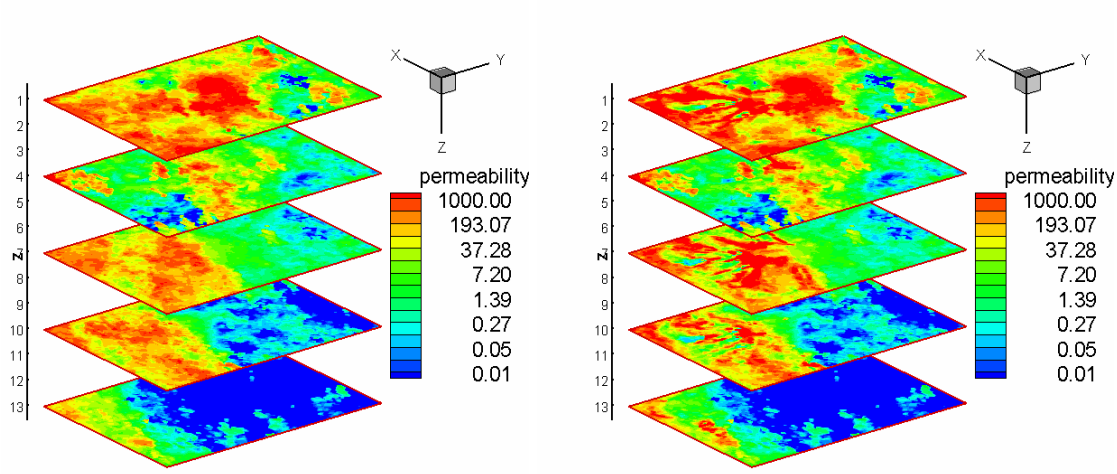

Figure 4.14 Initial upscaled permeability field (left) and final upscaled permeability field (right) after production data integration for the middle-eastern case.

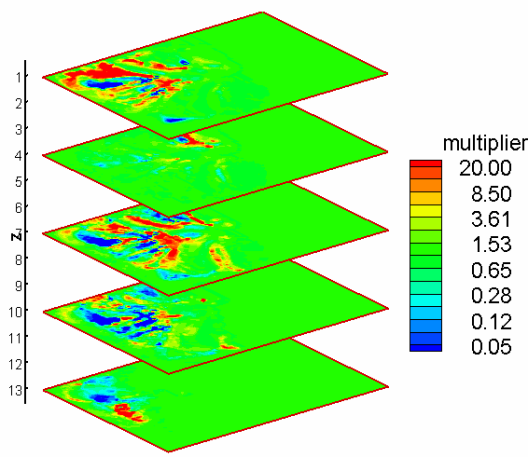

Figure 4.15 Permeability multiplier.

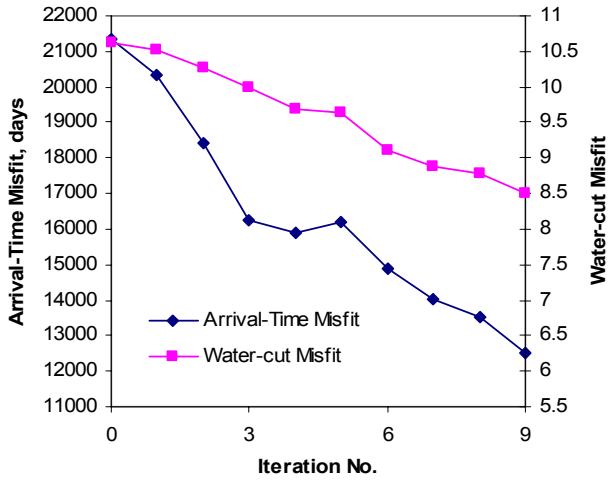

Figure 4.16 Misfit reduction for the middle-eastern case.

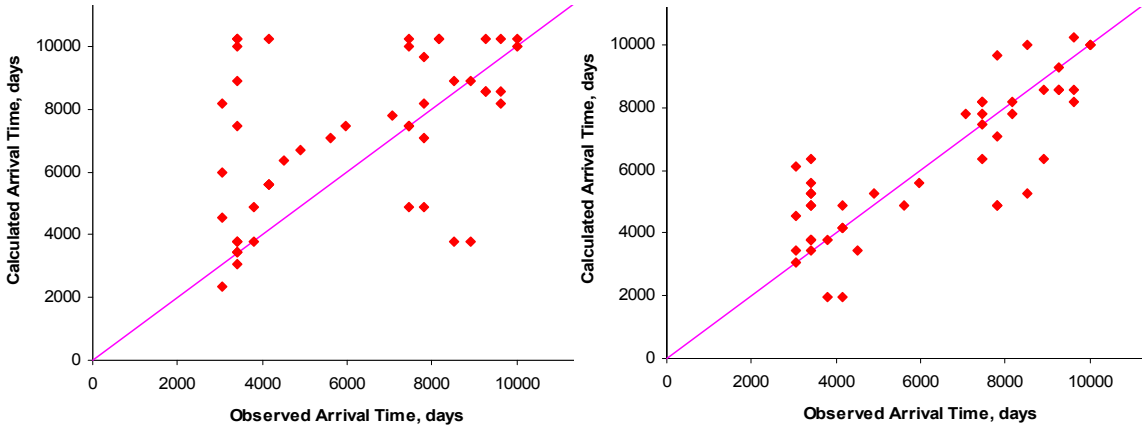

a. Initial b. Final

Figure 4.17 Arrival-time match for the giant middle-eastern case.

The water-cut match has significantly improved for most wells. Some examples of these matches are shown in **Fig. 4.18**. Specifically, the generalized travel-time inversion can match the water-cut history for wells with no calculated initial breakthroughs (Wells A, D, F, L, R, V, and X), wells with high initial water-cut (Wells J, Z, W, K, and Y), and wells with low initial water-cut and late breakthroughs (Wells M, P, G, E, and S). Generalized travel-time inversion improved the match even though the breakthrough-time is already matched (Wells Z and Y). Finally, the match in Well F shows its ability to match non-monotonic production history.

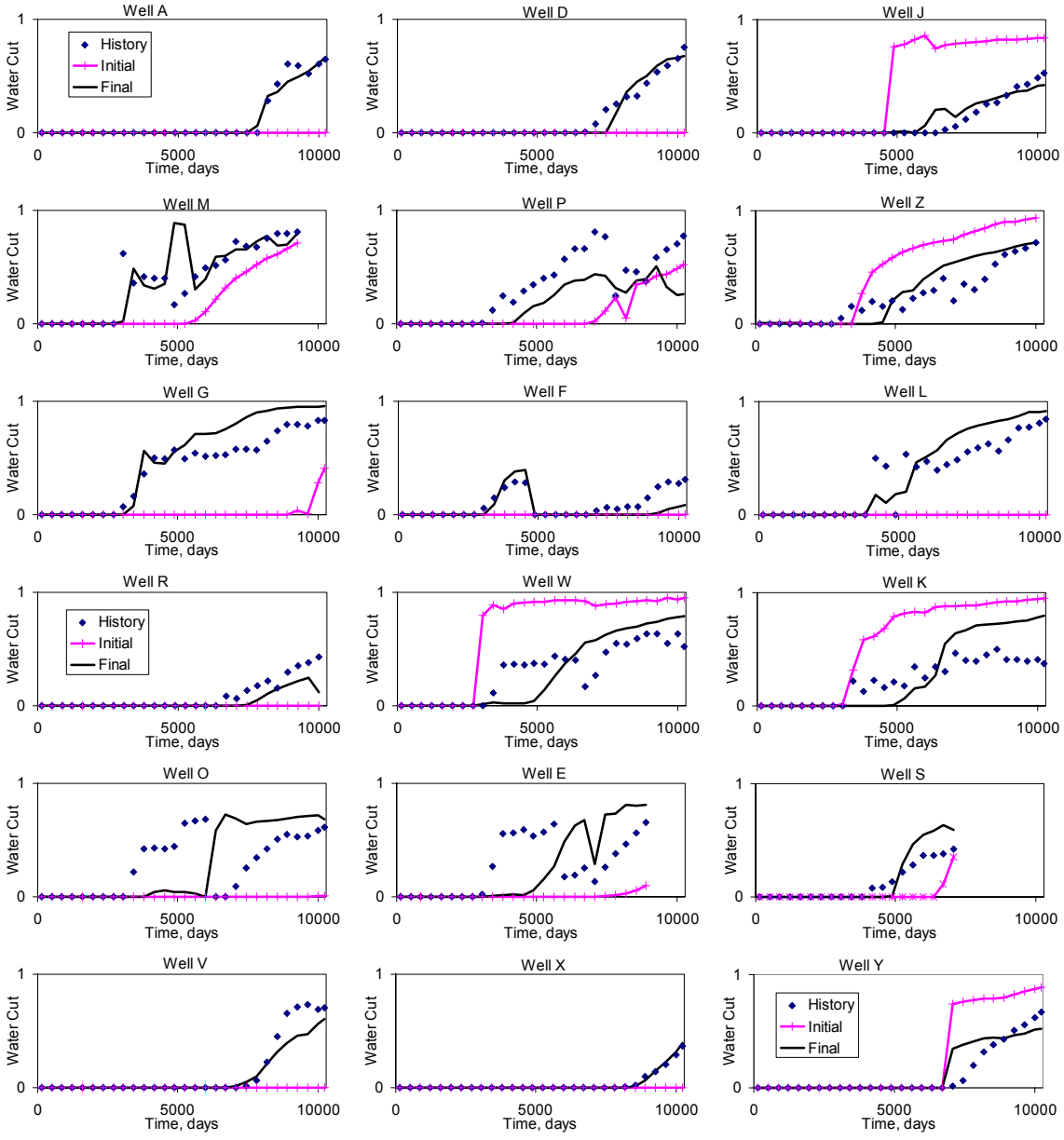

Figure 4.18 Examples of the water-cut match after history matching for the giant middle-eastern case.

The saturation distribution in the field at the end of the simulation is shown in **Fig. 4.19**. The water encroachment patterns and the unswept areas indicated by the simulation were found to be consistent with the field surveillance data.[55] The simulation model also shows evidence of water override as observed in field surveillance data.

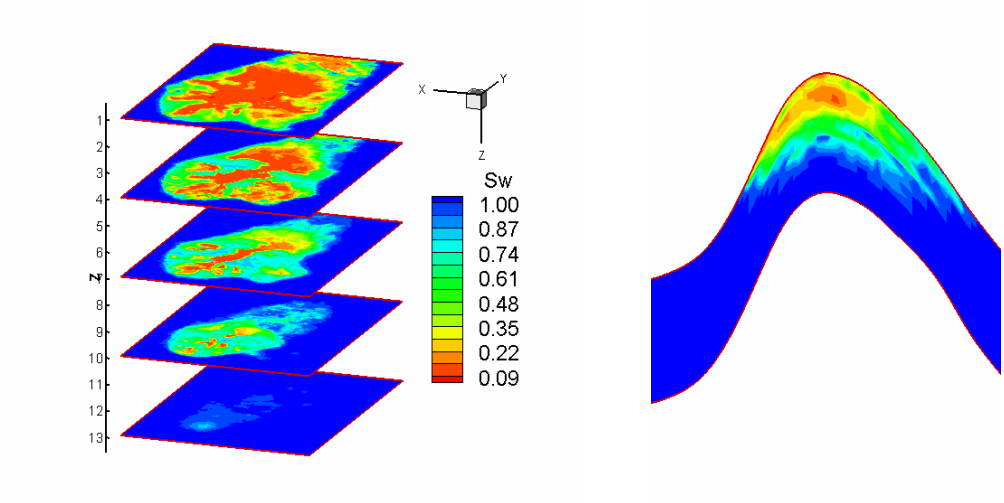

Figure 4.19 Saturation profile at 10290 days by final updated permeability. Water override is shown from the east-west cross section view.

Statistics After Inversion. We examined the impact of production data integration on the permeability distribution by comparing the statistics of the initial and the final permeability fields. As indicated in Fig. 4.20, the histograms of both the models are almost identical in terms of the median and the upper and the lower quantiles of permeability. In other words, the shape of the distribution has essentially remained unchanged. The mean permeability, however, is slightly higher after history matching. This is primarily because integration of production data has resulted in flow channels and preferential flow paths with higher permeabilities. As a result, the heterogeneity has increased in terms of standard deviation and coefficient of variation.

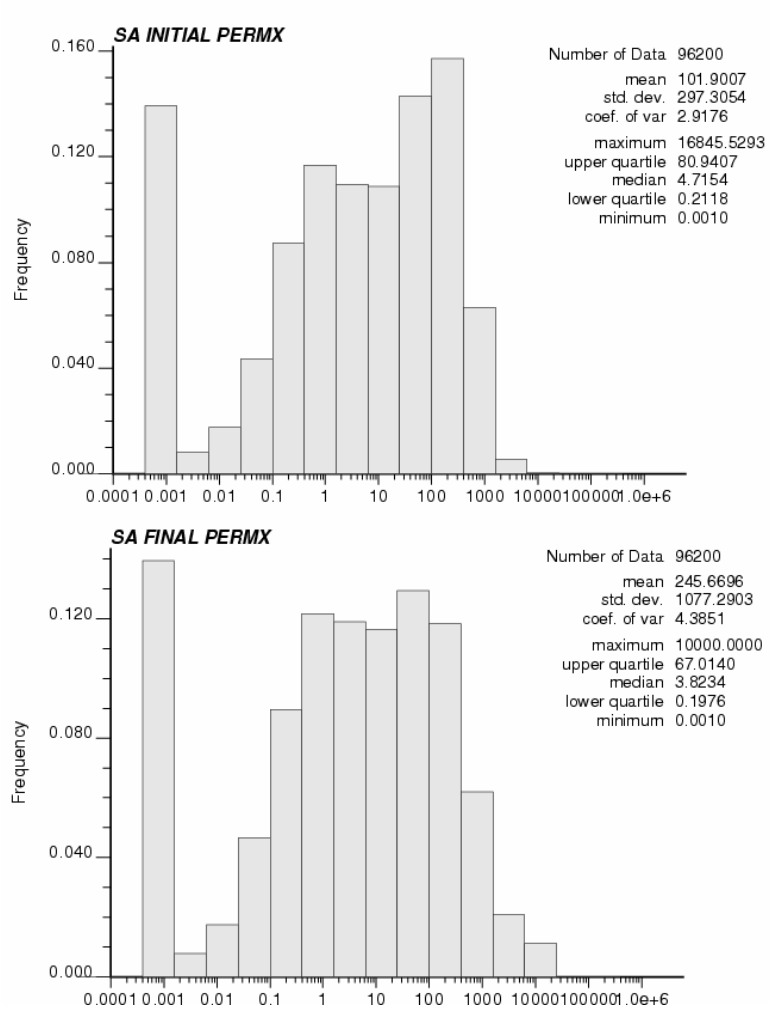

Figure 4.20 Histogram of the initial permeability and the final updated permeability for the giant middle-eastern case.

4.6 Chapter Summary

We have proposed a novel approach to history matching finite-difference models that combines the advantage of the streamline models with the versatility of finite-difference simulation. Streamline-based sensitivity calculations are shown to be adequate for finite-difference simulation with more comprehensive physical mechanisms. We have demonstrated the power and utility of our approach using both synthetic and field examples.

Some specific conclusions from this study can be summarized as follows:

1. A fast history matching approach for finite-difference models is proposed. The new approach combines the versatility of finite-difference simulation with the efficiency of streamline simulation. Use of finite-difference simulation allows us to account for detailed physics including compressibility and gravity effects and also cross-streamline mechanisms.
2. A key aspect of our proposed method is the use of streamline-based sensitivity during history matching finite-difference models. Although these sensitivities are approximate, they seem to be adequate for most purposes and do not significantly impact the quality of the match or the efficiency of the approach.
3. The generalized travel-time inversion for history matching is extremely robust because of its quasi-linear properties. It is computationally efficient, converges rapidly and is designed to preserve geologic realism during history matching. It also eliminates much of the time-consuming trial-and-error associated with manual history matching.
4. We have demonstrated the power and utility of our proposed approach using both synthetic and field examples. A full field application from a giant middle-eastern field with over 80 wells and 30 years of production history convincingly establishes the practical feasibility of the approach. The entire history matching for this field took 9 hours in a PC indicating the potential for cost savings in terms of time and manpower.

CHAPTER V

HISTORY MATCHING THREE-PHASE FLOW USING STREAMLINE MODELS

Reconciling high-resolution geologic models to field production history is still by far the most time-consuming aspect of the workflow for both geoscientists and engineers. Recently streamline-based assisted and automatic history matching techniques have shown great potential in this regard and several field applications have demonstrated the practical feasibility of the approach. However, most of these applications have been limited to two-phase water-oil flow because current streamline models are limited in their ability to incorporate highly compressible flow and cross-streamline mechanisms in a rigorous and computationally efficient manner.

In this chapter we propose an approach to history matching three-phase flow using a novel compressible streamline formulation and streamline-derived analytic sensitivities. We first generalize streamline models to account for compressible flow by introducing a relative density of total fluids along streamlines. This density term rigorously captures changes in total fluid volume with pressure and is easily traced along the streamlines. A density-dependent source term in the saturation equation accounts for the pressure effect during saturation calculations. Our approach preserves the 1-D nature of the saturation equation and all the associated advantages of the streamline approach with only minor modifications to existing streamline models. Second, we analytically compute parameter sensitivities that define the relationship between the reservoir properties and the production response, viz. water-cut and gas-oil ratio. These sensitivities are critical to history matching and streamline models allow us to compute them efficiently using a single flow simulation. Finally, for history matching we use ‘a generalized travel-time inversion’ that is shown to be extremely robust because of its quasi-linear properties and converges in only a few iterations. The approach is very fast and avoids much of the

subjective judgments and time-consuming trial-and-errors associated with manual history matching.

We demonstrate the power and utility of our approach using both synthetic and field examples. The synthetic cases include matching of water cut and gas oil ratios from a 9-spot pattern and are used to validate the method. The field-scale example is SPE ninth comparative example and consists 25 producers, 1 injector and aquifer influx. Starting with a prior geologic model, we integrate water-cut and GOR history using the generalized travel time inversion. Our approach takes only a few hours in a PC for the entire history matching without any apparent loss in geologic realism.

5.1 Introduction

In Chapter I we have already reviewed the minimization techniques and sensitivity calculation methods, here I will just mention the adjoint state method since recently it has been applied to history match three-phase flow.[58,59] The adjoint state method requires derivation and solution of adjoint equations that can be significantly smaller in number compared to the sensitivity equations. The adjoint equations are obtained by minimizing the production data misfit with flow equations as constraint and can be quite cumbersome for multiphase flow applications. Furthermore, the number of adjoint solutions will generally depend on the amount of production data and thus, length of the production history. And this restricts the application to small or synthetic cases.[58,59]

Although the streamline models have been extremely successful in bridging the gap between geologic modeling and flow simulation, they are currently limited in their ability to incorporate complex physical processes and cross-streamline mechanisms in a computationally efficient manner.[27] However, most of the applications have been limited to two-phase water-oil flow[14,15,22,26,45] because current streamline models are limited in their ability to incorporate highly compressible flow and cross-streamline mechanisms in a rigorous and computationally efficient manner.

Here for the first time we generalize streamline models to compressible flow using a rigorous formulation while retaining most its computational advantages. Our new formulation is based on three major elements and requires only minor modifications to existing streamline models. First, we introduce a relative density for the total fluids along the streamlines. This density captures the changes in the fluid volume with pressure and can be conveniently and efficiently traced along streamlines. Second, we incorporate a density-dependent source term in the saturation equation that accounts for the pressure effects during saturation calculations for compressible flow. Third, the relative density, the fluid volume, time-of-flight information are used to incorporate cross-streamline effects via pressure updates and remapping of saturations. Our proposed approach preserves the 1-D nature of the saturation calculations and all the associated advantages of the streamline approach. The saturation calculations are fully decoupled from the underlying grid and can be carried out using large time steps without grid-based stability limits.

We can history match three-phase flow using the rigorous streamline flow simulation. In addition, history matching three-phase flow using finite-difference flow simulation and streamline-based sensitivity is another option based on our vigorous streamline formulations. In order to get the sensitivities for three-phase flow, first, the velocity field from the finite-difference model is used to compute streamline trajectories and time of flight. Then the analytic sensitivities are calculated along the streamlines using a rigorous compressible streamline formulation. Our new rigorous compressible streamline sensitivity formulation is based on three elements as described above. The rigorous flow equation is used to derive water cut and gas/oil ratio sensitivities along the streamlines. Then, the relative density, the fluid volume, time-of-flight, and fractional flow information are used to map the streamline sensitivities to the cell sensitivities which are then utilized in an inversion algorithm to update the reservoir model during finite-difference simulation. For history matching, we use ‘a generalized travel-time inversion’ that is shown to be extremely robust because of its quasi-linear properties and converges in only a few iterations.

In this chapter, first a synthetic example is used to illustrate the procedure. Then the streamline formulations for compressible and three-phase flow are described. Comparison of incompressible and compressible streamline simulation will be shown. Then I will discuss analytical water-cut and gas/oil ratio sensitivity calculations for compressible and three-phase flow. A field-scale example is shown to validate this method.

5.2 Background and Illustration

Before going to the rigorous streamline mathematical formulations, a brief review of the production data integration procedure will be given and an illustrative example will be shown.

Streamline-based automatic history matching utilizes streamline-derived sensitivities to update geologic models. The major steps are: (i) Flow simulation to compute production response at the wells, either by commercial finite-difference simulators which can handle compressible and three-phase flow or by rigorous streamline simulation; (ii) Quantification of the mismatch between observed and computed production response; (iii) Streamline-based analytic sensitivity computation of the production response (water-cut and gas/oil ratio) with respect to reservoir parameters; (iv) Updating reservoir properties to match the production history via inverse modeling.

5.2.1 Synthetic Example

The synthetic case involves three-phase flow and includes matching water-cut and GOR from a 9-spot pattern starting with a homogeneous permeability distribution (**Fig.5.1a**). The mesh size used is 21×21×1. The reference permeability distribution consists of a low-permeability trend towards north and a high-permeability trend towards south. The water-cut and GOR simulation responses from the reference permeability field are shown in **Figs. 5.2** and **5.3**. We treat this as the observed data. Next, starting from a

homogeneous initial permeability model we jointly match the water-cut and GOR response via the generalized travel-time inversion. The permeability for each grid block is treated as an adjustable parameter for this example (a total of 441 parameters). The comparison of initial and final updated water-cut matches is shown in Fig. 5.2, and that of GOR is in Fig. 5.3. The final permeability distribution is shown in Fig. 5.1b. Clearly, the final permeability model captured the large-scale trend of the reference permeability field. The production data integration process is very efficient and takes only a few iterations to converge (**Fig. 5.4**). The CPU time required for this case is less than 10 minutes for 10 iterations in a PC (Intel Xeon 3.06 GHz Processor).

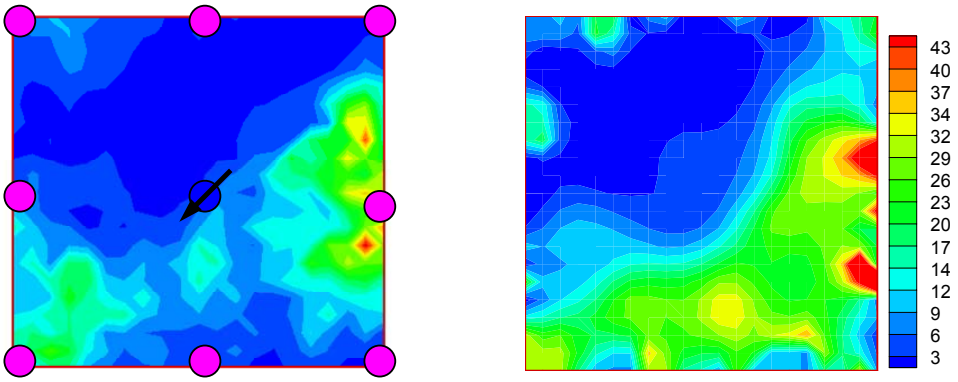

(a) reference permeability (b) final permeability

Figure 5.1 History matching 3-phase finite-difference model for a nine-spot heterogeneous case.

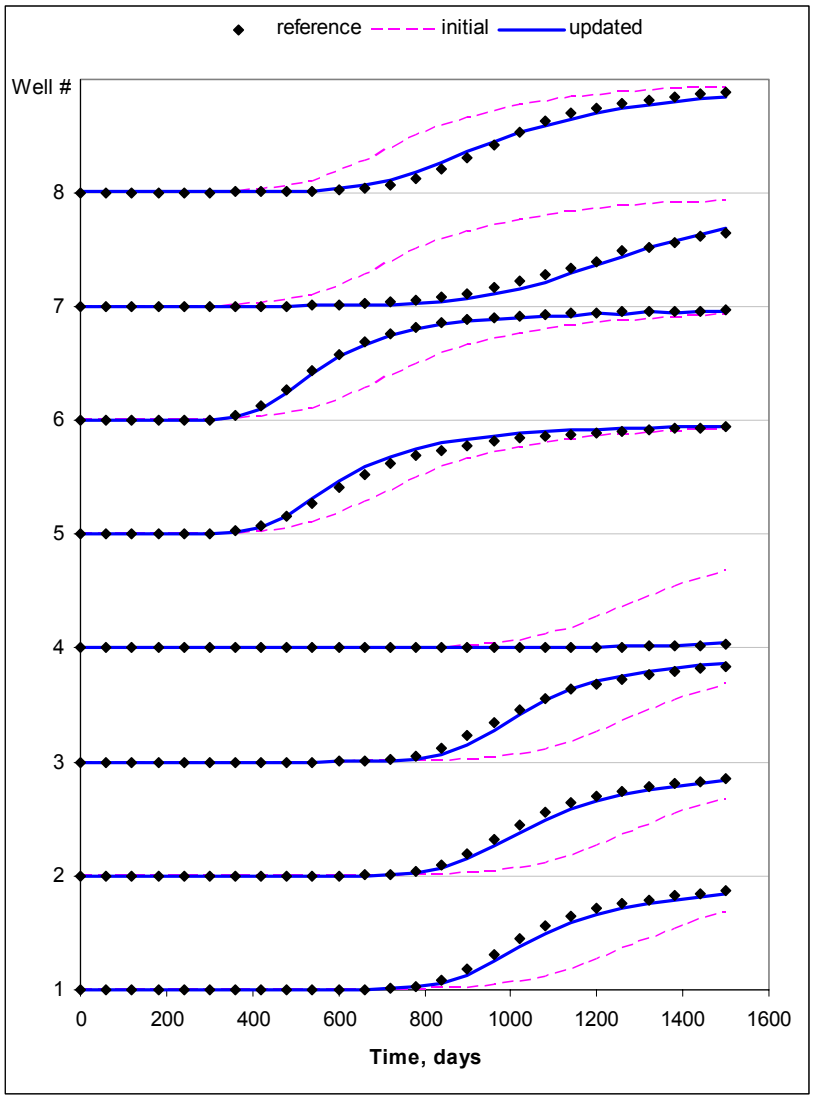

Figure 5.2 History matching 3-phase finite-difference model for a nine-spot heterogeneous case: water-cut match.

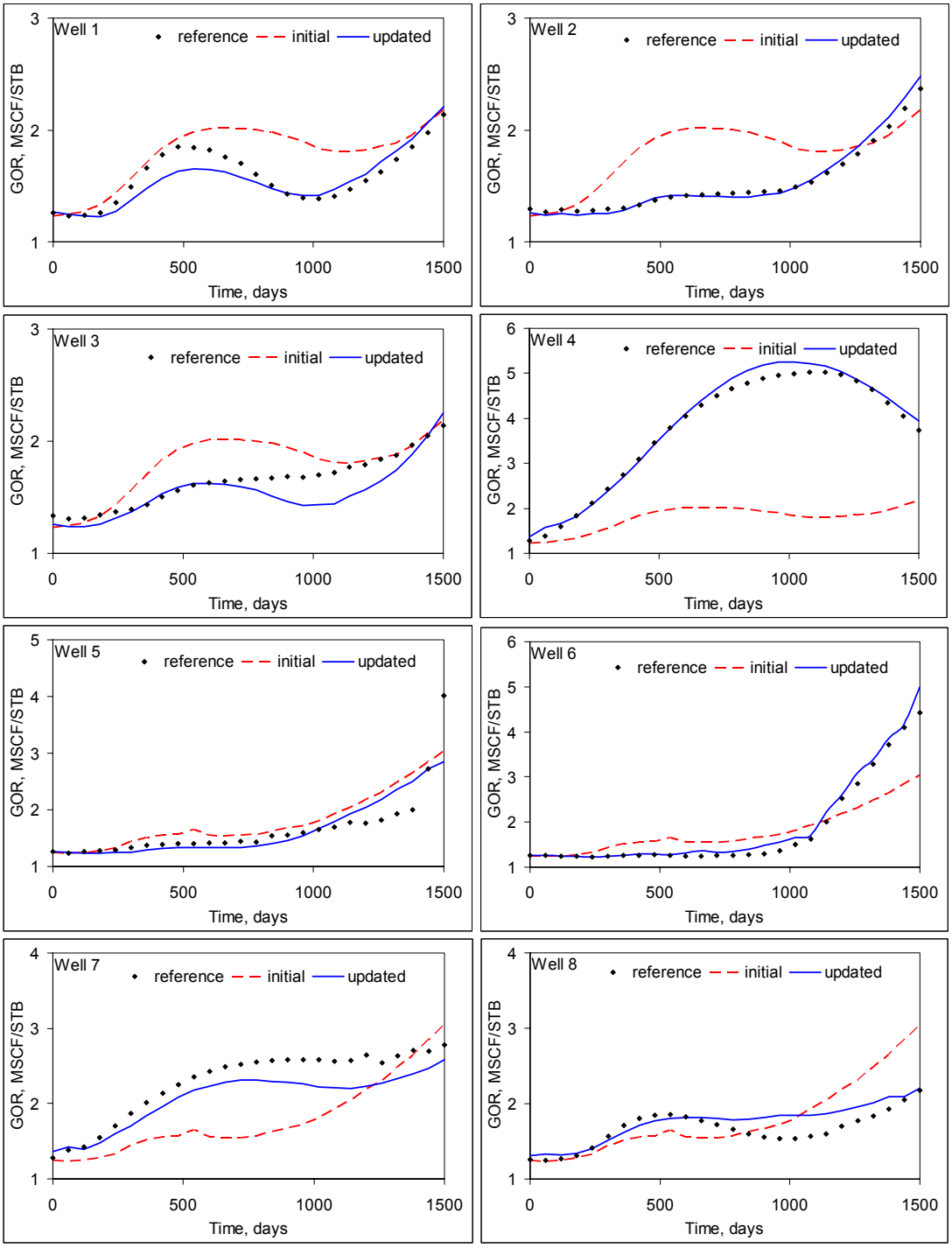

Figure 5.3 History matching 3-phase finite-difference model for a nine-spot heterogeneous case: gas/oil ratio match.

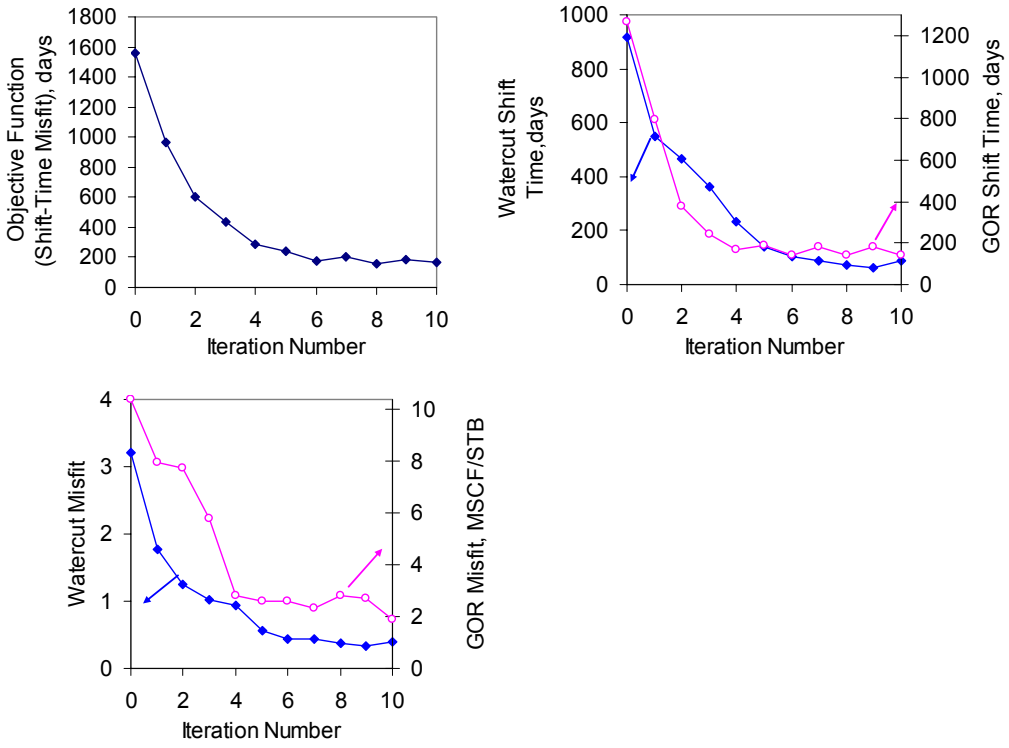

Figure 5.4 History matching 3-phase finite-difference model for a nine-spot heterogeneous case: objective function reduction, water cut and GOR shift-time misfit reduction, and water cut and GOR amplitude misfit reduction.

5.3 Mathematical Formulation

5.3.1 Compressible Streamline Simulation

Before going to sensitivity calculations, let's first examine the formulations for compressible and three-phase streamline simulation. Although streamline-based history matching techniques have shown great potential, most of the applications have been limited to two-phase water-oil flow because current streamline models are limited in their ability to incorporate highly compressible flow and cross-streamline mechanisms in a rigorous and computationally efficient manner. In the following sections, I will show how to rigorously extend streamline simulations to compressible and 3-phase flow.

Relative Density for Compressible Flow. From Bear (1972),[60] the mass conservation equation is

$$\nabla \cdot (\rho u) + \frac{\partial \rho}{\partial t} = 0 \tag{5.1a}$$

For steady state flow, although the divergence of volumetric flux of compressible fluid flow is not zero, the divergence of mass flux of that is going to be zero as follows,

$$\nabla \cdot (\rho u) = 0 \tag{5.1b}$$

Between pressure updating we can treat the flow as steady state.

If we expand it,

$$\nabla \cdot (\rho u) = u \cdot \nabla \rho + \rho \nabla \cdot u = 0 \tag{5.2}$$

Suppose we give $\nabla \cdot u = c$ [Constant], the equation above will be,

$$u \cdot \nabla \rho + \rho c = 0 \tag{5.3}$$

Introducing the time of flight equation, $u \cdot \nabla = \phi \frac{\partial}{\partial \tau}$,

$$u \cdot \nabla \rho + \rho c = \phi \frac{\partial \rho}{\partial \tau} + \rho c = 0 \tag{5.4}$$

Now the gradient of density is converted from three dimensional (*x,y,z*) coordinate to one dimensional (τ) coordinate by introducing the time of flight.

By using the above equation, we are able to trace the density from Injector to Producer as the example below,

$$\frac{\partial \rho}{\rho} = -\frac{c}{\phi} \partial \tau \rightarrow \int_{p_1}^{p_2} \frac{\partial \rho}{\rho} = -\frac{c}{\phi} \int_0^{\Delta \tau} \partial \tau \rightarrow \ln \frac{\rho_2}{\rho_1} = -\frac{c}{\phi} \Delta \tau \rightarrow \rho_2 = \rho_1 \exp(-\frac{c}{\phi} \Delta \tau) \tag{5.5}$$

The initial density ρ is starting from the unity at the injector.

The equation above simply shows that the density will vary with the divergence of flux (*c*, flux out minus flux in for x, y, z directions), porosity (ϕ) and the difference of (τ) within the particular interval along a streamline. If we have incompressible fluid flow which is simply $c = 0$, then the density will keep the initial unity value till the producer.

Mass Conservation Equation for Compressible Fluid Flow With Density-Dependent Source Term. The next question will be how we use the coordinate transformation. Mass conservation equation for compressible fluid flow will be given as follows,

$$\phi\frac{\partial}{\partial t}\left(\frac{S_w}{B_w}\right)+\nabla\cdot\left(\frac{f_w u_t}{B_w}\right)=0 \tag{5.6}$$

$$\phi\frac{\partial}{\partial t}\left(\frac{S_w}{B_w}\right)+\frac{f_w}{B_w}\nabla\cdot u_t+u_t\cdot\nabla\left(\frac{f_w}{B_w}\right)=0 \tag{5.7}$$

Again introducing the time of flight equation, $u\cdot\nabla=\phi\frac{\partial}{\partial\tau}$, and $\nabla\cdot u=c\,[\text{Constant}]$,

$$\phi\frac{\partial}{\partial t}\left(\frac{S_w}{B_w}\right)+\phi\frac{\partial}{\partial\tau}\left(\frac{f_w}{B_w}\right)=-\frac{f_w}{B_w}c \tag{5.8}$$

$$\frac{\partial}{\partial t}\left(\frac{S_w}{B_w}\right)+\frac{\partial}{\partial\tau}\left(\frac{f_w}{B_w}\right)=-\frac{c}{\phi}\frac{f_w}{B_w} \tag{5.9}$$

We can think the right hand term as the source term because of compressibility such as the expansion of the fluid. It is important to emphasize that we could transform the coordinate of the density from three dimensional to one dimensional along streamline.

By using the coordinate transform equation of the density,

$$\phi\frac{\partial\rho}{\partial\tau}+\rho c=0\rightarrow c=-\frac{\phi}{\rho}\frac{\partial\rho}{\partial\tau} \tag{5.10}$$

The divergence of the total flux is transformed into the time of flight. By using this coordinate transformation, saturation equation will be

$$\frac{\partial}{\partial t}\left(\frac{S_w}{B_w}\right)+\frac{\partial}{\partial\tau}\left(\frac{f_w}{B_w}\right)=-\frac{c}{\phi}\frac{f_w}{B_w}=\frac{1}{\rho}\frac{f_w}{B_w}\frac{\partial\rho}{\partial\tau} \tag{5.11}$$

Then we are able to solve the equation only along the streamline and we don't need to go back to the grid block coordinate which means we don't require operator splitting for this equation.

The discretization of the equation is as follows,

$$\frac{1}{\Delta t}\left(\left.\frac{S_w}{B_w}\right|^{n+1} - \left.\frac{S_w}{B_w}\right|^{n}\right) + \frac{1}{\Delta \tau}\left(\left.\frac{f_w}{B_w}\right|_{i-1/2}^{n} - \left.\frac{f_w}{B_w}\right|_{i+1/2}^{n}\right) = -\frac{c}{\phi}\left.\frac{f_w}{B_w}\right|_{i}^{n} \tag{5.12}$$

$$S_w^{n+1} = B_w^{n+1} \times \left[\left.\frac{S_w}{B_w}\right|^{n} - \frac{\Delta t}{\Delta \tau}\left(\left.\frac{f_w}{B_w}\right|_{i-1/2}^{n} - \left.\frac{f_w}{B_w}\right|_{i+1/2}^{n}\right) - \frac{\Delta t \cdot c}{\phi}\left.\frac{f_w}{B_w}\right|_{i}^{n}\right] \tag{5.13}$$

In detail,

$$\left.\frac{S_w}{B_w}\right|^{n} = \frac{S_{wi}^{n}}{B_{wi}^{n}} \tag{5.14}$$

$$\left.\frac{f_w}{B_w}\right|_{i-1/2}^{n} = \frac{f_i^n}{0.5 \times \left(B_{wi}^{n} + B_{wi-1}^{n}\right)} \tag{5.15a}$$

$$\left.\frac{f_w}{B_w}\right|_{i+1/2}^{n} = \frac{f_{i+1}^n}{0.5 \times \left(B_{wi}^{n} + B_{wi+1}^{n}\right)} \tag{5.15b}$$

Saturation Remapping. There is still one more step to take. The relative density, the fluid volume, time-of-flight information are used to incorporate cross-streamline effects via pressure updates and remapping of saturations. The new flow rate that a streamline carries at the location we investigate will be

$$q_{i\Psi} = q_{0\Psi}\frac{\rho_{0\Psi}}{\rho_{i\Psi}} = q_{0\Psi}\frac{1}{\rho_{i\Psi}}. \tag{5.16a}$$

Now the volumetric flux depends on the position along the streamline. When we are mapping from streamline segments to grid-block properties, we need to take into account the new q with compressibility.

The saturation in one grid block will be calculated using streamline segment saturation, streamline flow rate and streamline segment time of flight as follows

$$S_i = \frac{\sum_{\Psi} S_{i\Psi} \cdot q_{i\Psi} \cdot \Delta \tau_{i\Psi}}{\sum_{\Psi} q_{i\Psi} \cdot \Delta \tau_{i\Psi}}, \tag{5.16b}$$

where the streamline fluid volumetric rate is calculated by Eq. 5.16a.

We now illustrate the calculations using waterflooding in a ¼-spot pattern under black oil conditions and compare the results with incompressible flow. **Fig. 5.5** shows the pressure distribution for a two-phase flow black oil case. The initial pressure is set at 3000 psi and the producer is bottomhole pressure constrained at 1000 psi. The divergence of flux computed for each grid block is shown in **Fig. 5.6** and a contour of the streamline time of flight is shown in **Fig. 5.7**.

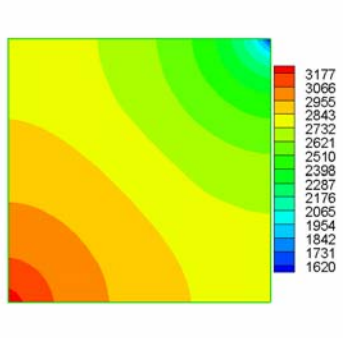

Figure 5.5 Pressure(psia) distribution for a ¼-five spot pattern, two-phase compressible flow.

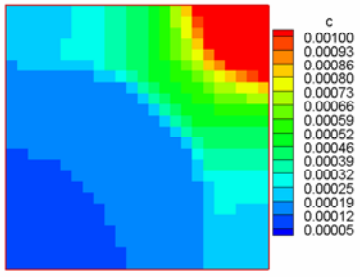

Figure 5.6 Total net flux distribution for a ¼-five spot pattern, two-phase compressible flow.

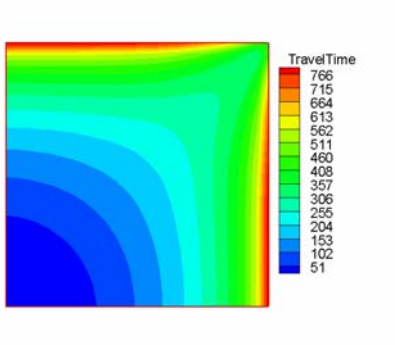

Figure 5.7 Streamline time-of-flight distribution for a ¼-five spot pattern, two-phase compressible flow.

We now calculate the effective densities along streamlines using Eq. 5.5. A contour of the 'local' changes in relative density is shown **Fig. 5.8** and a value less than unity indicates expansion of the fluid. Note that these changes are a function of fluid compressibility, porosity and time of flight. The relatively low values at the stagnant corners reflect the large cell time of flight there.

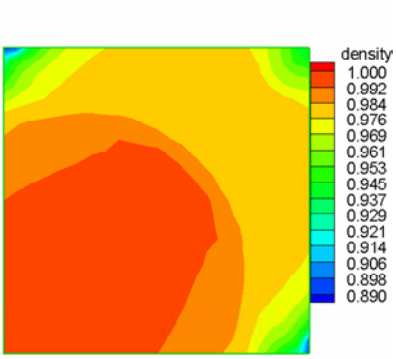

Figure 5.8 'Local' relative density distribution for a ¼-five spot pattern, two-phase compressible flow.

The accumulated relative densities along streamlines are contoured in **Fig. 5.9** and resemble the time of flight distribution. In fact, we can view the relative densities as scale factors for time of flight, 'accelerating' or 'retarding' the particle transport along streamlines. The oil rate at the producing well for the compressible streamline calculations is shown in **Fig. 5.10**. For comparison purposes, we have also shown the close correspondence with the results from finite difference calculations. The impact of fluid compressibility can also be easily seen in this figure.

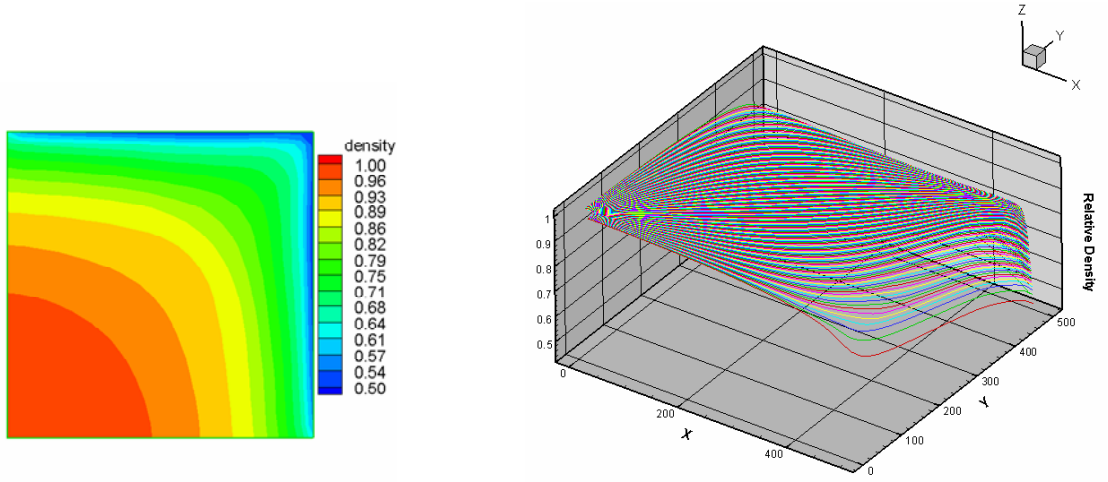

Figure 5.9 Accumulative relative density distribution (right side shows relative density traced along streamlines).

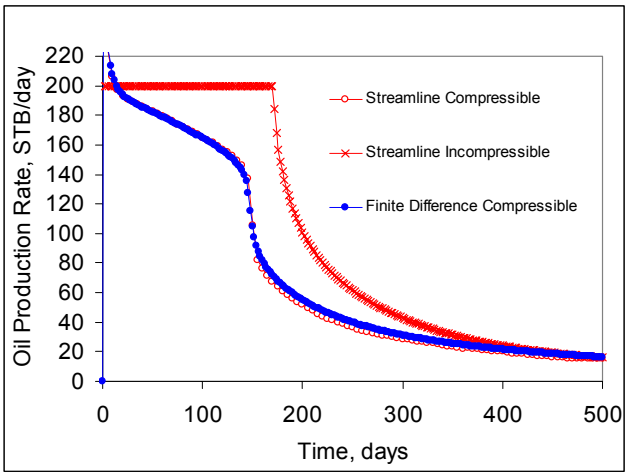

Figure 5.10 Comparison of oil rate at the producer.

In next case, we increased bottomhole pressure to 2500 psi. Average reservoir pressure is kept above initial reservoir pressure and fluid is under compression in most of the reservoir area. **Fig. 5.11** shows the tracing of relative density along the streamline. The contour of the relative density is shown in **Fig. 5.12**. For compression case, divergence of flux is negative and relative density is greater than 1. **Fig. 5.13** shows the oil production rate vs. time using compressible streamline formulation and commercial finite difference simulator. For comparison purpose we also show the results from the commercial streamline simulator. The improvement from the new formulation is quite obvious here.

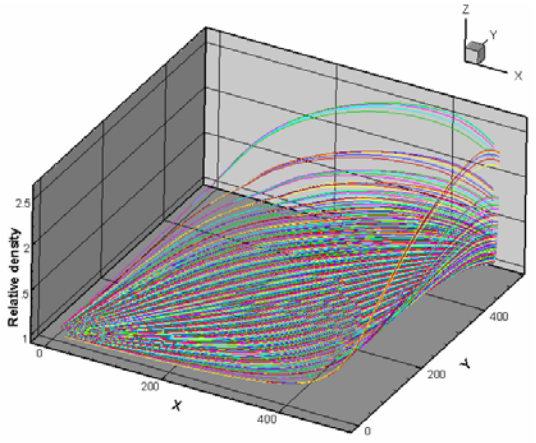

Figure 5.11 Tracing relative density along streamlines for a compression case.

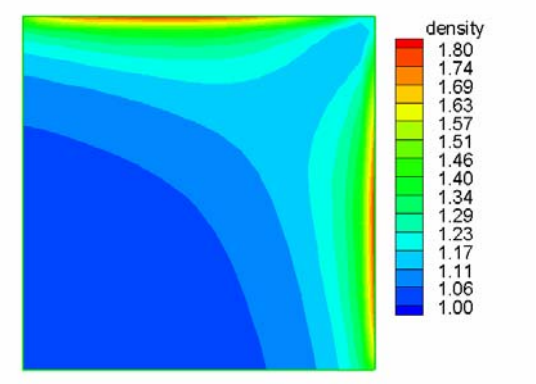

Figure 5.12 Contour plot of relative density for a compression case.

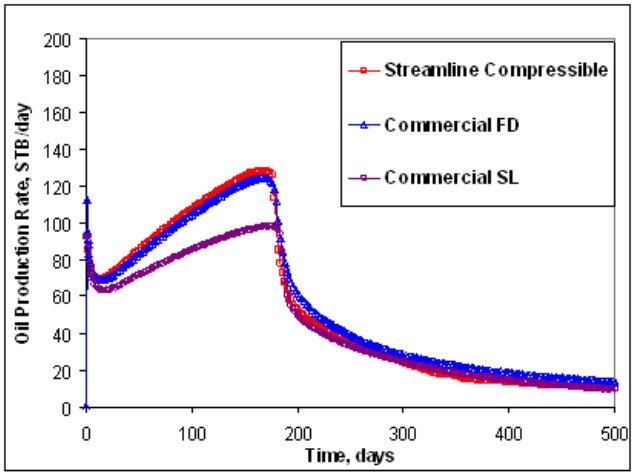

Figure 5.13 Oil production rate vs. time for a compression case.

5.3.2 Streamline Formulation for Three-Phase Flow

The mass conservation equation for gas is give by the same procedure,

$$\phi\frac{\partial}{\partial t}\left(\frac{S_g}{B_g}+\frac{S_oR_s}{B_o}\right)+\nabla\cdot\left(u_t\frac{f_g}{B_g}+u_t\frac{f_oR_s}{B_o}\right)=0 \tag{5.17}$$

$$\phi\frac{\partial}{\partial t}\left(\frac{S_g}{B_g}+\frac{S_oR_s}{B_o}\right)+\left(\frac{f_g}{B_g}+\frac{f_oR_s}{B_o}\right)\nabla\cdot u_t+u_t\cdot\nabla\left(\frac{f_g}{B_g}+\frac{f_oR_s}{B_o}\right)=0 \tag{5.18}$$

$$\phi\frac{\partial}{\partial t}\left(\frac{S_g}{B_g}+\frac{S_oR_s}{B_o}\right)+\phi\frac{\partial}{\partial\tau}\left(\frac{f_g}{B_g}+\frac{f_oR_s}{B_o}\right)=-\left(\frac{f_g}{B_g}+\frac{f_oR_s}{B_o}\right)c \tag{5.19}$$

or

$$\phi\frac{\partial}{\partial t}\left(\frac{S_g}{B_g}+\frac{S_oR_s}{B_o}\right)+\phi\frac{\partial}{\partial\tau}\left(\frac{f_g}{B_g}+\frac{f_oR_s}{B_o}\right)=\left(\frac{f_g}{B_g}+\frac{f_oR_s}{B_o}\right)\frac{\phi}{\rho}\frac{\partial\rho}{\partial\tau} \tag{5.20}$$

By eliminating ϕ,

$$\frac{\partial}{\partial t}\left(\frac{S_g}{B_g}+\frac{S_o R_s}{B_o}\right)+\frac{\partial}{\partial \tau}\left(\frac{f_g}{B_g}+\frac{f_o R_s}{B_o}\right)=-\left(\frac{f_g}{B_g}+\frac{f_o R_s}{B_o}\right)\frac{c}{\phi} \tag{5.21}$$

or

$$\frac{\partial}{\partial t}\left(\frac{S_g}{B_g}+\frac{S_o R_s}{B_o}\right)+\frac{\partial}{\partial \tau}\left(\frac{f_g}{B_g}+\frac{f_o R_s}{B_o}\right)=\left(\frac{f_g}{B_g}+\frac{f_o R_s}{B_o}\right)\frac{1}{\rho}\frac{\partial \rho}{\partial \tau} \tag{5.22}$$

Eq. 5.22 can be discretized and solved along streamlines using finite-difference as discussed for two-phase flow. Because of the high gas mobility, the three-phase flow equations need to be solved implicitly along streamlines.

An example using the new formulation is given below. We simulated water injection in a quarter five-spot pattern for three-phase flow. A homogeneous permeability model represented by 25×25 grid cells was used. The initial solution GOR is 1.27 Mscf/STB. Initial reservoir pressure is 3005 psi, which is a little bit higher than the bubble-point pressure, 3000 psi. There is no free gas at the initial state. The producer is bottomhole pressure constrained at 2500 psi, and the injector is rate constrained at 250 B/d. As the pressure drops, solution gas comes out from oil phase and accumulates to mobile free gas. **Fig. 5.14** shows the oil production rate, **Fig. 5.15** shows the gas production rate, and **Fig. 5.16** shows the water-cut. Our results match commercial finite-difference simulator.

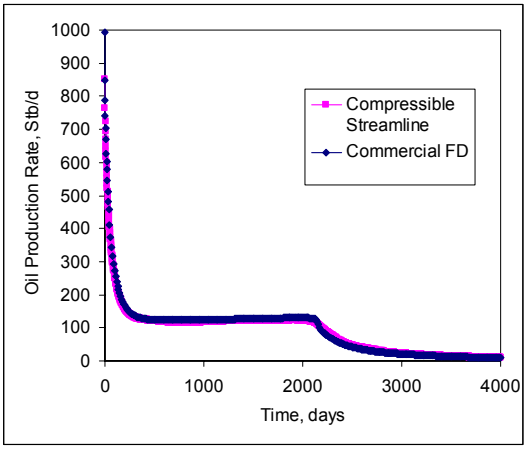

Figure 5.14 Oil production rate for a three-phase case.

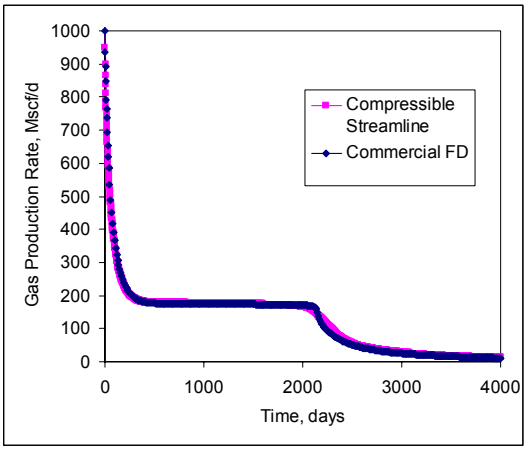

Figure 5.15 Gas production rate for a three-phase case.

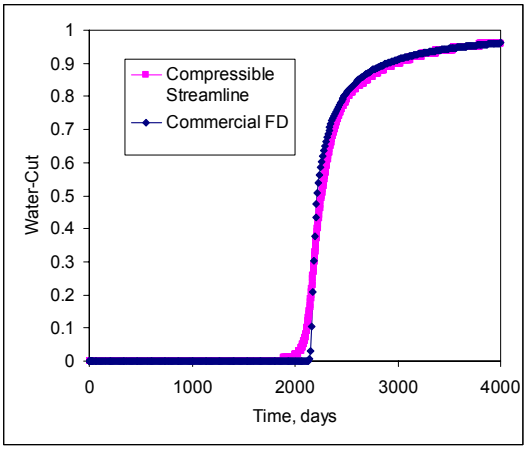

Figure 5.16 Water-cut curve for a three-phase case.

5.3.3 Sensitivity Calculation for Compressible and Three-Phase Flow

This section discusses the sensitivity calculation based on the rigorous streamline formulations.

Watercut Sensitivity. The component conservation equation for water is shown in Eq. 5.9. From Eq. 5.9,

$$\frac{\partial}{\partial t}\left(\frac{S_w}{B_w}\right) = -\frac{\partial}{\partial \tau}\left(\frac{f_w}{B_w}\right) - \frac{c}{\phi}\frac{f_w}{B_w} \tag{5.23}$$

$\frac{S_w}{B_w}$ is function of m and t. The implicit differentiation of $\frac{\partial t}{\partial m}$ will be

$$\frac{\partial t}{\partial m} = -\frac{\frac{\partial}{\partial m}\left(\frac{S_w}{B_w}\right)}{\frac{\partial}{\partial t}\left(\frac{S_w}{B_w}\right)} = -\frac{\frac{\partial \tau}{\partial m}\cdot\frac{\partial}{\partial \tau}\left(\frac{S_w}{B_w}\right)}{\frac{\partial}{\partial t}\left(\frac{S_w}{B_w}\right)} \tag{5.24}$$

$$\frac{\partial t}{\partial m} = \frac{\frac{\partial \tau}{\partial m}\frac{\partial}{\partial \tau}\left(\frac{S_w}{B_w}\right)}{\frac{\partial}{\partial \tau}\left(\frac{f_w}{B_w}\right)+\frac{f_w}{B_w}\frac{c}{\phi}} \tag{5.25}$$

or

$$\frac{\partial t}{\partial m} = \frac{\frac{\partial \tau}{\partial m}\frac{\partial}{\partial \tau}\left(\frac{S_w}{B_w}\right)}{\frac{\partial}{\partial \tau}\left(\frac{f_w}{B_w}\right)-\frac{f_w}{B_w}\frac{1}{\rho}\frac{\partial \rho}{\partial \tau}} \tag{5.26}$$

For incompressible flow, c=0, B_w is constant and Eq. 5.25 reduces to our previous sensitivity formulation Eq. 4.18.

Gas/Oil Ratio Sensitivity. The component conservation equation for gas is shown in Eq. 5.19. Let's define $S'_g = \frac{S_g}{B_g}+\frac{S_o R_s}{B_o}$, then

$$\frac{\partial S'_g}{\partial t}+\frac{\partial}{\partial \tau}\left(\frac{f_g}{B_g}+\frac{f_o R_s}{B_o}\right) = -(\frac{f_g}{B_g}+\frac{f_o R_s}{B_o})\frac{c}{\phi} \tag{5.27}$$

$$\frac{\partial S'_g}{\partial t} = -\frac{\partial}{\partial \tau}\left(\frac{f_g}{B_g}+\frac{f_o R_s}{B_o}\right)-(\frac{f_g}{B_g}+\frac{f_o R_s}{B_o})\frac{c}{\phi} \tag{5.28}$$

If we assume that the streamlines do not shift because of small perturbations in reservoir properties, changes in S'_g (gas saturation, including the solution gas in oil phase) at the outlet node of a streamline can be expressed as $S'_g = S'_g(t, \boldsymbol{m})$, so

$$\delta S'_g = \frac{\partial S'_g}{\partial t}\delta t + \frac{\partial S'_g}{\partial \tau}\left[\frac{\partial \tau}{\partial \boldsymbol{m}}\right]^T \delta \boldsymbol{m} \tag{5.29}$$

The implicit differentiation of $\frac{\partial t}{\partial m}$ will be

$$\frac{\partial t}{\partial m} = -\frac{\frac{\partial S'_g}{\partial m}}{\frac{\partial S'_g}{\partial t}} = -\frac{\frac{\partial S'_g}{\partial \tau}\frac{\partial \tau}{\partial m}}{\frac{\partial S'_g}{\partial t}} \tag{5.30}$$

We can now combine Eq. 5.30 with Eq. 5.28 in order to obtain the following expression for travel time sensitivity in terms of the streamline time of flight,

$$\frac{\partial t}{\partial m} = \frac{\frac{\partial \tau}{\partial m}\frac{\partial S'_g}{\partial \tau}}{\frac{\partial}{\partial \tau}\left(\frac{f_g}{B_g} + \frac{f_o R_s}{B_o}\right) + \left(\frac{f_g}{B_g} + \frac{f_o R_s}{B_o}\right)\frac{c}{\phi}}, \tag{5.31}$$

$$\frac{\partial t}{\partial m} = \frac{\frac{\partial \tau}{\partial m}\frac{\partial}{\partial \tau}\left(\frac{S_g}{B_g} + \frac{S_o R_s}{B_o}\right)}{\frac{\partial}{\partial \tau}\left(\frac{f_g}{B_g} + \frac{f_o R_s}{B_o}\right) + \left(\frac{f_g}{B_g} + \frac{f_o R_s}{B_o}\right)\frac{c}{\phi}}. \tag{5.32}$$

We can get fluxes and saturation from Eclipse, then trace streamlines and map block properties to streamline coordinate properties and obtain the $\frac{\partial(\cdot)}{\partial \tau}$ values at the streamline outlet nodes. If we use compressible streamline simulation, these values are already available along the streamlines.

Now let's discuss the parameters relevant to Eq. 5.32.

The fractional flow of water, oil, and gas is calculated by

$$f_w = \frac{\frac{k_{rw}}{\mu_w}}{\frac{k_{rg}}{\mu_g} + \frac{k_{ro}}{\mu_o} + \frac{k_{rw}}{\mu_w}},\ f_g = \frac{\frac{k_{rg}}{\mu_g}}{\frac{k_{rg}}{\mu_g} + \frac{k_{ro}}{\mu_o} + \frac{k_{rw}}{\mu_w}}, \text{ and } f_o = 1 - f_w - f_g. \tag{5.33}$$

The default k_{ro} model is given according to Eclipse,[61]

$$k_{ro} = \frac{S_g k_{rog} + (S_w - S_{wco}) k_{row}}{S_g + S_w - S_{wco}} \tag{5.34}$$

Since Stone's second model[62,63] (modified) is commonly used in industry, it is also provided as an option:

$$k_{ro} = k_{rocw}\left[\left(\frac{k_{row}}{k_{rocw}} + k_{rw}\right)\left(\frac{k_{rog}}{k_{rocw}} + k_{rg}\right) - k_{rw} - k_{rg}\right], \tag{5.35}$$

where μ_g is the dry gas viscosity, and μ_o is the live oil (with dissolved gas) viscosity. Fluid viscosity, solution GOR, and formation volume factors are functions of pressure.

$$\mu_w = \mu_w(P) \tag{5.36a}$$

$$\mu_o = \begin{cases} \mu_o(P) & (P > P_b) \\ \mu_o(R_s(P)) & (P < P_b) \end{cases} \tag{5.36b}$$

$$\mu_g = \mu_g(P) \tag{5.36c}$$

$$R_s = R_s(P) \tag{5.36d}$$

$$B_w = B_w(P) \tag{5.36e}$$

$$B_o = B_o(P) \tag{5.36f}$$

$$B_g = B_g(P) \tag{5.36g}$$

Production GOR (the ratio of produced gas to produced oil) is

$$GOR = \frac{Q_g}{Q_o} = \frac{Q_{g,free} + R_s Q_o}{Q_o} = \frac{Q_{g,free}}{Q_o} + R_s = \frac{k_{rg}\mu_o B_o}{k_{ro}\mu_g B_g} + R_s \tag{5.37}$$

If $P>P_b$, for undersaturated reservoir, production *GOR* is contributed by R_s only. Reexamining Eq. 5.32, we see that the travel-time sensitivity for production GOR is valid for situations where there is free gas and/or solution gas.

5.4 Sensitivity Verification

In order to verify the travel-time sensitivity in Eqs. 5.25 and 5.32 we compared our results with sensitivities obtained by numerical perturbation. For this purpose, we simulated water injection in a quarter five-spot pattern for three-phase flow. A homogeneous permeability model represented by 21×21 grid cells was used for this comparison. The initial solution GOR is 1.27 Mscf/STB. The reservoir was produced by a production/injection ratio of 1.25 starting with the bubble-point pressure. As the pressure drops, solution gas comes out from oil phase and accumulates to mobile free gas. We perturbed every grid block permeability by 5%, one grid block at a time and numerically computed the partial derivative of the arrival time of a fixed watercut and GOR with respect to permeability. **Fig. 5.17** shows the results for watercut of 0.47, and **Fig. 5.18** shows the result for GOR of 4 Mscf/STB. Clearly, we obtain a good agreement between analytical travel time sensitivities calculated from Eqs. 5.25 and 5.32 and numerical travel time sensitivities. The locations of the negative and positive sensitivities are in close agreement. The shape of the watercut analytical sensitivity is a little bit different from the perturbation sensitivity since the analytical sensitivities are calculated along the streamlines thus the shape is in accordance with the streamline trajectory. The differences are also because of the approximations inherent in the analytical computations, particularly the assumption that the streamlines do not shift because of small perturbation in reservoir properties. Nevertheless, as we will see later, the streamline-based sensitivities are adequate for history matching purposes under a wide variety of conditions.

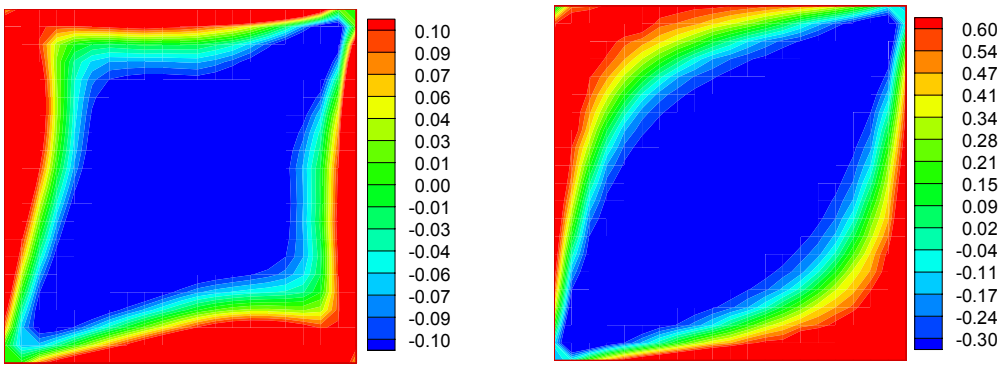

a. numerical b. analytical

Figure 5.17 Comparison of numerical and analytical sensitivity in a ¼-five spot pattern at water cut of 0.47.

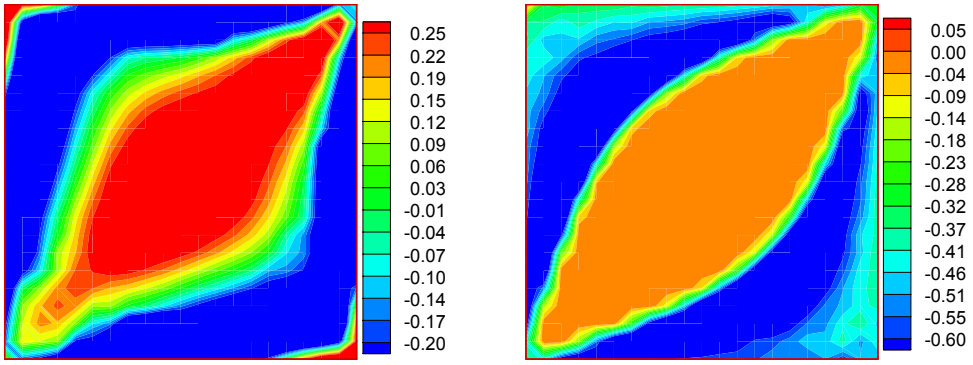

a. numerical b. analytical

Figure 5.18 Comparison of numerical and analytical sensitivity in a ¼-five spot pattern at GOR of 4 Mscf/STB.

5.5 Field-Scale Example

In this section I demonstrate the feasibility of the approach for field studies by application to a large-scale 3-D example. As mentioned before, streamlines and time of flight are used to compute the sensitivity of the production data with respect to reservoir parameters as described in the mathematical formulation section. In this field example, watercut and GOR were matched jointly to update the reservoir permeability model.

5.5.1 Model Description

Ninth SPE benchmark problem[64] was used to validate the methodology. The SPE ninth problem studies a bottom waterflooding in a dipping reservoir with natural water encroachment from an aquifer. The reservoir (**Fig. 5. 19**) is represented by a 24×25×15 mesh system with conventional rectangular coordinates. The dimensions of the grid blocks are 300 feet in both the X- and Y- directions. Cell (1,1,1) is at a depth of 9000 feet subsea at the center of the cell top. The remaining cells dip in the X-direction at an angle of 10 degrees. Values of porosity and thickness can be found in Ref. 64. The total thickness from Layers 1 to 13 is 209 feet (16 feet per layer in average), and Layer 14 and 15 has a thickness of 50 and 100 feet respectively.

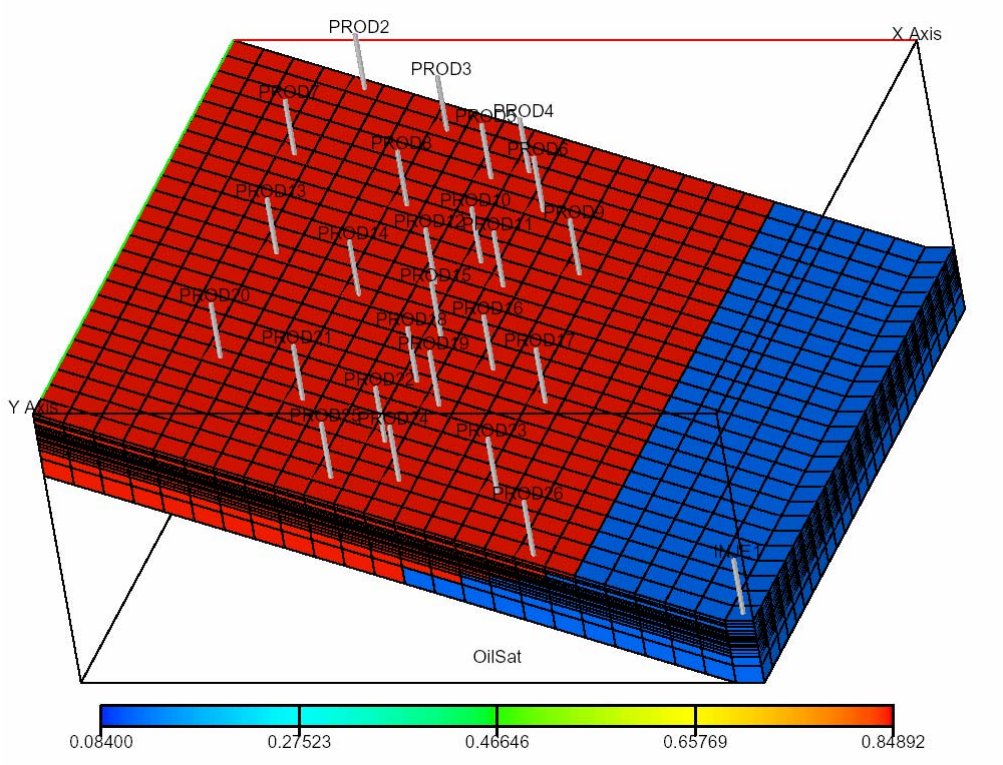

Figure 5.19 Initial oil saturation for the reservoir.

Solution gas/oil ratio and gas formation volume factor are shown in **Fig. 5.20**. Relative permeabilities are shown in Fig. **5.21**. Modified Stone's second model was used to compute oil relative permeability.

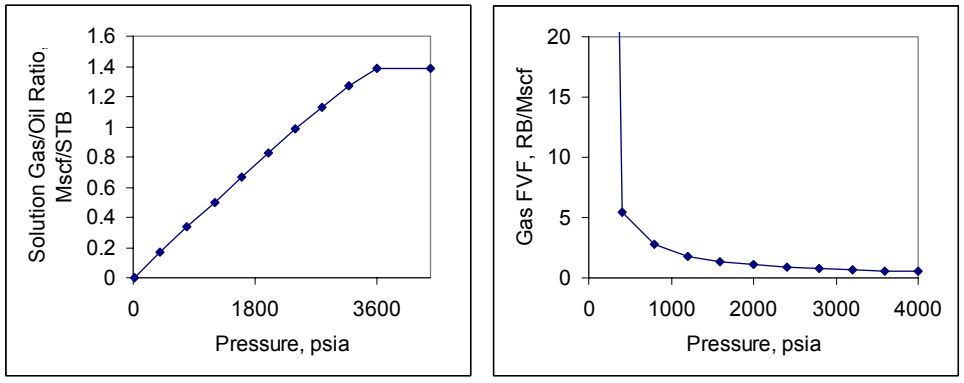

Figure 5.20 Solution gas/oil ratio and gas formation volume factor curves.

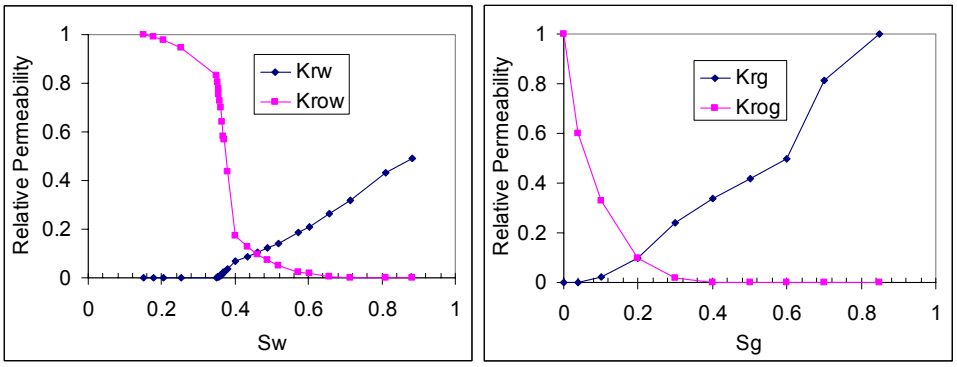

Figure 5.21 Relative permeability curves.

The initial oil phase pressure at 9035 feet subsea is 3600 psia which is the bubble-point pressure. The oil/water contact is 9950 feet subsea. There is no free gas initially in the reservoir. After 900 days of production, there is plenty of free gas (**Fig. 5.22**).

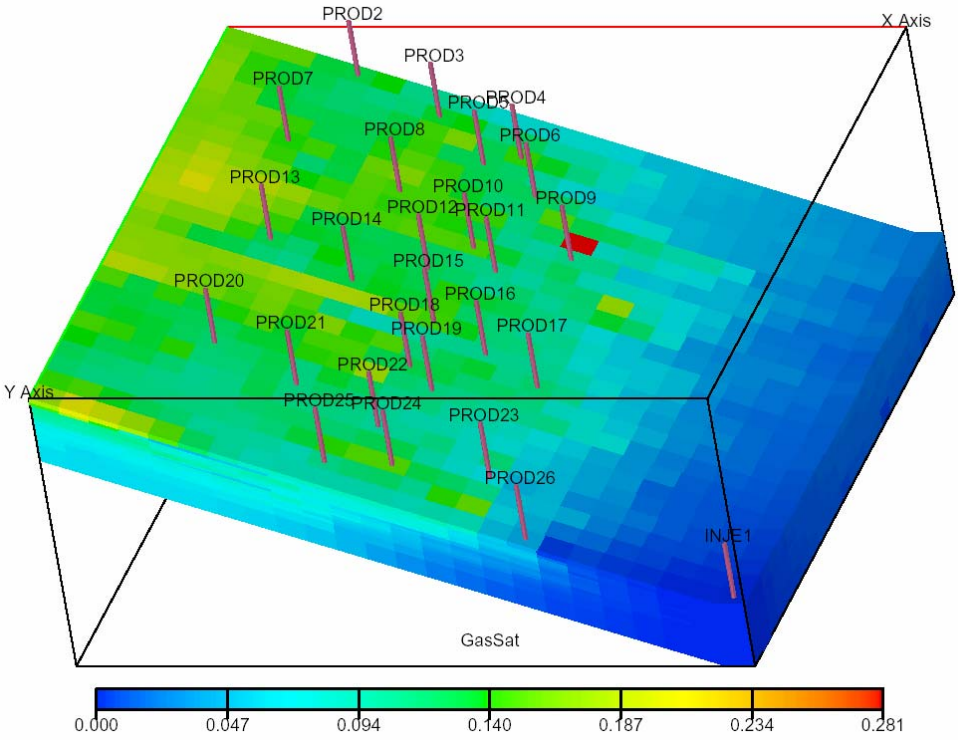

Figure 5.22 Gas saturation distribution at the end of simulation time (900 days).

The permeability field used by the original SPE ninth problem was generated geostatistically on a cell by cell basis. The permeability is log-normally distributed with a mean of 108 md, a minimum of 0.003 md and a maximum of 10054 md. The correlation length in the X-direction is about 6 grid blocks, and there is no correlation in the Y- and Z- directions. For validation purpose, this permeability field was used as a true or reference model to generate production history by running flow simulation.

A total of 1 water injector (I1) and 25 producers (named as P2 to P26) were included in the reservoir. The injector was completed from layers 11 through 15. In the original SPE9 problem, all producers were completed in layers 2, 3, and 4 only. For validation purpose, all producers except produces 9, 17, 23, and 26 were changed to be completed in layers 1 to 13. Producers 9, 17, 23, and 26 are completed in layers 1 to 5 so that wells will not be perforated in the water leg. The water injector was injecting at a maximum

bottomhole pressure of 4500 psia at a reference depth of 9110 feet subsea, and the producers were producing with a constant reservoir volume rate of 1800 RB/D and minimum flowing bottomhole pressure of 1000 psia.

5.5.2 Production Data Integration

To generate an initial permeability model to start with, the permeability values at the well blocks are regarded as known hard data. Analysis of the variogram indicated a correlation length of about 2100 feet (7 grids) in the X-direction and about 2 grids in the Y-direction (**Fig. 5.23**). No correlation in the Z-direction was found. Using these variogram parameters, the condition data at well locations, and the histogram of the hard data, sequential Gaussian simulation was used to generate 10 realizations of the permeability model. One model was randomly picked up as the initial model.

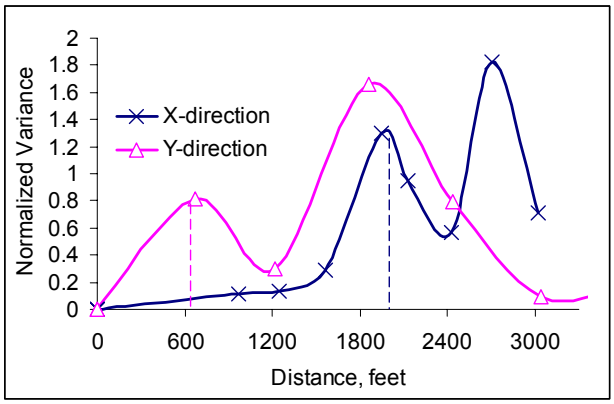

Figure 5.23 Semi-variogram for the permeability known at the well locations (about 600 and 2100 feet range in the X- and Y- directions respectively).

In 5 iterations, all misfit indexes dropped obviously, including the objective function (GOR and water cut total shift time misfit), GOR shift time misfit, water-cut shift-time misfit, GOR amplitude misfit, and water-cut amplitude misfit (**Fig. 5.24**).

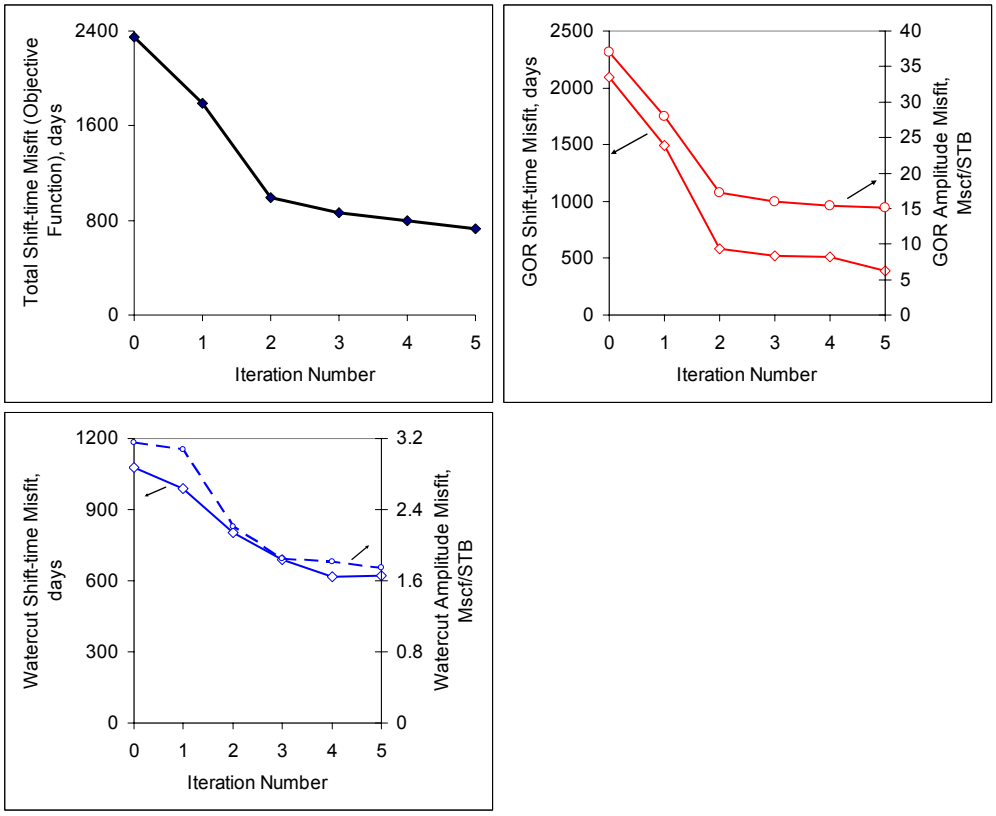

Figure 5.24 Shift time and amplitude misfit reduction for joint watercut and GOR matching for SPE9 problem.

The reference, initial, and final matched production GOR are shown in **Fig. 5.25**. Most of the wells gained a satisfactory match.

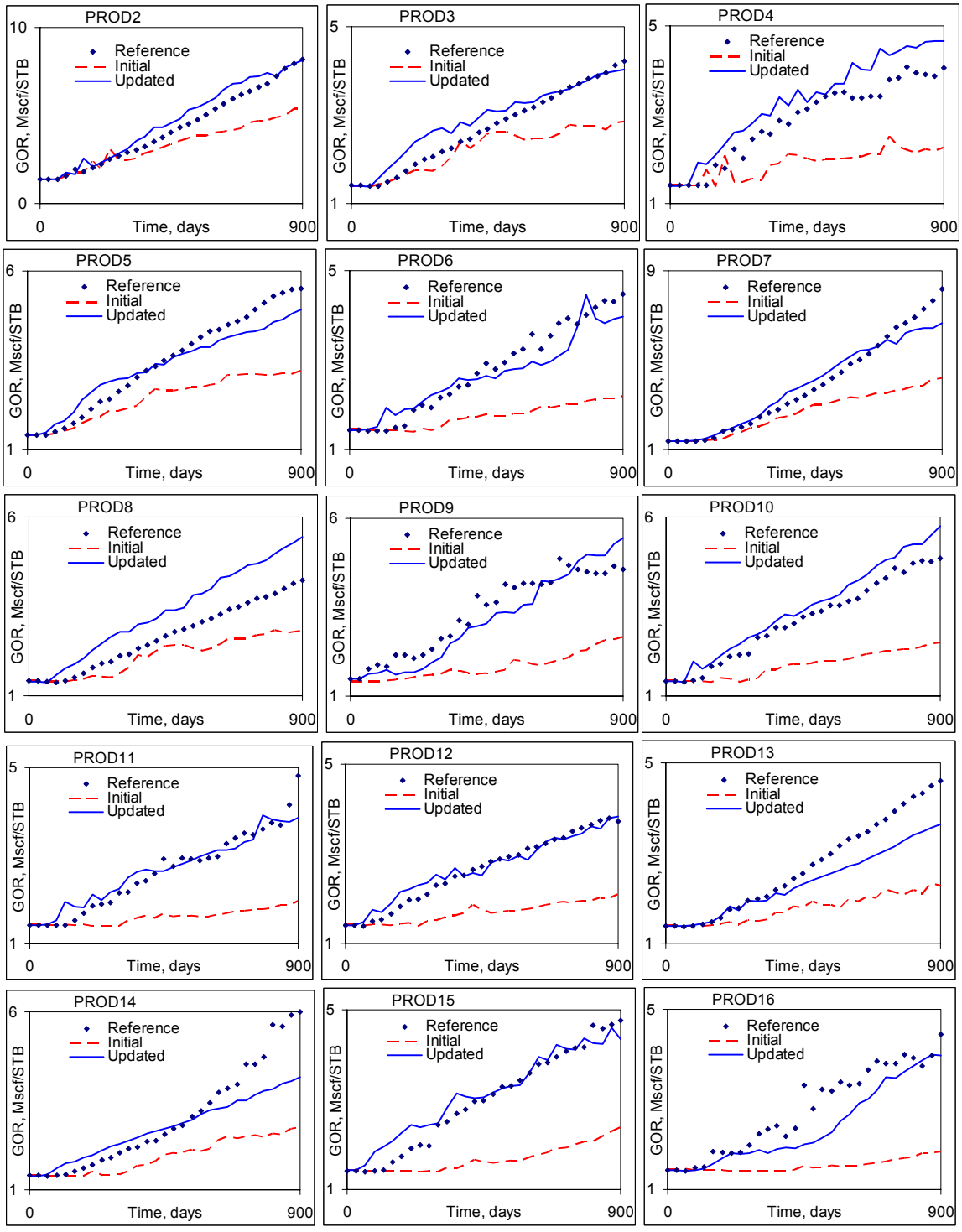

Figure 5.25 Production GOR match for all the 25 producers (named from PROD2 to PROD26) for SPE9 problem.

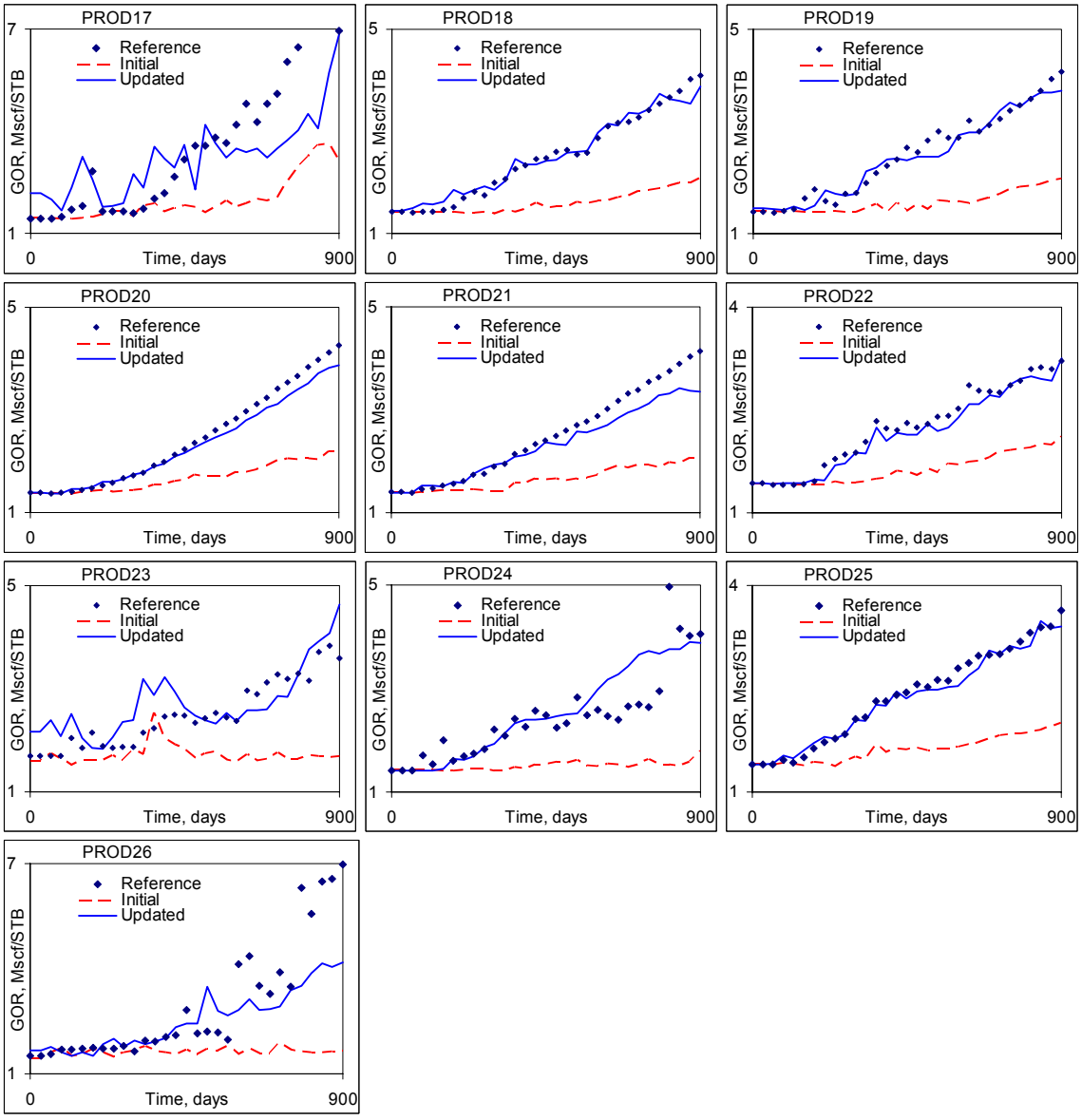

Figure 5.25 Continued.

Although only five wells showed obvious water breakthrough by the true reference model, all the wells were used in the production data integration. By the initial permeability model, only two wells showed significant water breakthrough. After joint integration of GOR and water cut data, all five wells showed significant water breakthrough, although the amplitude match is not perfect (**Fig. 5.26**).

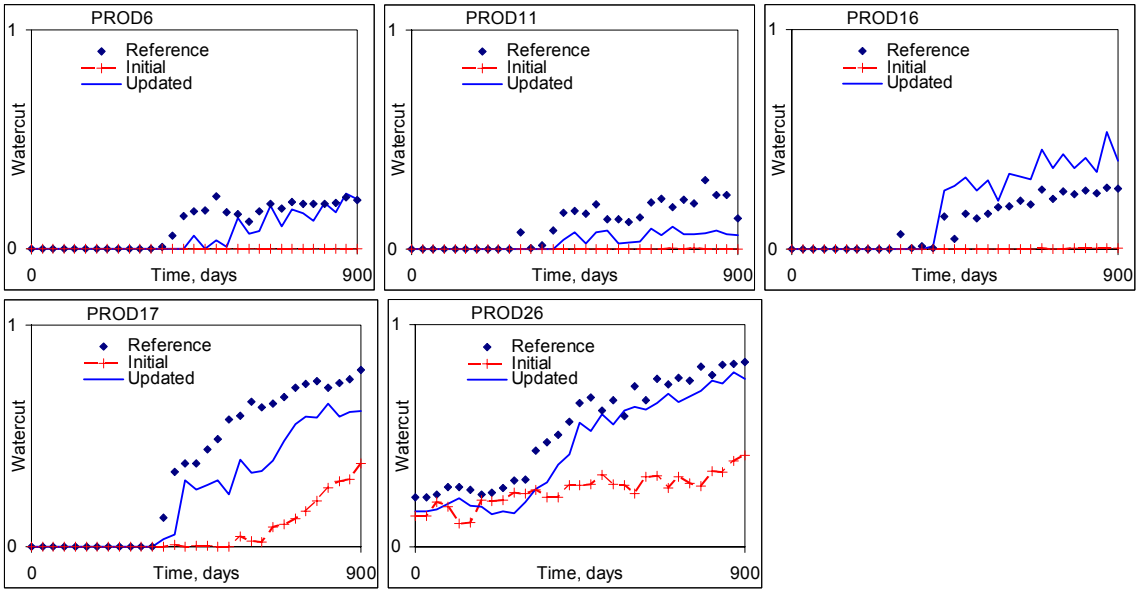

Figure 5.26 Watercut match for wells showing observed breakthrough for SPE9 problem.

Fig. 5.27 compared the initial permeability model, the true (reference) model, and the derived (updated) model. The scale is logarithmic. As mentioned before, minimum is 0.003 md and maximum is 10054 md. It is hard to tell the difference between the derived and the initial model by visual comparison. But still they are detailed changes. For example, the permeability in Layer 3 was reduced to be closer to the true model. We can conclude from the comparison that the geologic realism of the initial model is retained in the final derived model.

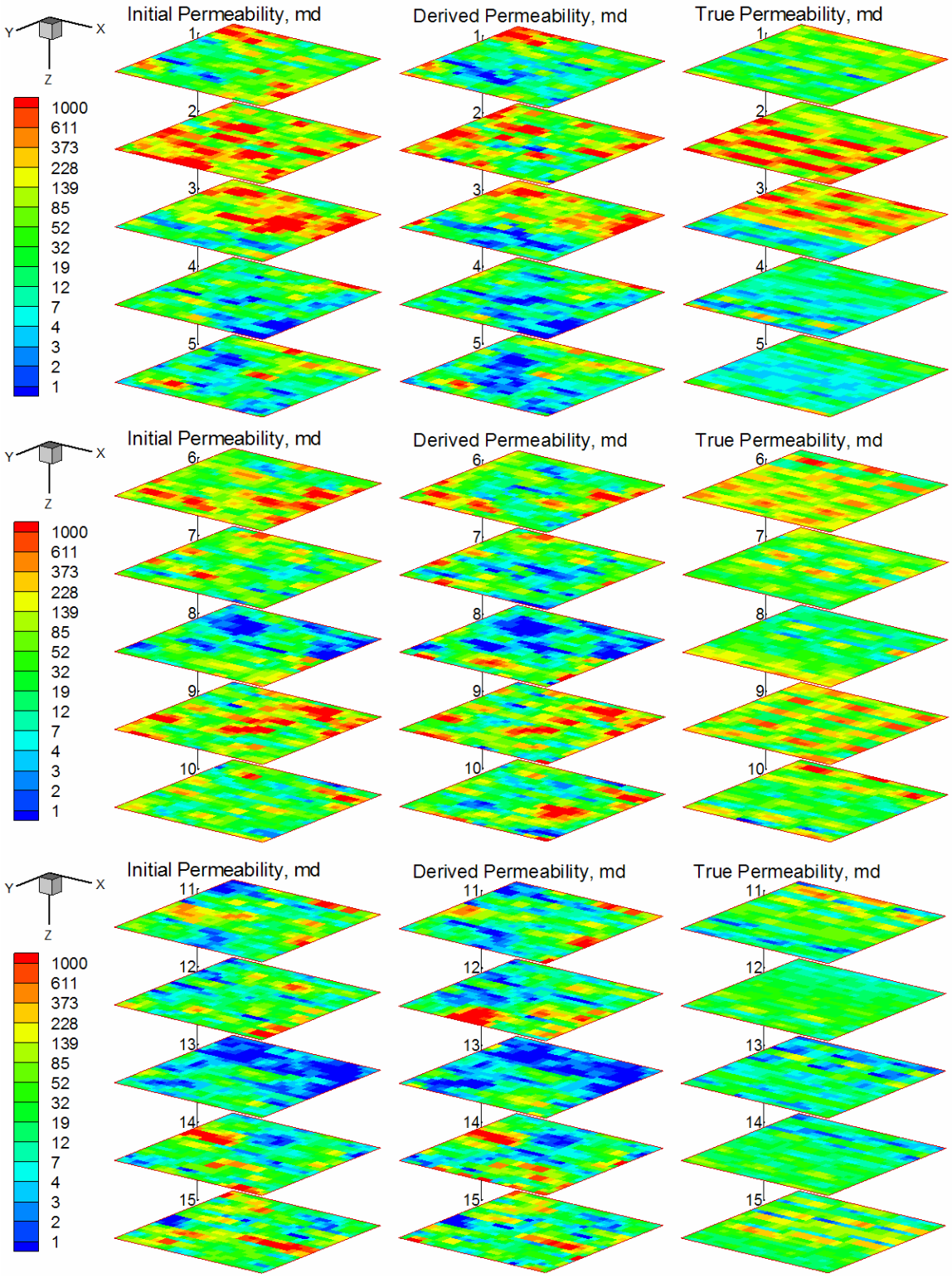

Figure 5.27 Initial, derived (updated), and true (reference) permeability model comparison for SPE9 problem.

It is hard to discern the changes made to the initial model since the method is designed to preserve the initial geologic realism. But if we compare the "true-initial" permeability difference and the "derived-initial" permeability difference (**Fig. 5.28**), we find that the derived model made most of the needed changes, especially the close agreement in the areas where permeability needs to be reduced. There is some discrepancy in the areas where there are very few streamlines (**Fig. 5.29**) since there is not enough information to guide the change (for example, near the boundary or in the areas where there is no well), or in the areas near the aquifer (the area far from Y-axis, also refer to Fig. 5.19) since the streamline time-of-flight is extremely large and was not used in the sensitivities. The agreement in the areas where permeability needs to be reduced (dark areas) is very satisfactory.

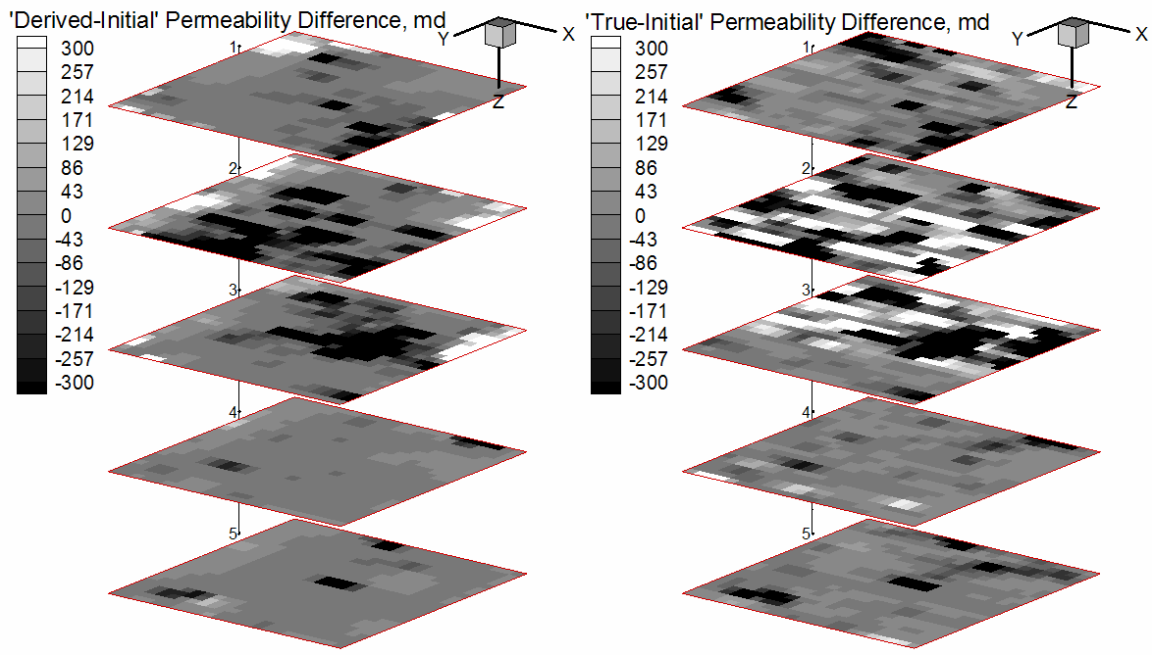

Figure 5.28 Comparison of the "derived-initial" permeability difference and the "true-initial" permeability difference (All 15 layers are shown).

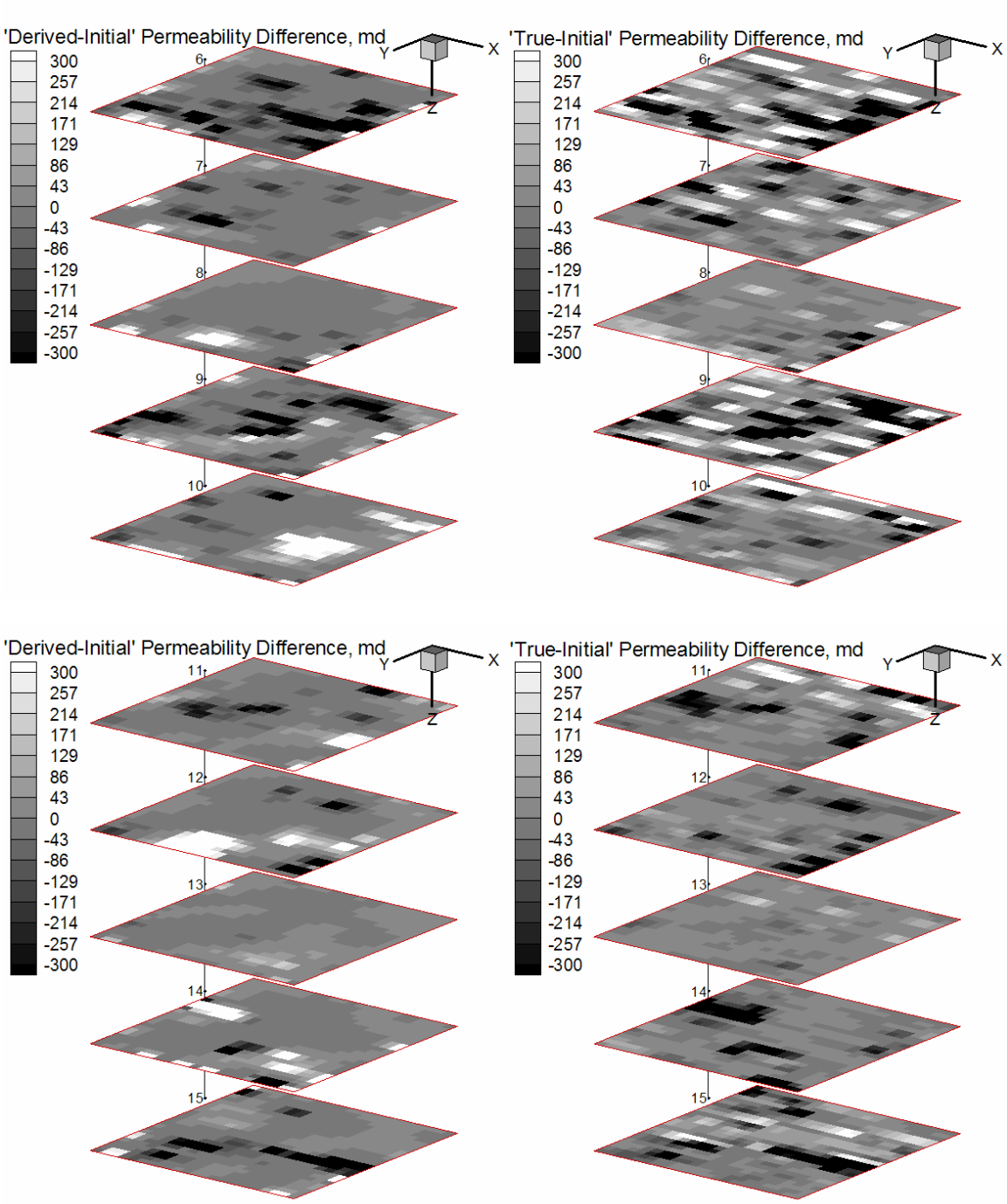

Figure 5.28 Continued.

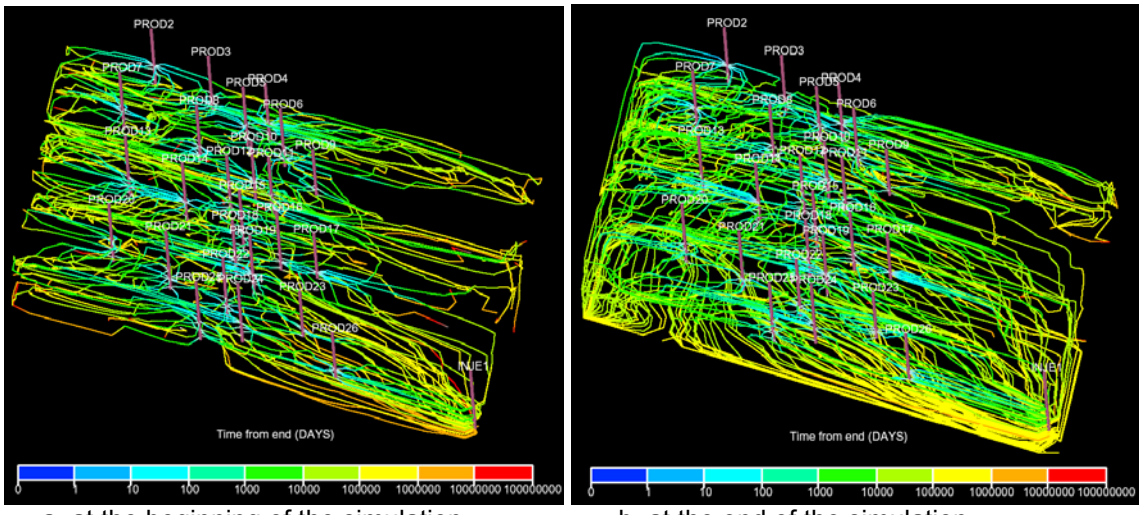

a. at the beginning of the simulation b. at the end of the simulation

Figure 5.29 Streamline and time-of-flight distribution.

For this field case, it took about 50 minutes in 5 iterations to get a good history match running at a computer with 1.5 GHz Pentium 4 processor.

This field-scale example shows that the methodology is working and the approach is very efficient.

5.6 Chapter Summary

An approach to history matching three-phase flow using a novel compressible streamline formulation and streamline-derived analytic sensitivities was developed. Streamline models were generalized to account for compressible flow by introducing a relative density of total fluids along streamlines. A density-dependent source term in the saturation equation accounts for the pressure effect during saturation calculations.

Parameter sensitivities that define the relationship between the reservoir properties and the production response, viz. water cut and gas-oil ratio, were analytically computed. This calculation is very efficient. Also the analytical sensitivities were verified by comparing with the perturbation sensitivity.

Generalized travel-time inversion is extremely robust and converges in only a few iterations for joint inversion of water cut and gas-oil ratio.

The power and utility of the approach were demonstrated using both synthetic and field-scale examples. The synthetic case includes matching of water cut and gas oil ratios from a 9-spot pattern and is used to validate the method. The field-scale example is modified SPE ninth comparative example and consists 25 producers, 1 injector and aquifer influx. Starting with a prior geologic model, water-cut and GOR history were integrated using the generalized travel time inversion. The approach took less than one hour in a PC for the entire history matching without any apparent loss in geologic realism.

CHAPTER VI

CONCLUSIONS AND RECOMMENDATIONS

In this work, I have quantified the degree of non-linearity for amplitude inversion, travel-time inversion, and generalized travel-time inversion; developed approaches to history matching streamline models using generalized travel time inversion which can be applied to large real field cases; developed approaches to fast history matching finite-difference models which can be applied to large real field cases; and developed approach to efficient history matching compressible, three-phase flow production data. The power and utility of these techniques have been demonstrated using synthetic and field applications.

6.1 Conclusions

Some specific conclusions can be made from this work:

1. We have quantitatively investigated the non-linearities associated with travel time and amplitude inversion for production data integration. The non-linearity is expressed in terms of a simple and intuitive geometric measure of curvature as proposed by Bates and Watts and later used by Grimstad and Mannseth.
2. The non-linearity in travel time inversion is found to be orders of magnitude smaller than the conventional amplitude inversion. As a result, the travel time inversion has better convergence properties and is less likely to be trapped in local minimum.
3. Travel time sensitivity is more uniform between the wells. In contrast, the amplitude sensitivity can be localized near the wells. The higher magnitude of the travel time sensitivity also contributes to its quasilinearity and improved convergence properties.

4. The generalized travel time inversion effectively combines travel time and amplitude inversion while retaining most of the desirable properties of the travel time inversion. For the field example studied here, the generalized travel time inversion outperformed both travel time and amplitude inversion.
5. Use of streamline-derived sensitivities can significantly improve the efficiency of assisted history matching. In particular, the sensitivities can be utilized to directly obtain the changes in reservoir properties necessary to improve the history match in a more objective way. This eliminates the time-consuming and subjective manual adjustment of parameters in the assisted history matching process. By intervening at every stage of the iterative process, we can retain control over the history matching process to preserve plausibility and geologic realism.
6. Streamline-based sensitivities and inversion allow us to take into account the full coupling of the streamlines in the reservoir rather than changing individual wells or streamline bundles at a time. This not only significantly increases the efficiency, but also preserves geologic continuity and minimizes the chances of introducing non-physical artifacts during the history matching process.
7. The power and utility of streamline-based inversion is demonstrated using two field examples with model sizes ranging from 10^5 to 10^6 grid blocks and with over one hundred wells. In both the cases, the streamline-based automatic history matching led to better individual well matches as well as field-wide matches compared to assisted history matching and with no apparent loss of geologic realism. We have shown that the automatic history matching can be used both for conditioning geologic models and also to further improve the models derived from the assisted history matching.
8. The use of sensitivities during assisted history matching can lead to significant savings in computation time and manpower. For the field examples presented here, the automatic history matching took days compared to months for assisted history matching. This makes it possible to generate multiple history-matched models to perform uncertainty analysis.

9. A fast history matching approach for finite-difference models is proposed. The new approach combines the versatility of finite-difference simulation with the efficiency of streamline simulation. Use of finite-difference simulation allows us to account for detailed physics including compressibility and gravity effects and also cross-streamline mechanisms.
10. A key aspect of our proposed method is the use of streamline-based sensitivity during history matching finite-difference models. Although these sensitivities are approximate, they seem to be adequate for most purposes and do not significantly impact the quality of the match or the efficiency of the approach.
11. We have demonstrated the power and utility of our proposed approach using both synthetic and field examples. A full field application from a giant middle-eastern field with over 80 wells and 30 years of production history convincingly establishes the practical feasibility of the approach. The entire history matching for this field took 9 hours in a PC indicating the potential for cost savings in terms of time and manpower.
12. An approach to history matching three-phase flow using a novel compressible streamline formulation and streamline-derived analytic sensitivities was developed. Streamline models were generalized to account for compressible flow by introducing a relative density of total fluids along streamlines. A density-dependent source term in the saturation equation accounts for the pressure effect during saturation calculations.
13. We analytically computed parameter sensitivities that define the relationship between the reservoir properties and the production response, viz. water-cut and gas-oil ratio. This calculation is very efficient. Also we verified the analytical sensitivities by comparing with the perturbation sensitivity.
14. Generalized travel-time inversion is extremely robust and converges in only a few iterations for joint inversion of watercut and gas-oil ratio.
15. We demonstrate the power and utility of our approach using both synthetic and field-scale examples. The synthetic cases include matching of water cut and gas oil ratios

from a 9-spot pattern and are used to validate the method. The field-scale example is SPE ninth comparative example and consists 25 producers, 1 injector and aquifer influx. Starting with a prior geologic model, we integrate water-cut and GOR history using the generalized travel time inversion. Our approach takes less than one hour in a PC for the entire history matching without any apparent loss in geologic realism.

6.2 Recommendations

Our experience with amplitude inversion indicates that the results tend to be more sensitive to the choice of inversion parameters. For homogeneous or smooth starting models, we can obtain a reasonable solution by careful choice of inversion parameters. We have cases where amplitude inversion works when starting with a smooth model. Further investigation is needed to explore the success possibility of amplitude inversion.

Generalized travel-time inversion succeeded for integration of non-monotonic tracer response. One reason is that the tracer response shapes calculated from different geologic models are more or less similar (bell shape with a peak or peaks), thus this helps getting a correct shift time. Another reason might reside in the sensitivity formulation. We have tried to apply the same sensitivity formulation (Luo and Schuster's formulation) to integrate non-monotonic water cut data but did not get very positive result. One reason is that water cut responses in real life is erratic and have multiple up-and-downs. We still need to investigate how to better match this kind of water cut responses, maybe by incorporating Luo and Schuster's formulation, or by master-point amplitude inversion to reduce the degree of non-linearity.

Currently, the gas/oil ratio shift time is calculated from the amplitude difference and the tangent of the observed gas/oil ratio if the response is flat and causes difficulty for shift time calculation. It is recommended to investigate other ways to get a correct shift time.

Gas/oil ratio response is very sensitive to three-phase relative permeability and PVT properties. We should also investigate the GOR sensitivity to relative permeability and PVT properties.

NOMENCLATURE

A = maximum amplitude of tracer concentration

B_g = gas formation volume factor

B_o = oil formation volume factor

B_w = water formation volume factor

c = divergence of flux

C_c = calculated tracer concentration

C_o = observed tracer concentration

$\boldsymbol{C}_D$ = data error covariance

$\boldsymbol{C}_M$ = prior model parameter covariance

$\boldsymbol{d}$ = data vector

D = dispersion coefficient

$\boldsymbol{F}_k$ = tangent vector

$\boldsymbol{F}_{kk}$ = acceleration vector

f_g = fractional flow of gas

f_o = fractional flow of oil

f_w = fractional flow of water

$\boldsymbol{G}$ = sensitivity matrix

GOR = production gas/oil ratio

$\boldsymbol{I}$ = identity matrix

J = misfit function

k = permeability

k_{rg} = gas phase relative permeability

k_{ro} = oil phase relative permeability

k_{rw} = water phase relative permeability

k_{rog} = oil relative permeability in gas/oil saturation function

k_{row} = oil relative permeability in water/oil saturation function

k_{rocw} = k_{row} at connate water saturation

$\boldsymbol{L}$ = spatial difference operator

m = reservoir parameter

$\boldsymbol{m}$ = reservoir parameter vector

$\boldsymbol{m_p}$ = prior reservoir model parameter

n_b = number of grid blocks

n_o = number of dynamic data observations

N_{dj} = number of dynamic data observations of jth well

N_w = number of wells

P = pressure

P_b = bubble point pressure

q = streamline flow rate

Q_g = gas production rate

$Q_{g,free}$ = free gas production rate

Q_o = oil production rate

$\boldsymbol{R}$ = reservoir parameter vector

R_s = solution gas/oil ratio

R^2 = coefficient of determination

s = slowness

$\boldsymbol{S}$ = sensitivity matrix

S_g = gas saturation

S_o = oil saturation

S_w = water saturation

S_{wco} = connate water saturation

t = time

Δt = travel-time shift

$\Delta\tilde{t}$ = generalized travel-time

u = Darcy velocity

v = Interstitial velocity

y^{obs} = observed response

$\overline{y^{obs}}$ = averaged observed response

y^{cal} = calculated response

β_1 = weighting factor for the prior model

β_2 = weighting factor for the roughness term

κ_{am} = measure of nonlinearity for amplitude inversion

κ_{gt} = measure of nonlinearity for generalized travel-time inversion

κ_{tt} = measure of nonlinearity for travel-time inversion

ρ = relative density

τ = time of flight

$\Delta\tau$ = generalized travel-time or travel-time shift

μ_g = gas viscosity

μ_o = oil viscosity

μ_w = water viscosity

λ_{rt} = total relative mobility

ϕ = porosity

Ψ = streamline trajectory

REFERENCES

1. Deutsch, C.V. and Journel, A.G.: *GSLIB: Geostatistical Software Library and User's Guide*. 2nd edition, Oxford University Press, New York (1998).
2. Sun N.-Z.: *Inverse Problem in Groundwater Modeling*. Kluwer Academic Publishers, Boston (1994).
3. Tarantola, H.: *Inverse Problem Theory: Methods for Data Fitting and Model Parameter Estimation*. Elsevier, Amsterdam, Netherlands (1987).
4. Milliken, W.J. and Emanuel, A.: "History Matching Finite Difference Models with 3D Streamlines," paper SPE 49000 presented at the 1998 SPE Annual Technical Conference and Exhibition, New Orleans, 27-30 September.
5. Milliken, W.J., Emanuel, A. and Chakravarty, A.: "Application of 3D Streamline Simulation to Assist History Matching," paper SPE 63155 presented at the 2000 SPE Annual Technical Conference and Exhibition, Dallas, 1-4 October.
6. Baker R.O: "Streamline Technology: Reservoir History Matching and Forecasting = Its Success, Limitations, and Future," Distinguished Author Series, *Journal of Canadian Petroleum Technology* (April 2001) **40**, No. 4, 23-27.
7. Yeh, W. W.-G.: "Review of Parameter Identification Procedures in Groundwater Hydrology: The Inverse Problem," *Water Resources Research* (1986) **22**, No. 2, 95.
8. Wen, X.-H, Deutsch, C.V. and. Cullick, A.S.: "A Review of Current Approaches to Integrate Flow Production Data in Geological Modeling," Report 10, Stanford Center for Reservoir Forecasting, Stanford, CA (1997).
9. Cheng, H., Khargoria, A., He, Z. and Datta-Gupta, A.: "Fast History Matching of Finite-Difference Models Using Streamline-Derived Sensitivities," *SPE Reservoir Evaluation & Engineering* (2005), to appear.
10. Landa, J.L. and Horne, R.N.: "A Procedure to Integrate Well Test Data, Reservoir Performance History and 4-D Seismic Information into a Reservoir Description," paper SPE 38653 presented at the 1997 SPE Annual Technical Conference and Exhibition, San Antonio, TX, 5-8 October.

11. Landa, J.L.: "Technique to Integrate Production and Static Data in a Self-Consistent Way," paper SPE 71597 presented at the 2001 SPE Annual Technical Conference and Exhibition, New Orleans, 30 September-3 October.
12. Wen, X.-H., Deutsch, C.V. and Cullick, A.S.: "High Resolution Reservoir Models Integrating Multiple-Well Production Data," *SPE Journal* (December 1998) 344-355.
13. Vasco, D.W., Yoon, S., and Datta-Gupta, A.: "Integrating Dynamic Data into High-Resolution Reservoir Models Using Streamline-Based Analytic Sensitivity Coefficients," *SPE Journal* (December 1999) 389.
14. Wen, X.-H, Deutsch, C.V. and Cullick, A.S.: "Integrating Pressure and Fractional Flow Data in Reservoir Modeling with Fast Streamline-Based Inverse Method," paper SPE 48971 presented at the 1998 SPE Annual Technical Conference and Exhibition, New Orleans, 27-30 September.
15. Wang, Y. and Kovscek, A.R.: "Streamline Approach for History Matching Production Data," *SPE Journal* (December 2001) 353-363.
16. Caers, J., Krinshnan, S., Wang, Y. and Kovscek, A.R.: "A Geostatistical Approach to Streamline-Based History Matching," *SPE Journal* (September 2002) 250-266.
17. Agarwal, A. and Blunt, M.J.: "Streamline-Based Method with Full-Physics Forward Simulation for History-Matching Performance Data of a North Sea Field," *SPE Journal* (June 2003) 171-180.
18. Wen, X.-H., Deutsch, C.V. and Cullick, A.S.: "Inversion of Dynamic Production Data for Permeability: Fast Streamline-Based Computation of Sensitivity Coefficients of Fractional Flow Rate," *J. of Hydrology* (2003) **281**, 296-312.
19. Bissel, R.C.: "Calculating Optimal Parameter for History Matching," Proc. of the 4th European Conference on the Mathematics of Oil Recovery, Topic E: History Match and Recovery Optimization, Røros, Norway (1994).
20. Oliver D.S., Reynolds, A.C., Bi, Z., Abacioglu, Y.: "Integration of Production Data into Reservoir Models," *Petroleum Geoscience* (May 2001) 65-73.
21. Datta-Gupta, A., Yoon, S.S., Nordaas, K., and Vasco, D.W.: "Streamlines, Ray

Tracing and Production Tomography: Generalization to Compressible Flow," *Petroleum Geoscience* (May 2001), 75.

22. Yoon, S., Malallah, A.H., Datta-Gupta, A. and Vasco, D.W..: "A Multiscale Approach to Production Data Integration Using Streamline Models," *SPE Journal* (June 2001) 182-192.
23. Landa, J.L., Kamal, M.M., Jenkins, C.D., and Horne, R.N.: Reservoir Characterization Constrained to Well Test Data: A Field Example," paper SPE 36511 presented the 1996 SPE Annual Technical Conference and Exhibition, Denver, 6-9 October.
24. Wu, Z. and Datta-Gupta, A.: "Rapid History Matching Using a Generalized Travel Time Inversion Method," *SPE Journal* (June 2002) 113-122.
25. Reynolds, A. C., He, N., and Oliver, D.S.: "Reducing Uncertainty in Geostatistical Description with Well Testing Pressure Data," in the Proc. of the 1997 International Reservoir Characterization Conference, Houston, 2-4 March.
26. He, Z., Datta-Gupta, A., and Yoon, S.: "Streamline-Based Production Data Integration with Gravity and Changing Field Conditions*," SPE Journal* (December 2002) 423-436.
27. King, M.J. and Datta-Gupta, A.: "Streamline Simulation: A Current Perspective," *In Situ* (1998) **22**, No. 1, 91.
28. Luo, Y. and Schuster, G.T.: "Wave-Equation Traveltime Inversion," *Geophysics* (1991) **56,** No. 5, 645.
29. Anterion, F., Eymard, R. and Karcher, B. : "Use of Parameter Gradients for Reservoir History Matching," paper SPE 18433 presented at the 1989 SPE Symposium on Reservoir Simulation, Houston, 6-8 February.
30. Sun, N-Z and Yeh, W. W.-G.: "Coupled Inverse Problems in Groundwater Modeling, I, Sensitivity Analysis and Parameter Identification," *Water Resources Research* (1990) **26**, 2507.

31. Cheng, H., Datta-Gupta, A., and He, Z.: "A Comparison of Travel-Time and Amplitude Matching for Production Data Integration Into Field-Scale Geologic Model," *SPE Journal* (March 2005) 75-90.
32. Bates, D.M. and Watts, D.G.: "Relative Curvature Measures of Nonlinearity," *J. R. Statist. Soc. B* (1980) **42**, No. 1, 1.
33. Grimstad, A.-A. and Mannseth, T.: "Nonlinearity, Scale, and Sensitivity for Parameter Estimation Problems," *SIAM J. Sci. Comput.* (2000) **21**, No. 6, 2096.
34. Mannseth, T., Nordtvedt, J.-E., Brusdal, K., Grimstad, A.-A., Kolltveit, K., and Watson, A.T.: "Functional Representation and Model Nonlinearity in Estimation of Porous Media Properties From Laboratory Experiments," presented at the 4th SIAM Conference on Mathematical and Computational Issues in the Geosciences, Albuquerque, NM, 16-19 June, 1997.
35. Bissel, R.C., Killough, J.E., and Sharma, Y.: "Reservoir History Matching Using the Method of Gradients," paper SPE 24265 presented at the 1992 SPE European Petroleum Computer Conference, Stavanger, 25-27 May.
36. Datta-Gupta, A. and King, M.J.: "A Semianalytic Approach to Tracer Flow Modeling in Heterogeneous Permeable Media," *Advances in Water Resources* (1995) **18**, No. 1, 9.
37. Parker, R.L.: *Geophysical Inverse Theor*y, Princeton University Press, Princeton, New Jersey (1994).
38. Paige, C.C. and Saunders, M. A.: "LSQR: An Algorithm for Sparse Linear Equations and Sparse Least Squares," *ACM Trans. Math. Software* (1982) **8**, No. 1, 43.
39. Nolet, G.: "Seismic Wave Propagation and Seismic Tomography," *Seismic Tomograph*y, G. Nolet (Ed.), D. Reidel, Dordrecht, (1987) 1-23.
40. Lichtenberger, J.: "Field Application of Interwell Tracers for Reservoir Characterization of Enhanced Oil Recovery Pilot Areas," paper SPE 21652 presented at the 1991 SPE Production Operations Symposium, Oklahoma City, 7-9 April.
41. Allison, S.B., Pope, G.A., and Sepehrnoori, K., "Analysis of Field Tracers for Reservoir Description," *J. Pet. Sci. Eng.* (1991), **5,** 173-186.

42. Iliassov, P.A., Datta-Gupta, A., and Vasco, D.W.: "Field-Scale Characterization of Permeability and Saturation Distribution Using Partitioning Tracer Tests: The Ranger Field, Texas," *SPE Journal* (December 2002) 409-423.
43. Agarwal, B., and Blunt, M. J.: "A Streamline-Based Method for Assisted History Matching Applied to an Arabian Gulf Field," paper SPE 84462 presented at the SPE Annual Technical Conference and Exhibition, Denver, CO, October 5-8, 2003.
44. Caers, J.: "Geostatistical History Matching Under Training-Image Based Geostatistical Model Constraints," *SPEJ* (2003), 218-226.
45. Liu, N., Betancourt, S., and Oliver, D.S.: "Assessment of Uncertainty Assessment Methods," paper SPE 71624 presented at the 2001 SPE Annual Technical Conference and Exhibition, New Orleans, 30 September-3 October.
46. King, M.J. and Datta-Gupta, A.: "Streamline Simulation: A Current Perspective," *In Situ* (1998) **22**, No. 1, 91.
47. Datta-Gupta, A., "Streamline Simulation: A Technology Update," SPE Distinguished Author Series, *Journal of Petroleum Technology* (December 2000) 68-73.
48. Bratvedt, F., Gimse, T. and. Tegnander, C.: "Streamline Computations for Porous Media Flow Including Gravity," *Transport in Porous Media* (1996) **25**(1), 63.
49. Vega, L., Rojas, D. and Datta-Gupta, A.: "Scalability of the Deterministic and Bayesian Approaches to Production Data Integration into Field-Scale Reservoir Models," SPE 79666 presented at the 2003 SPE Reservoir Simulation Symposium, Houston, 3-5 February.
50. Durlofsky, L. J., Jones, R.C. and Milliken, W. J., "A New Method for the Scale Up of Displacement Processes in Heterogeneous Reservoirs," 4th European Conference on Mathematics of Oil Recovery, Røros, Norway (June 1994).
51. Schlumberger GeoQuest: *FrontSim User Guide 2003A*, Schlumberger , Houston (2003).
52. Schlumberger GeoQuest:*ECLIPSE Reference Manual 2003A*,Schlumberger, Houston 2003).
53. Provost, M.: "The Streamline Method for Unstructured Grids," M.S. Thesis, Stanford University, Palo Alto, CA, June 2000.
54. Sabir, K. : "Velocity Models, Material Balance and Solution Convergence in

Streamline-Based Simulation," M.S. Thesis, Texas A&M University, College Station, Texas, December 2002.

55. Qassab, H, Khalifa, M, Pavlas, R., Khargoria, A., He, Z., Lee, S. H. and Datta-Gupta, A.: "Streamline-based Production Data Integration Under Realistic Field Conditions: Experience in a Giant Middle-Eastern Oil Reservoir," SPE 84079 presented at the SPE Annual Technical Conference and Exhibition, Denver, CO, 5-8 October, 2003.
56. Oliver, D. S.: "Incorporation of Transient Pressure Data into Reservoir Characterization," *In Situ* (1994)**18**, No. 3, 243-275.
57. Reynolds, A. C., He, N., and Oliver, D.S.: "Reducing Uncertainty in Geostatistical Description with Well Testing Pressure Data," in Proc. of the 1997 International Reservoir Characterization Conference, Houston, 2-4 March.
58. Li, R., Reynolds, A. C., and Oliver, D.S.: "History Matching of Three-Phase Flow Production Data," *SPE Journal* (December 2003) 328-340.
59. Reynolds, A. C., Li, R., and Oliver, D.S.: "Simultaneous Estimation of Absolute and Relative Permeability by Automatic History Matching of Three-Phase Flow Production Data," *JCPT* (March 2004) **43**, No. 3, 37-45.
60. Bear, J.: *Dynamics of Fluids in Porous Media*. Dover Publications, Inc., New York (1972).
61. Schlumberger GeoQuest: *ECLIPSE Technical Description 2003A*, Schlumberger (2003).
62. Stone, H.L.: "Estimation of Three-Phase Relative Permeability and Residual Oil Data," *JCPT* (1973) **12**, 53-61.
63. Aziz, K. and Settari, A., 1979. *Petroleum Reservoir Simulation*. Elsevier Applied Science Publishers, London.
64. Killough, J.E.: "Ninth SPE Comparative Solution Project: A Reexamination of Black-Oil Simulation," paper SPE 29110 presented at the 13th SPE Symposium on Reservoir Simulation held in San Antonio, TX, 12-15 February 1995.

VITA

Hao Cheng
7510 Brompton Street, Apt. 156, Houston, TX 77025
Cell: (979)587-1714
haocheng@spemail.org

Education

Ph.D., Petroleum Engineering, Texas A&M University, College Station, TX, Aug. 2005
Ph.D., Petroleum Engineering, University of Petroleum, Beijing, China, June 2001
B.S., Petroleum Engineering, Xi'an Petroleum Institute, Xi'an, China, June 1996

Journal Articles

1. Hao Cheng, Akhil Datta-Gupta, and Zhong He, "A Comparison of Travel-Time and Amplitude Matching for Production Data Integration Into Field-Scale Geologic Model: Sensitivity, Non-Linearity and Practical Implications," *SPE Journal*, 10(1), 75-90, March 2005
2. Hao Cheng, Arun Khargoria, Zhong He, and Akhil Datta-Gupta, "Fast History Matching of Finite-Difference Models Using Streamline-Derived Sensitivities," *SPE Reservoir Evaluation & Engineering*, 2005 (to appear)
3. Mishal Al-Harbi, Hao Cheng, Zhong He, and Akhil Datta-Gupta, "Streamline-Based Production Data Integration in Naturally Fractured Reservoirs," *SPE Journal*, to appear
4. Hao Cheng, Wenliang Zhang, and Yanmei He, "Advances in Numerical Simulation of Foam Flow in Porous Media," *Fault-Block Oil & Gas Field*, Vol. 7, No. 5, 26-30, September 2000
5. Hao Cheng, Chenggang Xian and Zhaoxin Lang, "A New Chemical Reaction Equilibrium Model in Alkaline-Surfactant-Polymer Flood and Its Application," *Journal of the University of Petroleum*, China (Edition of Natural Science), Vol. 24, No. 2, 64-69, April 2000
6. Hao Cheng, Zhaoxin Lang, "Capillary Crossflow in Foam Flood and Its Numerical Simulation," *Journal of Chongqing University* (Natural Science Edition, China), Vol. 23, Supplement, 161-165, October 2000
7. Chenggang Xian, Hao Cheng, Zhaoxin Lang and Lihua Zhang, "Well Patterns for Low Permeability Oilfield," *Journal of the University of Petroleum*, China (Edition of Natural Science), Vol. 23, No. 2, 51-54, April 1999
8. Chenggang Xian, Zhaoxin Lang and Hao Cheng, "Development and Application of Mathematical Models for Alkaline-Surfactant-Polymer Flooding," *Journal of the University of Petroleum*, China (Edition of Natural Science), Vol. 24, No. 2, 61-63, April 2000

This dissertation was typed by the author.